The effect of oil emplacement on quartz cementation in a deeply buried sandstone reservoir

Richard H Worden[1], Mohammed Bukar[1], Philip Shell[2]

1 Department of Earth, Ocean and Ecological Sciences, University of Liverpool, Liverpool, L69 3GP, UK

2. BP Exploration (Epsilon) Ltd, Oman Branch, PC 130 (Al Azaiba), Muscat, Sultanate of Oman

Key words: quartz cementation, quartz cement inhibition, diagenesis, oil charging, reservoir quality

Abstract

Quartz is an important, porosity-occluding cement in sandstone reservoirs that have been subjected to elevated temperature (>80 º-100 ºC) for a substantial period of time. The effect of oil emplacement on quartz cementation in reservoir sandstones is controversial; some studies have concluded that early oil emplacement can inhibit quartz cementation leading to the preservation of porosity, while other studies have concluded that quartz cementation appears largely unaffected by oil emplacement. Here we have studied shallow marine, Upper Jurassic sandstones from Ula Field, Norwegian North Sea, with reservoir temperatures of approximately 150 ºC, in order to determine whether oil emplacement had a significant impact on diagenesis with

particular attention to quartz cementation. Following sedimentological description of cores, samples above and below the oil-water contact have been collected, adjacent to core analysis plug points. These samples then underwent a series of studies, including petrographic point counting with a transmitted light microscope, scanning electron microscopy (SEM), backscattered electron microscopy (BSEM), cathodoluminescence microscopy (SEM-CL), and fluid inclusion studies. These data were integrated with routine core analysis and petrophysical log data. Density and resistivity log data have been used to determine the precise oil saturation of each sample studied. The distributions of all potential controls on porosity and permeability, such as grain size, sorting, matrix clay content, degree of bioturbation, the presence of grain coatings, and dolomite cement, as well as the amount of quartz cement, have been assessed. The presence of primary oil inclusions within quartz cement shows that oil ingress into the Ula reservoir commenced prior to the onset of quartz cementation. Very fine-grained, matrix-rich, bioturbated and microquartz-cemented sandstones have uniformly low quartz cement contents irrespective of oil saturation. Medium-grained, graded, matrix-poor, microquartz-poor sandstones have quartz cement ranging from 1 % to greater than 17 %, associated with core porosities of about 22 % and 7 %, respectively. Higher oil saturations equate to higher porosities and permeabilities in the medium-grained, graded, matrix-poor, microquartz-poor sandstones, which cannot be explained by any control other than the amount of quartz cement as a function of pore fluid type. Oil emplacement therefore appears to have inhibited quartz cementation at high oil saturations and can be viewed as a significant control on reservoir quality. The significance of this study is that the presence of oil in a sandstone reservoir, at the time that quartz cement was growing, can have a considerable impact on reservoir quality. Models that seek to predict quartz cement and reservoir quality in sandstones need to account for the timing of oil emplacement compared to other diagenetic processes.

Introduction

The aim of this paper is to determine whether oil charge exerted a control on quartz cementation, and consequently preserved porosity, in sandstones from the Upper Jurassic Ula Formation in Ula Field, Norwegian North Sea.

Understanding whether oil charge has stopped or retarded quartz cementation in the Ula Formation could impact the prediction of porosity and permeability (reservoir quality) distribution, leading to (i) increased accuracy in volumetric reserve estimation (e.g. stock tank oil initially in place: STOIIP) and (ii) being able to forecast well performance pre-drill, allowing wells with better delivery to be drilled first. The accurate understanding and prediction of reservoir quality is therefore key in order to obtain predictable well flow-rates throughout the lifetime of a field/reservoir (Sneider, 1990). However, the prediction of reservoir quality is, and will continue to be, a key challenge for petroleum exploration and reservoir development. Defining and reducing risk associated with reservoir quality is especially important in sandstone reservoirs that have been subjected to elevated temperatures (typically taken to be >100 $^{\circ}C$) because of quartz, and other deep burial-related, cements, or high effective stress because of compaction (Taylor et al., 2010).

Quartz is volumetrically the most important cement in deeply buried sandstones (Worden and Morad, 2000). The ability to predict areas within reservoirs, or individual sandstone units, where quartz cement quantity appears to be anomalously low could lead to improved prediction of the distribution of porosity and permeability in reservoirs where quartz cement has been demonstrated to be the main control on reservoir quality. The concept that oil emplacement could inhibit quartz cementation and influence preservation of porosity in sandstone reservoirs became known to many geologists from Johnson's (1920) publication “The cementation process”, later developed in a series of papers (Hawkins, 1978; Lowry, 1956; Scholle, 1977; Scholle and Halley, 1985). However, the question of the inhibiting effect of oil on mineral reactions in oil fields remains open and is highly contentious (Sathar et al., 2012; Taylor et al., 2010).

All diagenetic reactions take place through an aqueous phase, by dissolution, transport and re-precipitation (Worden and Morad, 2000). Hence, for diagenetic reaction to occur there must be aqueous fluid present to dissolve the mineral grains, to transport dissolved material, and to facilitate mineral precipitation. In an oil or gas field, displacement of the aqueous fluid by hydrocarbons within the pore space disrupts the pathway between the reactants and sites of precipitation. As oil saturation increases (i) the residual (irreducible) water becomes isolated within a continuous hydrocarbon phase, (ii) the aqueous pathway becomes tortuous and diffusion rate decreases, or (iii) grain surfaces become coated by oil if the sandstone is mixed- or oil-wet (Barclay and Worden, 2000a). As a consequence, most of those working on diagenesis and sandstone reservoir quality assumed, up to the early-to-mid 1990s, that early oil emplacement halted cementation and preserved porosity.

Many empirical studies from different basins and from reservoirs of different ages have used, or discussed, the concept that early oil emplacement is a mechanism for porosity preservation in sandstones (Bjørnseth and Gluyas, 1995; Dixon et al., 1989; Emery et al., 1993; England et al., 2003; Gluyas and Cade, 1997; Gluyas et al., 1993; Haszeldine et al., 2003; Higgs et al., 2007; Marchand et al., 2000; Marchand et al., 2001; Marchand et al., 2002; Robinson and Gluyas, 1992; Saigal et al., 1992; Wilkinson and Haszeldine, 2011; Wilkinson et al., 2004; Wilkinson et al., 2006). These studies assumed that replacing formation water with oil simply stopped water-mediated geochemical reactions. However, several other workers have suggested that quartz cementation can continue unhindered even after oil emplacement (Aase and Walderhaug, 2005; Bjørkum and Nadeau, 1998; Ehrenberg, 1990, 1993; Midtbø et al., 2000; Molenaar et al., 2008; Ramm and Bjorlykke, 1994). To explain this rather different interpretation of diagenetic processes, it was assumed that the combined diagenetic processes of dissolution-diffusion-precipitation utilise residual water that clings to grain surfaces, and that this film of water apparently permits mineral diagenesis to continue unhindered.

Comprehensive overviews of the empirical and theoretical arguments for and against oil emplacement inhibiting quartz cementation (Worden and Morad, 2000; Worden et al., 1998) concluded that the rate of quartz cementation that is synchronous with, or after, oil emplacement in sandstone is probably reduced relative to rates of quartz cementation in the underlying aquifer. These reviews concluded that quartz cementation should be strongly inhibited if (i) the system has mixed wettability or is oil-wet, (ii) the silica is externally supplied, (iii) the rate of diffusion is rate controlling, or (iv) advection is an important part of the transport process. However, even in internally-sourced silica systems with diffusion as the transport control, the overall rate of quartz cementation should be inhibited due to added tortuosity reducing the net rate of diffusion.

One of the main difficulties in definitively addressing the controversial question of oil inhibition of quartz cement is the large number of potential controls on quartz cementation, such as: (i) primary depositional factors (e.g. facies, grain size, sorting, detrital mineralogy, matrix clay content), (ii) diagenetic factors (e.g. grain coating clay and other minerals, pre-quartz, pore-filling cements, the source of silica), and (iii) pore system characteristics (e.g. wettability and tortuosity). It is also important to consider the oil-filling history of each facies. It is, therefore, possible that previous studies have compared fundamentally different rocks, with different controls on quartz cementation, when attempting to prove or disprove the effect of oil emplacement on quartz cementation. In this study, we have taken samples with variable oil and water saturations, as defined by wireline log data. We have been careful to only compare sandstones from the same facies. We have also carefully quantified the presence, type and extent of grain coating materials and taken account of pore-filling cements and only made comparisons between rocks that appear to be as similar as possible (apart from oil saturation). Key questions to be addressed are;

1. What was the timing of oil emplacement relative to quartz cementation in the Ula Formation?
2. What other potential influences/controls are there on quartz cementation in the Ula Formation?

3. Is there a difference in the quartz cement volume as a function of oil saturation for rocks that share similar pre-oil filling characteristics?
4. Can any differences in quartz cement volume be attributed to oil emplacement?

Geological background

Ula Field is an offshore oil accumulation located in blocks 7/12 in the southern Norwegian sector of the North Sea (Fig. 1). Ula is located 280 km (149 miles) southwest of Stavanger at the eastern margin of the Central Graben along the Hidra Fault zone (Fig. 1) (Nedkvitne et al., 1993). In addition to Ula Field, three other fields, Gyda, Tambar and Tambar East, combine to make up the Ula-Gyda-Tambar (UGT) area (O'Connor et al., 2011). Ula Field was chosen to undertake this study due to the abundance of available core and supporting downhole data, which not only gives good geographical coverage of the whole field but also gives good stratigraphic coverage through the oil leg, transition zone and water leg.

Ula Field consists of Mesozoic sediments in an anticlinal structure formed by late Jurassic rifting and subsequent inversion in the Cretaceous and Tertiary (Brown et al., 1992). The main reservoir in the field is the Upper Jurassic Ula Formation (Fig. 2) (Bergan et al., 1989; Karlsen et al., 1993; Partington et al., 1993; Underhill, 1998). The Upper Jurassic Mandal Formation is considered to be the source of the petroleum, beginning expulsion from the deeper parts of the Central Graben during the late Cretaceous. Petroleum is still being generated in the UGT area from the Mandal

Formation source rock (Taylor et al., 1999). Within the UGT area, the Mandal Formation also provides the seal for the underlying Jurassic sandstones (Bjørnseth and Gluyas, 1995).

The Upper Jurassic Ula Formation is a marine sandstone, up to 200m thick, that prograded across Haugesund Formation outer-shelf mudstones following a sea level drop in the Kimmeridgian (Harris, 2006). Ula sandstones are typically very fine- to medium-grained, well-sorted, and locally can be glauconitic with some beds rich in shale fragments. Ula Formation sandstones have been described as arkosic (using the McBride, 1963, classification scheme) and were probably sourced from nearby Triassic sandstone outcrops (Gluyas, 1997). Much of the Ula Formation has been interpreted to be intensively burrowed (Baniak et al., 2014; Baniak et al., 2015) and, even where no burrows are evident, physical sedimentary structures can be absent, suggesting that the unit has been intensively bioturbated. Facies subdivisions are largely based on grain size and matrix content ; facies 1 is a normally-graded, medium-grained sandstone, with low detrital clay content, facies 2 is a bioturbated fine- to medium-grained sandstone with variable detrital clay content, facies 3 is a very fine to fine-grained sandstone that is intensively bioturbated with a high detrital clay content. Trace fossils are dominated by *Ophiomorpha*, suggesting a high energy, shallow marine (*Skolithos* ichnofacies) origin for the sandstone (Baniak et al., 2015). The Ula Formation contains pervasively carbonate-cemented intervals that have negligible porosity and have been interpreted to result from bedded accumulation of shell debris followed by early diagenetic dissolution and reprecipitation as calcite cement (Gluyas, 1997). Core analysis porosity in the Ula Formation typically lies between 7 and 28%. Permeability mostly falls between 650 to 850 mD for the better reservoir units (with extremes between 0.2 and 2800 mD) (Karlsen et al., 1993).

The Ula Formation in Ula Field underwent more than 2000m of subsidence after the early Oligocene and is slightly overpressured, possibly as a result of the rapid late Tertiary subsidence (Fig. 3) (Harris, 2006; O'Connor et al., 2011). The Ula reservoir has been reported to have a slightly tilted oil-water contact (O'Connor et al., 2011). Reservoir temperature at 3,450 m (11,319 ft) is 143 to 145^{o}C (Home, 1987).

Methods and material

One hundred and twenty two samples of conventional core plugs from four wells were obtained for petrographic analysis from the BP core store at Reslab laboratories in Stavanger, Norway (Appendix 1). These petrographic samples were taken directly adjacent to plug points for conventional core analysis, thus ensuring that the petrographic data tied to the core analysis data. Of the four wells, well 7/12-2 is in the oil leg, and 7/12-A8 is in the water leg, 7/12-3A and 7/12-A13 traverse the oil and water legs. The core sample suite covers the range of present subsurface depths between about 3350 and 3850 m (10,991 and 12,631 ft) TVD, and spans the thickness of the whole reservoir.

Samples were impregnated with blue resin and then made into polished thin sections. Sandstone modal composition was obtained, in the laboratories at Liverpool University, by point counting all thin sections at 400 counts per section. Point counting was performed using a x10 objective but higher power objectives were used where necessary, e.g. for finer grained materials and grain coatings. The grid-spacing was selected to ensure that the whole thin section was covered. Quartz cement was differentiated from quartz grains by virtue of the presence of a trail of inclusions on quartz grain surfaces. Grain sizes and grain coatings were determined for each sample using a Meiji 9000 microscope fitted with an Infinity 1.5 camera. Images were collected and long axes of 100 grains per sample and were measured using Infinity Analyser software, with the images and camera calibrated to standards of known size. Fifty quartz grains per sample were measured in the laboratories at Liverpool University, for the percentage of grain-coating microcrystalline quartz coverage (noting that negligible clay mineral coats were observed) of the freely-exposed grain surfaces, using visual estimates compared to standard grain-coverage images. Only potential sites for quartz cementation (i.e. facing pores, not coated with dead-oil or with clay matrix) that were coated with microcrystalline quartz were measured and expressed as a percentage of all potential sites for quartz cementation.

Scanning electron microscope (SEM) examination of all samples was undertaken using a Philips XL 30 SEM with tungsten filament with an accelerating voltage of 20 kV, and 8 nA beam current for both secondary electron (SE) and backscattered electron microscopy (B)SEM. The SEM examination was carried out on polished sections and freshly fractured, stub-mounted samples coated with carbon and gold respectively. Energy dispersive X-ray analysis (EDAX) provided qualitative compositional analysis of clay minerals, carbonate cements and feldspars. Oil-stained samples were soaked in acetone to remove the oil stains which caused problems for the vacuum system in the gold coater. The scanning electron microscope-cathodoluminescence (SEM-CL) images of quartz cemented grains were collected at

10 kV by integrating the signals from 16 discrete frames using a slow scanning raster; this took about 8 minutes for each image. The petrographically-defined quartz cement content was compared to the amount of quartz cement discernible from SEM-CL images for three samples, one with high, one with intermediate, and one with a low quartz cement content, to ensure that the point count determination of quartz cement was consistent.

Doubly polished fluid inclusion wafers for fluid inclusion microthermometric studies were selected to cover all facies from both the water leg and the oil leg and prepared from core samples. An Olympus BX-60 petrographic microscope was used for thermometry equipped with a Linkam THMSG 600 heating and cooling stage. This enabled the measurement of the phase transition temperatures from -180 to 600 °C with an accuracy of between ± 0.1 to ± 1.0. Observations were made with different magnifications (objectives 10x, 20x, 50x and 100x). Inclusions were photographed with Digital Camera Olympus DP71 for the purpose of the fast mapping of inclusion locations. Homogenisation temperature measurements were made on each inclusion in each small piece of fluid inclusion wafer and then freezing point depression measurements were made on each identified inclusion to prevent modification of the homogenisation temperature (Worden et al., 1995). Fluid inclusion samples were also studied using a mercury UV source to differentiate oil inclusions from aqueous inclusions with a record being kept of the presence and absence (and relative abundance) of petroleum inclusions.

Petrophysical and conventional core analysis data were made available by BP Norway. Porosity and permeability were measured for BP Norway using modern industry-standard methods and corrected for confining stress. The permeability data reported here were all collected from plugs drilled parallel to bedding (horizontal permeability). The provided data excluded any anomalous data from fractured plugs. The plugs were collected using industry standard approaches at one every 25 cm (9.84 inches), irrespective of be boundaries to ensure a representative petrophysical dataset. The petrophysical log suites provided for this study were: caliper, bulk density, neutron porosity, sonic transit time, gamma ray, and shallow and deep resistivity. Porosity was calculated for each of the logs using the bulk density log (g/cm^3) and the following relationship:

$$\text{fractional porosity} = (\rho_{mbd} - \rho_{amd})/(\rho_{fd} - \rho_{amd}) \qquad \text{(eq 1)}$$

Where:

ρ_{mbd} = measured bulk density for each sample (from petrophysical logs)

ρ_{amd} = average mineral density

ρ_{fd} = fluid density

The average mineral density employed was 2.66 g/cm^3 (the density of quartz); this average is reasonable since there is a proportion of feldspar with lower density and a proportion of carbonate minerals with higher density. The average fluid density was assumed to be 1.00 g/cm^3.

Water saturation was calculated from the petrophysical log data for each 10 cm depth-interval using the Archie equation. Hole conditions were not an issue in the studied section because it did not include poorly-lithified or soluble sections such as mudstones or evaporites. Values of n, a, and m were fixed at 2.0, 0.81 and 2.0, respectively, as used by the field operators, following industry standard methods and calibration. Deep induction resistivity log data were used since these give true formation resistivity, unaffected by invasion of the formation by drilling fluids (Asquith and Gibson, 1982). The reported formation water resistivity for Ula Field is 0.025 ohm.m (Oxtoby, 1994).

Results

Wireline and core analysis data

The calculated density log porosity values correlate well with the core analysis porosity values suggesting that the (wireline) density log porosity values are credible (Fig. 4). The density log-derived porosity and water saturation values for each well are illustrated in Figure 5. The log-derived porosity of the four wells seems to be highest at the shallowest positions with porosity routinely > 20% at the crest of the field but no higher than 10-15 % at the flanks of the field (Fig. 5). The wells included in this study show a wide variation in water saturations; well 7/12-2 has low water saturation, wells 7/12-A13 and 7/12-A08 have high water saturation. Well 7/12-3A has low to intermediate water saturation. The very low porosity and high water saturation spikes (e.g. for well 7/12-2) represent pervasively calcite cemented intervals.

The core analysis data have been split between the three main facies as determined by sedimentological facies description of the core and then further split by the wireline-calculated water saturations (Fig. 5). Porosity-permeability data for each facies, split by water saturation, are displayed in Figure 6 showing that samples with lowest water saturations, especially from facies 1 and facies 2, have the highest porosity and permeability values.

Facies and detrital minerals

The point count data confirm that the Ula Formation reservoir is an arkosic sandstone (Fig. 7). The wells used in this study and different facies within the core are not differentiated on the ternary QFL diagram since the data lie in one cluster. The main variations in different facies are in terms of: grain size, clay content and degree of bioturbation. A full listing of petrographic data is given in Appendix 1.

Facies 1 is medium-grained, moderately well-sorted (0.52 ϕ), with low detrital clay content (mean 4.2 %, Table 1) and no direct sign of bioturbation. Facies 1 tends to be in upward-fining (i.e. graded) beds that are devoid of small-scale sedimentary structures. Point counting results show that the most dominant detrital mineral is monocrystalline quartz (mean 34 %), followed by K-feldspar (mean 11 %) and plagioclase (14 %). Polycrystalline quartz and traces of rock fragments are also present in this facies.

Facies 2 is a fine- to medium-grained sandstone that is moderately- to well-sorted (0.62 ϕ), with a variable detrital clay content ranging from 0.8 to 13.0 % (mean 6.5 %) (Table 1). Facies 2 is bioturbated with no remaining primary sedimentary structures due to bioturbation with cm-scale horizontal burrows, identified as *Ophiomorpha* or *Palaeophycus*. The dominant detrital mineral grains in facies 2 are monocrystalline quartz (mean 28 %), K-feldspar (mean 9 %), plagioclase (mean 15%) and rock fragments (<3 %).

Facies 3 is a very fine- to fine-grained sandstone that is moderately-sorted (0.83 ϕ) with a high detrital clay content, based on point-count data ranging from 5.7 to 23.2 % (mean 11.5 %) (Table 1). Facies 3 is intensively bioturbated with vertical and horizontal burrows identified as *Teichichnus* or *Rhizocorallian*. The dominant detrital mineral grains in facies 3 are monocrystalline quartz (mean 27 %), K-feldspar (mean 7 %), and plagioclase (mean 11 %). This facies has localised accumulations of stratigraphically-localized shell fragments and only a small amount of rock fragments.

Detrital clays are present as mm- to cm-sized patches and thin discontinuous layers. Detrital clay is most abundant in the very fine to fine-grained bioturbated facies. Up to 26 % detrital clay is found in the very fine- to fine-grained, highly bioturbated facies and the lowest clay of <1 % are found in the medium-grained graded sandstones devoid of evidence of bioturbation. SEM observations indicate that the detrital clay matrix is dominated by illite and chlorite, confirmed by XRD analyses (trace not illustrated in this paper).

Overall paragenesis

A summary paragenetic sequence is presented in Figure 8, with supporting photomicrographs and SEM images in Figures 9, 10, 11 and 13. The sequence is subdivided into ‘early’ and ‘late’ diagenesis. Early diagenetic events took place in depositional pore waters, at relatively shallow depths, with an influence of depositional and influxing meteoric water (Morad et al., 2010), whereas subsequent diagenesis during burial occurred after the main phase of compaction and is characterised by growth at higher temperatures.

Early diagenesis

Early diagenesis commenced with admixing and infiltration of detrital clay into the newly deposited sediment, largely due to bioturbation. This resulted in patchy distribution of detrital clays and created locally cleaner pathways that potentially promoted later throughput of diagenetic fluids. This was accompanied by initial compactional porosity-loss, mainly through the reorganisation of grains and mechanical compaction into a stable framework. Framboidal pyrite (Fig. 9a) is associated with detrital clay and precipitated in a reducing environment at relatively shallow depth, during the decay of organic fragments by sulphate-reducing bacteria (Burley & Worden, 2003). Some beds are completely cemented with early diagenetic calcite and have negligible porosity. Dissolution of stratigraphically-restricted shelly carbonate fragments, and the growth of locally pervasive minor non-ferroan calcite within primary pores, occurred during early diagenesis. This led to total occlusion of porosity (see later section on wireline log analysis). Some beds are thus completely cemented with early diagenetic calcite and have negligible porosity. These nodular or bedded early calcite-cemented samples have been excluded from further data analysis (i.e. no point count data for samples with pervasive calcite cement included in Appendix 1) since they do not inform the discussion about the effect of oil emplacement on burial diagenesis (quartz cementation).

Bacterial sulphate reduction, responsible for framboidal pyrite growth (Fig. 9a), led to acidification, which resulted in minor dissolution of unstable grains and created minor amounts of secondary porosity (Fig. 9b). These minor, partially-dissolved grains were typically replaced by small quantities of patchy, early diagenetic chlorite

(Fig. 9c). Chlorite predominantly occurs as minor pore-filling rosettes. Volumetrically, pore-filling chlorite is present in small quantities (typically < 1 %). Chlorite appears to be facies-related with the majority occurring in the very fine- to fine-grained, matrix rich, bioturbated facies 3. Grain-coating chlorite is not present in the studied Ula Formation reservoir sandstones.

Microcrystalline quartz locally coats grains (Fig. 9d). By reference to evidence from equivalent Upper Jurassic outcrops at Brora, on the NE coast of Scotland, UK, microcrystalline quartz was probably sourced from the dissolution of unstable siliceous bioclasts (e.g. sponge spicules), at shallow burial depths (< 60 °C) (Vagle et al., 1994).

Further dissolution of feldspar (Fig. 9e) seems to have resulted in the precipitation of a small quantity of early (i.e. pre-compactional) quartz overgrowths, present within quartz-quartz grain contact zones (Figs. 9e-f). Early diagenesis terminated with the end of the main phase of burial-related compaction, which is generally assessed as moderate to strong as evidenced by the prevalence of long and sutured grain contacts.

Late diagenesis

Minor feldspar dissolution continued beyond the main phase of compaction, as indicated by locally significant, but volumetrically-minor, secondary pores that have no evidence of compaction. This phase of grain dissolution liberated Al and Si and potentially contributed to the precipitation of the diagenetically-dominant, post-compactional quartz overgrowths (Table 1) and minor quantities of clay minerals

(Fig. 9e) (Barclay and Worden, 2000b). The switch from feldspar dissolution to feldspar growth (Worden and Rushton, 1992), required a switch from cation-poor and/or low pH to cation rich and/or moderate pH pore-waters (Fig. 9e). This change also led to local growth of minor quantities of dawsonite (sodium aluminum hydroxycarbonate) within primary pores (Worden, 2006). Minor quantities of late illite precipitated, locally coating quartz overgrowths at this late stage (Fig. 9d).

Non ferroan and ferroan dolomite cement are present in the Ula Formation (Ula field), with the most volumetrically-important being rhombic ferroan dolomite (Fig. 10a). The mean point count volume for total dolomite is ~0.7 %, (Table 1). Ferroan and non-ferroan dolomite are only present in very fine to fine bioturbated sandstones with abundant matrix (facies 3; Table 1). The ferroan dolomite replaces and locally crosscuts quartz cement and so formed after quartz cement. Hydrocarbon influx started after the onset of the main phase of quartz cement growth since residual hydrocarbon is present on quartz cement surfaces (Fig. 10b).

Quartz diagenesis

Both grain-coating microcrystalline quartz and quartz overgrowths are present in the Ula Formation. The Ula sandstones have variable amounts of quartz overgrowth cement ranging from high porosity sandstones with relatively small amounts of quartz cement (i.e. a few percent quartz cement) (Figs. 10a, b and c) to pervasively quartz-cemented samples in which the porosity is almost totally occluded (Figs. 10,d, e and f). Quartz overgrowths are not visibly zoned when studied using SEM-CL (Figs. 10e and f). The euhedral edges of quartz overgrowths are locally stained by dead oil or bitumen (Fig. 10b). However, some low porosity sandstones in the finest grained and most clay-rich facies 3 have little quartz cement due to other pore-filling materials such as abundant pore-filling clay and localised Fe-dolomite (Fig. 10a, Table 1). Quartz overgrowths are euhedral when facing open pores (Figs. 10b, c and e). The boundaries between detrital quartz grains and quartz overgrowths are typically characterized by a dust rim composed of fine-grained clay minerals or fluid inclusions (Figs. 10b, c and d). Quartz overgrowths can range in thickness from < 10 µm to > 50 µm. At sites where overgrowths from neighbouring grains interlock, porosity tends to be locally fully occluded. Quartz overgrowths are least abundant in facies type 3 but facies 1 and 2 have highly variable quantities of quartz overgrowths (Table 1).

The quartz cement-poor, medium-grained graded samples from low water saturation samples from 7/12-2 notably have relatively clean, largely unmodified (i.e. as-deposited) detrital quartz grain surfaces (Fig. 11). Such grains are marked by a lack of microquartz cement coatings and no more than nascent, patchy and very thin quartz overgrowths (Figs. 11b and d). These clean quartz grains from the oil leg have subtly uneven surfaces that resemble detrital grains from modern environments.

Quartz cement seems to increase in overall abundance with increasing depth for the medium-grained graded facies 1 (Fig. 12). The same pattern of increasing quartz cement with depth can be discerned for the fine- to medium-grained bioturbated facies 2 but there is no pattern for the relatively quartz cement-poor very fine to fine-grained bioturbated facies 3 (Fig. 12)

Light optics revealed a very fine-grained, colourless mineral coating with low to intermediate birefringence in some samples (Fig. 13a); SEM observation confirmed that this is microcrystalline quartz (Fig. 13b, Table 1). The quantity of microquartz is greatest in the very fine- to fine-grained bioturbated facies 3, with much less in the fine- to medium-grained and bioturbated facies 2 and medium-grained graded facies 1 (Figs. 12 and 14a, Table 1). There is no systematic pattern of microquartz variation with depth of burial (Fig. 12). Some samples have unusually large amounts of microquartz, others have low to negligible amounts. The microquartz crystals tend to be < 5 µm in size and vary in shape from anhedral (typically rounded) to euhedral. Microquartz tends to sit on detrital grain surfaces but locally forms thick irregular coatings that extend into neighbouring pores and pore-filling patches. Microcrystalline quartz cement appears to be dominant only in facies 3 (very fine to fine bioturbated sandstone with abundant matrix) but it is typically present in small amounts in the coarser facies although one or two samples from the medium-grained graded facies 1 and fine- to medium-grained bioturbated facies 2 contain several percent microquartz. Facies 3 samples tend to have commensurately smaller amounts of quartz cement than the microquartz-poor medium-grained graded facies 1 and fine- to medium-grained bioturbated facies 2 (Table 1; Fig. 14a). As well as point counting microquartz, the percentage of detrital quartz grains that are coated with microcrystalline quartz was determined by visually estimating 50 grains per section for a subset of the samples (Fig. 14b). Medium-grained graded facies 1 sandstones have grains that are, on average, about 10 to 20% coated with microquartz and have low overall point counted quantities of microquartz (Figs. 14a and b). Very fine- to fine-grained bioturbated facies 3 sandstones contain some grains that are approaching 100% grain coating with microquartz. Fine- to medium-grained bioturbated facies 2 sandstones tend to have intermediate degrees of grain coating by microquartz (Fig. 14b).

Fluid inclusion Analysis

Samples for fluid inclusion study were selected from both oil and water legs. Homogenization temperatures were measured for aqueous inclusions and petroleum inclusions in 12 samples in wells 7/12-2, 7/12-A3, 7/12-5, 7/12-A08, and 7/12-A13 of the Ula Formation. Primary fluid inclusions that fluoresced under UV illumination are present in quartz overgrowths (Fig. 15) showing that some oil was present during the growth of quartz. Non-fluorescent primary aqueous fluid inclusions are also present in quartz overgrowths. Petroleum inclusions are generally larger in size (Fig. 15a-d) and have a higher vapour-liquid ratio than aqueous inclusions and were therefore easier to work with. Aqueous inclusions range in diameter from 1 to 17 µm. Petroleum inclusions range in diameter from 7 to 38 µm. The liquid to vapor ratio for aqueous fluid inclusion was consistently about 8:1 and for petroleum inclusion was about 5:1. All the homogenisation temperatures recorded here are from inclusions within quartz overgrowths or located between detrital quartz grains and their quartz overgrowths. Only homogenization temperatures that were reproducible within (<5 ºC) were recorded. All inclusions homogenised to liquid upon heating. Aqueous inclusion populations tend to be unimodal between 120 and 174 ºC with the lowest recorded aqueous inclusion homogenization temperature being 103 °C. Petroleum inclusions homogenized between about 80 and 142 ºC. Pressure corrections were not made to the aqueous inclusion homogenisation temperatures because the formation water was probably saturated with methane at the time of trapping (Hanor, 1980), implying that the measured homogenisation temperatures are representative of the actual trapping temperature for the aqueous inclusions. Homogenisation temperatures of inclusions trapped in quartz are not likely to have been re-equilibrated and so represent the true trapping temperature (Worden et al., 1995). The oil inclusions cannot easily be used to reveal the conditions of trapping since the precise PVT properties of the trapped petroleum are not known.

Histograms of homogenization temperatures four representative samples are given in Figure 16 and summarized in Table 2. The present-day formation temperature for well 7/12-A3 is 154°C (determined from drill stem testing) which compares favorably with the homogenisation temperatures (Fig. 16) although the modal fluid inclusion homogenization temperature is lower than the present day temperature.

Discussion

Quartz cementation in the presence of oil

The presence of primary oil inclusions in quartz cement indicates that some oil was present in the reservoir when this authigenic mineral was being precipitated. The very lowest homogenisation temperatures for the aqueous inclusions is 103°C, although a more typical minimum homogenisation temperatures for the aqueous inclusions is 120°C (Fig. 16) which is somewhat higher than the threshold of 80°C widely assumed to be the temperature above which quartz cement grows (Walderhaug, 1996). The oil saturation at the time of the growth of quartz cement, and thus inclusion trapping, is not known although it is noteworthy that the fluid inclusion sample with highest oil saturation at the present day (7/12-2, 3403.00m) has the lowest percentage of quartz cement (Table 2) and was visually estimated to have a relatively great abundance of petroleum inclusions (Fig. 15). Having some oil in the pore network clearly does not automatically preclude quartz cementation.

Quartz cement modeling in the presence of oil

Simple modeling approaches have been developed to try to link quartz cement abundance with burial and thermal histories (Bjørkum et al., 1998; Lander and Walderhaug, 1999; Walderhaug, 1990, 1994a, b, 1996; Walderhaug et al., 2000). These models were calibrated by examining quartz cement quantities in different sandstones from one basin (Norwegian North Sea) and relating these quantities to the burial history of each sandstone reservoir in the calibration dataset. All of these models assumed that quartz cement is internally-derived and that the main control is the rate of quartz precipitation. The timing of quartz cementation in each well was derived by using aqueous fluid inclusion temperatures from the sandstones in the calibration dataset and the assumption that quartz cementation was continuous from the lowest recorded aqueous inclusion homogenization temperature onwards (despite there being punctuated fluid inclusion records reported) (Walderhaug, 1994a). Geometric characteristics were accounted for by examining grain size (and relating this to available surface area) and the fraction of grains that are quartz (as opposed to feldspars, lithics, etc.). The published models were thus calibrated using a number of basic assumptions. Interestingly, the models were also calibrated utilising the fundamental assumption that emplacement of oil did not inhibit quartz cementation. Since the published models (Walderhaug, 1990, 1994a, b, 1996; Walderhaug et al., 2000) involved the assumption that oil had no effect on quartz cement growth. These models therefore seem to be fundamentally unsuitable for attempting to model any effect of oil emplacement on quartz cementation. However, for medium-grained graded facies 1 and fine- to medium-grained bioturbated facies 2 in the oil leg of Ula oil field, the relative quantity of quartz cement and the elevated porosity look anomalous compared to the quantities found in the water leg (Table 1, Fig. 12). There are a finite number of controls on anomalously high porosity-low quartz cemented sandstones (Bloch et al., 2002); these possible controls will now be examined.

Main controls on porosity-loss above and below the oil-water contact

A comparison of the effects of cementation and compaction using a plot of pore-filling cement versus intergranular volume (also known as a Houseknecht-type plot) (Fig. 17) shows that there is a difference in what process has controlled porosity-loss as a function of position in the oil field. On average, the oil leg samples occupy a central position in the diagram showing a combination of compaction and cementation leading to the final porosity. In contrast the water leg samples sit mainly within the cementation field. The main cement is quartz so that it could be concluded that quartz cement dominates in the high water saturation zone while there has been less cement in the high oil saturation zones (Fig. 17). In contrast, it could also be concluded that compaction has been relatively more important than cementation in the oil leg compared to the water leg so that there is a need to compare cement volumes for initially similar samples (same facies) between the oil and water legs.

Grain size, detrital clay and grain-coating microcrystalline quartz and quartz cementation

Grain size is broadly uniform within each facies so that this cannot be invoked as the primary cause of variable amounts of quartz cement in the various facies (Table 1, Appendix 1). Similarly, both fine- to medium-grained bioturbated and medium-grained graded sandstone samples each have approximately consistent quantities of detrital matrix clay, so this, too, can be excluded as a control on quartz cement within each facies (Fig. 12; Table 1). It is noteworthy that very fine to fine bioturbated facies 3 has a far higher quantity of matrix clay than medium and coarse facies 1 and 2. However, for the water leg samples from the three facies, there is a well-developed, inverse correlation between the amount of detrital clay and the amount of quartz cement (Table 1). This suggests that the more argillaceous-rich, finer-grained, heavily bioturbated samples have experienced inhibition of quartz cement compared to the cleaner medium- and coarse-grained sandstones. Ferroan dolomite is not a major mineral cement but it too correlates with primary facies and detrital clay content possibly (Table 1).

Microquartz is an abundant, and pervasively grain-coating, cement found on detrital quartz grains in the very fine- to fine-grained bioturbated facies 3 (Fig. 14). Quartz cementation appears to have been inhibited by microquartz coats irrespective of pore fluid type (Fig. 12; Table 1). This effect has been reported previously (Aase et al., 1996; French and Worden, 2013; French et al., 2010; French et al., 2012; Hendry and Trewin, 1995; Ramm et al., 1997; Weibel et al., 2010; Worden et al., 2012). It is significant that a small subset of fine- to medium-grained bioturbated facies 2 samples contain measurable microquartz (Fig. 14a). These samples have commensurately reduced amounts of quartz cement and elevated porosity. For example, samples of fine- to medium-grained bioturbated facies 2 in well 7/12-3A at 3,559-3,566 m (11,677-11,699 ft) TVDss contain a few percent microquartz (Fig. 12) and have anomalously elevated porosity as a consequence of the inhibition of quartz cement (Figs. 5 and 12).

When grain-coating microquartz percentage, and percentage of surface area of grain-coating by microquartz, are plotted against quartz cement (Fig. 14a), it is apparent that samples from medium-grained graded facies 1 (and fine- to medium-grained bioturbated facies 2) show a large range of quartz cement volumes irrespective of the amount of microquartz. Although microquartz exerts a control on the development of quartz overgrowths, it is not particularly abundant in medium-grained graded facies 1 or fine- to medium-grained bioturbated facies 2 and it cannot explain the full range of abundance of quartz cement. This suggests that there is an additional control, other than microquartz, that has determined the amount of quartz cement in facies 1 and 2.

Since grain-coating microquartz is only observed in large amounts in very fine- to fine-grained bioturbated facies 3, it seems likely that this is the only facies in which there was an abundant potential source for the microquartz. Microquartz in Upper Jurassic sandstones from the North Sea is typically attributed to detrital sponge spicules (Aase et al., 1996; Vagle et al., 1994). Based on the literature-based interpretation that the microquartz was sourced from replaced sponge spicule fragments, it can thus be inferred that detrital fragments of sponge spicules were preferentially concentrated in the finest-grained sand fraction. We here speculate that the grading of the silica bioclasts into the finest sand fraction may be a consequence of their fragility and consequent attritional diminution during transport from their original location on the marine shelf. While these silica bioclasts have successfully led to the inhibition of quartz cement (good for reservoir quality), they are found in the finest sandstones (facies 3) that also contain abundant matrix clay so that the reservoir quality has been detrimentally controlled by other factors.

Quantity of quartz cement above and below the oil-water contact for rocks of the same pre-oil filling characteristics?

The characteristics of the three different primary facies above and below the oil-water contact (and in the transition zone) are summarized in Table 1. The three facies have been defined by grain size, matrix clay content and sedimentary structures (including grading and degree of bioturbation) and so have self-consistent grain size and sorting characteristics and detrital mineralogy (Fig. 7). They also have consistent quantities of detrital clay and grain-coating microcrystalline quartz (Table 1). Samples that have been fully cemented with early diagenetic calcite, i.e. with all pore space filled very soon after deposition, have been removed from the analysis since they cannot record the effects of oil emplacement of burial diagenetic processes. The amounts of ferroan dolomite observed in pores are approximately consistent for the different facies (Table 1). The quantity of petrographically-defined quartz cement has been plotted against specific water saturation for each sample, derived using log data with the data split by the petrographically-defined microquartz content (Fig. 18). This approach shows that low water saturations (and therefore high oil saturations) equate to less quartz cement in medium-grained graded facies 1 (Fig. 18a) and fine- to medium-grained bioturbated facies 2 (Fig. 18b), relative to samples of these same facies from the water leg. There does not appear to be a simple relationship between water saturation and quartz cement content for very fine to fine bioturbated facies 3 (Fig. 18c) although large quantities of microquartz in this facies equate to negligible amounts of quartz cement in all cases. The lack of correlation of water saturation with quartz cement for the very fine to fine bioturbated facies may be a result of: (1) the large quantity of pre-existing detrital clay that left less room for quartz cement to grow (Fig. 12; Table 1), or (2) the great abundance of grain-coating microquartz that prevented quartz cement precipitating (Figs. 12, 14, 18c; Table 1).

Focusing on the medium-grained graded facies 1 sandstones that have less than 20% grain coating, it is possible to discern a good correlation between water saturation and quartz cement content (Fig. 19a). There are good inverse relationships between water saturation and core analysis porosity and permeability (Figs. 19b-c). There is also a good inverse relationship between quartz cement and core analysis porosity (Fig. 19d) confirming that quartz cement is the master control on reservoir quality.

The conclusion from the data detailed in Table 1 and Figures 18 and 19 is that for medium-grained graded facies 1 sandstones, that have virtually identical and small amounts of detrital clay, ferroan dolomite, and grain-coating microquartz, samples from the oil leg appear to have less quartz cement, higher porosity and higher permeability than samples from the water leg. The same is broadly true for fine- to medium-grained bioturbated facies 2 sandstones (Table 1) but very fine to fine bioturbated facies 3 samples tend to have a relatively small quantity of quartz cement irrespective of oil saturation. Facies 3 sandstones have smaller quantities of quartz cement than facies 1 and 2 due to the combined effects of grain coating microquartz

(Fig. 14) and relatively minor extra amounts of ferroan dolomite and abundant matrix clay (Table 1).

The assessment of the effects of compaction versus cementation (Fig. 17) shows that water leg samples tend to be more cementation-dominated than oil leg samples. For samples of the same facies, with the same microquartz content, this difference is the result of there being more quartz cement in the water leg than the oil leg (Fig. 18a). We can thus surmise that the growth of quartz cement in the oil leg has been inhibited relative to growth in the water leg.

Synthesis: has oil slowed quartz cementation and therefore caused preservation of porosity?

The key question addressed by this study is whether emplacement of oil during diagenesis led to inhibition of quartz cementation in the Ula Formation in Ula Field. Samples from the oil leg have higher porosities and less quartz cement than comparable samples from the water leg for facies 1 and facies 2 (Table 1, Fig. 18). This difference cannot be explained by demonstrable variances in abundance of microcrystalline quartz coatings (Figs. 12 and 14), grain size, grain-coating chlorite or the presence of other subordinate pore-filling cements (Table 1). We therefore propose that the differences in porosity and quartz cement abundance as a function of oil saturation may be directly attributed to differences in the dominant fluid type within the pore space of these samples.

In essence, the rate of quartz cement growth will be limited to the slowest step in the sequence of steps: supply, transport and precipitation. Having oil present in the pore space during quartz cementation (as shown by oil inclusions in quartz cement; Figs. 15, 16) may have caused the rate of quartz *precipitation* to slow significantly relative to similar samples with high water saturation and therefore led to less quartz cement being precipitated. However, the recorded reduced abundance of quartz cement in the oil leg samples (in medium-grained graded facies 1 and fine- to medium-grained bioturbated 2) could also be the result of reduced rates of silica *supply* in the oil leg (presumably from internal, stylolite-related sources). Alternatively, there may have been reduced rates of silica *transport* in the presence of oil due either to slowed advection (resulting from relative permeability effects) or slowed diffusion (resulting from tortuosity effects) (Worden et al., 1998). The lack of correlation between IGV and quartz cement content (Table 1, Appendix 1) could be used to infer that pressure solution (chemical compaction) has not been affected by the emplacement of oil if we assume that quartz cement was only supplied by local, intra-facies pressure solution. However we cannot be sure that quartz cement in facies 1 and 2 sandstones has not been supplied by feldspar-clay reactions (Barclay and Worden, 2000b), pressure solution in surrounding mudstones (Land and Millken, 2000) or clay-rich sandstones (Trewin and Fallick, 2000), export of biogenic silica from finer sandstone facies (e.g. facies 3) (Worden and Morad, 2000) or even mass flux from deeper in the basin (Giles et al., 2000). Although we cannot be sure which of supply, transport and precipitation rate has been slowed by the presence of oil we can state that the overall process of quartz cementation has been significantly slowed in cleaner, less fine-grained, minimally microquartz-coated sandstones, by the presence of oil in the pore network.

Conclusion

1. Oil was present during quartz cementation in the Ula Formation in Ula Field as revealed by the presence of oil inclusions suggesting oil ingress into the reservoir began when the reservoir was at a temperature of about 100-120°C.
2. Aqueous fluid inclusion homogenisation temperature data from primary inclusions in quartz cement shows that quartz cementation seems to have started at an absolute minimum of 103°C with most quartz cement growing at >120°C, if assume that the lower homogenisation temperatures for aqueous inclusions in quartz are regarded as being representative of minimum growth temperature.
3. For sandstones of the same depositional facies, with similar grain size, similar detrital clay content, similar low quantity of grain coating microquartz and similar low quantity of ferroan dolomite, there is less quartz cement in the oil leg than in the water leg, particularly for facies 1 (medium-grained graded sandstone) and facies 2 (fine- to medium-grained bioturbated sandstone).
4. For facies 3 (fine- to very fine-grained bioturbated sandstone) there appears to be little quartz cement, regardless of whether oil was present during diagenesis or not. This can be attributed to the (relatively) large quantity of grain-coating microquartz and detrital clay associated with this facies.

5. A small number of the coarse-grained sandstone samples in the water leg also have a few percent grain-coating microquartz. These have unusually reduced quantities of quartz cement showing that microquartz, as well as oil emplacement, can inhibit quartz cementation.
6. Emplacement of oil before, or during, quartz cementation has inhibited the growth of quartz cement in the Ula Formation in the cleaner, fine- to medium-grained and medium-grained graded, minimally microquartz cemented sandstones.

FIGURE CAPTIONS

Figure 1. Location map of the Central Graben showing Ula Field with insert map of the North Sea region (lower left). The map shows the study area in the black square and inserted field structural map right showing major bounding faults structures and well locations (modified from Nedkvitne et al., 1993).

Figure 2. Generalized stratigraphy of Ula Field. The Mandal Formation is the main regional source rock; the Ula Formation is the reservoir under consideration.

Figure 3. Thermal curves for Ula Field from well 7/12-6 (Fig. 1), the heavier black line represents the top of the Ula reservoir interval. The combined burial and thermal history was modelled using BasinMod software.

Figure 4. Comparison of core analysis porosity and wireline-derived porosity for well 7/12-A13.

Figure 5. Plots of density-derived porosity and Archie-derived water saturation (S_w) from four of the five Ula field wells used in this study.

Figure 6. Plots of core analysis porosity and permeability subdivided by wireline derived water saturations for the three facies; (a) Medium-grained graded sandstone facies, (b) Fine- to medium-grained bioturbated sandstone facies, (c) Very fine- to fine-grained bioturbated sandstone facies.

Figure 7. Ternary diagram showing the Ula Formation sandstone classification (McBride, 1963).

Figure 8. Generalised paragenetic sequence for the Ula Sandstone in Ula Field (7/12-2, 7/12-A3, 7/12-5, 7/12-A08 and 7/12-A13). Age ranges of diagenetic phases are estimated based on thin section and SEM observations.

Figure 9 a) SEM image showing framboidal pyrite (py) and microcrystalline quartz (μqz) formed early within intergranular area (7/12-A3, 3520.36 m TVD, Sw 0.61) b) SEM image showing partial dissolution of detrital K-feldspar grain (KF) and later authigenic quartz within the secondary intragranular pore (sip) (Well 7/12-5, 3894.00 mDD, Sw 0.78). (c) quartz overgrowth (qzo) encloses pore-filling chlorite (ch) shown by circle (Well 7/12-5, 3894.00 mDD, Sw 0.78) suggesting quartz precipitation after chlorite. (d) late hairy illite (i) draped quartz overgrowths (7/12-A3 , 3520.36 m TVD, Sw 0.61). (e) Optical thin section photomicrograph (plane polarised) showing feldspar overgrowths (kfo) and quartz overgrowths both of which thin at grain contacts (circled) suggesting precipitation after main phase of compaction (7/12-A3, 3515.76 m TVD, Sw 0.35). (f) residual hydrocarbons (rh) which stain earlier quartz overgrowths (7/12-2, 3407.93 m TVD, Sw 0.06).

Figure 10 (a) Thin section photomicrograph (plane polarised light) showing patchy clay minerals (PC) and dolomite cement (dol) (7/12-2, 3389.92 m TVD, Sw 0.05). (b) Thin section image (plane polarised) showing quartz overgrowths which partially fills primary intergranular pore (PP) and stained by residual hydrocarbons (rh) (7/12-2, 3427.67 m TVD, Sw 0.13). (c) Thin section photomicrograph (plane polarised light) showing clean primary porosity (PP) medium to high volume of quartz overgrowths (qzo) and uncoated quartz grain (Q) (7/12-A13, 3706.32 m TVD, Sw 0.62). (d) Thin section photomicrograph (plane polarised light) showing quartz overgrowths (qzo) occluding primary pores around quartz grain 7/12-A3, 3525.35 m

TVD, SW 0.31). (e and f) Backscattered electron image and cathodoluminescence image of the same sample differentiating between detrital quartz (Q) and quartz overgrowths (qzo) in the later. Note that it much easier to observe quartz cement-grain boundaries using light optical images than backscattered electron images. (7/12-A3, 3525.35 m TVD, SW 0.31).

Figure: 11. SEM micrographs of minimally quartz cemented samples of medium-grained graded facies 1 from the oil leg revealing the lack of microquartz or any other sort of grain coating material. The exposed quartz grain surfaces contain nascent quartz cement but are largely in their original, depositional, state. qzo: quartz overgrowth, cs: clean grain surface free of microquartz but also with no quartz cement growing. (a and inset b) 7/12-2, 3389.92 m TVD; Sw 0.05. (c and inset d) 7/12-2 3384.98 m TVD depth; Sw 0.05.

Figure: 12. Variation of log-derived water saturation, core analysis porosity, quartz cement, microquartz and detrital clay with true vertical depth for all the wells studied. Samples have been split into the three main facies. The diagram represents the aggregation of data from four wells; the data are in depth order and do not represent the stratigraphic succession.

Figure 13. (a) Thin section image of microquartz-coated sandstone (7/12-2; 3365.40; m TVD; Sw 0.19). (b) SEM image showing grain-coating microcrystalline quartz (µqz) and mesoquartz (mqz) crystals (7/12-A3; 3534.87 m TVD; Sw 0.55).

Figure14. Point-counted quartz cement plotted against: (a) point-counted microquartz cement for all samples, and (b) for a subset of the samples, the percentage of grains coated with microquartz. Samples with abundant microquartz (and grain coating) have little quartz cement suggesting that microquartz has effectively inhibited quartz

overgrowths. However, there are many samples with little microquartz (and grain coating) that also have little low quantities of quartz overgrowths suggesting that there is another factor that has significantly affected the growth of quartz cement.

Figure 15. Thin section photomicrograph showing fluid inclusions; see Table 2 for details of samples in the images. (a) Plane polar showing fluid inclusion assemblage in quartz cement. (b) Plane polar photomicrograph showing fluid inclusion rim at the boundary between detrital quartz grain and quartz cement samples from water zone well 7/12-A3. (c and d) petroleum inclusion under fluorescence light samples from oil leg of 7/12-2.

Figure 16. Homogenization temperature measurements for aqueous and petroleum inclusions in selected samples of the Ula Formation. Note present-day reservoir temperature is only available for well 7/12-A3

Figure 17. Diagram, based on petrographic data, illustrating styles of porosity loss in the Ula Formation (after Houseknecht, 1984). The oil leg samples ($Sw < 0.5$) have relatively more porosity lost to compaction than cementation. In contrast, the water leg samples ($Sw > 0.5$) have more porosity lost to cementation than compaction. This diagram suggests that, on average, the water leg is more cemented than the oil leg.

Figure 18. Point-counted quartz cement volume versus wireline-derived water saturation; (a) medium-grained graded sandstone facies 1 (b) fine- to medium-grained bioturbated sandstone facies 2 (c) very fine- to fine-bioturbated facies 3. This diagram shows that the fine- to medium-grained bioturbated and medium-grained graded facies have less quartz cement in samples with low water saturation than those with higher water saturation. This suggests that oil emplacement has inhibited

the growth of quartz cement. Note that microquartz coatings also play a role in diminishing the amount of amount of quartz cement.

Figure 19. Wireline-derived water saturation values for medium-grained graded sandstone facies 1 samples, that have less than 20% grain coating, compared to quartz cement and core analysis data. (a) Water saturation compared to quartz cement showing that these sandstones have decreasing quartz cement in samples with decreasing water saturations. Sandstones with water saturations less than 0.5 have less than 5% quartz cement; those with water saturations greater than 0.5 have up to 15% quartz cement. There is a good correlation between water saturation and quartz cement; this relationship could be used to predict quartz cement as a function of water saturation. (b) Water saturation compared to core analysis porosity showing that these sandstones have increasing porosity with decreasing water saturation. (c) Water saturation compared to core analysis permeability showing that these sandstones have increasing permeability with decreasing water saturation. (d) Quartz cement compared to core analysis porosity showing that less quartz cement equates to higher porosity.

TABLE CAPTIONS

Table 1. Average values of core analysis horizontal permeability porosity, and point count quartz cement, detrital clay, microquartz and ferroan dolomite volumes for the different facies, subdivided by high and low water saturation. A full listing of all petrographic and related data is available in Appendix 1.

Table 2. The properties of fluid inclusion samples in different wells of Ula Field.

References

Aase, N. E., P. A. Bjorkum, and P. H. Nadeau, 1996, The effect of grain-coating microquartz on preservation of reservoir porosity: American Association of Petroleum Geologists Bulletin, v. 80, p. 1654-1673.

Aase, N. E., and A. Walderhaug, 2005, The effect of hydrocarbons on quartz cementation: diagenesis in the Upper Jurassic sandstones of the Miller Field, North Sea, revisited: Petroleum Geoscience, v. 11, p. 215-223.

Asquith, G. B., and C. R. Gibson, 1982, Basic well log analysis for geologists: American Association of Petroleum Geologists, Methods in Exploration, p. 216.

Baniak, G. M., M. K. Gingras, B. A. Burns, and S. G. Pemberton, 2014, An example of a highly bioturbated, storm- influenced shoreface deposit: Upper Jurassic Ula Formation, Norwegian North Sea: Sedimentology, v. 61, p. 1261-1285.

Baniak, G. M., M. K. Gingras, B. A. Burns, and S. G. Pemberton, 2015, Petrophysical characterization of bioturbated sandstone reservoir facies in the Upper Jurassic Ula Formation, Norwegian North Sea, Europe: Journal of Sedimentary Research, v. 85, p. 62-81.

Barclay, S. A., and R. H. Worden, 2000a, Effects of reservoir wettability on quartz cementation in oil fields, *in* R. H. Worden, and S. Morad, eds., Quartz cementation in sandstones, v. 29, Special Publication of the International Association of Sedimentologists, p. 103-117.

Barclay, S. A., and R. H. Worden, 2000b, Geochemical modelling of diagenetic reactions in a sub-arkosic sandstone: Clay Minerals, v. 35, p. 57-67.

Bergan, M., B. Tørudbakken, and B. Wandås, 1989, Lithostratigraphic correlation of Upper Jurassic sandstones within the Norwegian Central Graben: sedimentological and tectonic implications, *in* J. D. Collinson, ed., Correlation in hydrocarbon exploration, Norwegian Petroleum Society, Graham and Trotman, London, p. 243-251.

Bjørkum, P. A., and P. H. Nadeau, 1998, Temperature controlled porosity/permeability reduction, fluid migration, and petroleum exploration in sedimentary basins: Australian Petroleum Production and Exploration Association Journal, v. 38, p. 453-464.

Bjørkum, P. A., E. H. Oelkers, P. H. Nadeau, O. Walderhaug, and W. M. Murphy, 1998, Porosity prediction in quartzose sandstones as a function of time, temperature, depth, stylolite frequency, and hydrocarbon saturation: American Association of Petroleum Geologists Bulletin, v. 82, p. 637-648.

Bjørnseth, H. M., and J. Gluyas, 1995, Petroleum exploration in the Ula Trend: Norwegian Petroleum Society Special Publications, v. 4, p. 85-96.

Bloch, S., R. H. Lander, and L. Bonnell, 2002, Anomalously high porosity and permeability in deeply buried sandstone reservoirs: Origin and predictability: American Association of Petroleum Geologists Bulletin, v. 86, p. 301-328.

Brown, A., A. W. Mitchell, I. R. Nilssen, I. J. Stewart, and P. T. Svela, 1992, Ula field: relationship between structure and hydrocarbon distribution: Structural and tectonic modelling and its application to petroleum geology: Norwegian Petroleum Society Special Publication, v. 1, p. 409-420.

Dixon, S. A., D. M. Summers, and R. C. Surdam, 1989, Diagenesis and preservation of porosity in Norphlet Formation (Upper Jurassic), southern Alabama: Americam Association of Petroleum Geologists Bulletin, v. 73, p. 707-728.

Ehrenberg, S. N., 1990, Relationship between diagenesis and reservoir quality in sandstones of the Garn Formation, Haltenbanken, mid-Norwegian continental shelf: American Association of Petroleum Geologists Bulletin, v. 74, p. 1538-1558.

Ehrenberg, S. N., 1993, Preservation of anomalously high porosity in deeply buried sandstones by grain-coating chlorite: examples from the Norwegian continental shelf: American Association of Petroleum Geologists Bulletin, v. 77, p. 1260-1260.

Emery, D., P. C. Smalley, N. H. Oxtoby, K. V. Ragnarsdottir, P. Aagaard, A. Halliday, M. L. Coleman, and R. Petrovich, 1993, Synchronous oil migration and cementation in sandstone reservoirs demonstrated by quantitative description of diagenesis [and discussion]: Philosophical Transactions of the Royal Society of London. Series A: Physical and Engineering Sciences, v. 344, p. 115-125.

England, G. L., R. S. Haszeldine, J. Cleverley, S. A. Barclay, B. W. D. Yardley, Q. J. Fisher, C. Graham, and A. Fallick, 2003, Applying Ion-Microprobe Technology in Reconstructing Quartz Cement History in an Upper Jurassic Sandstone Reservoir of the Outer Moray Firth Basin, North Sea, United Kingdom: American Association of Petroleum Geologists Annual meeting, South Lake Tulsa, Oklahoma.

French, M. W., and R. H. Worden, 2013, Orientation of microcrystalline quartz in the Fontainebleau Formation, Paris Basin and why it preserves porosity: Sedimentary Geology, v. 284, p. 149-158.

French, M. W., R. H. Worden, E. Mariani, W. C. Horn, C. E. Kliewer, W. A. Lamberti, R. R. Mueller, and C. Fischer, 2010, Low temperature porosity preserving microquartz from Upper Cretaceous sandstones of the Subhercynian Basin (Germany): Geochimica et Cosmochimica Acta, v. 74, p. A305-A305.

French, M. W., R. H. Worden, E. Mariani, R. E. Larese, R. R. Mueller, and C. E. Kliewer, 2012, Microcrystalline quartz generation and the preservation of porosity in sandstones: evidence from the Upper Cretaceous of the Sub-Hercynian Basin, Germany: Journal of Sedimentary Research, v. 82, p. 422-434.

Giles, M. R., S. L. Indrelid, G. V. Beynon, and J. Amthor, 2000, The origin of large-scale quartz cementation: evidence from large data sets and coupled heat-fluid mass transport modelling, *in* R. H. Worden, and S. Morad, eds., Quartz cement in sandstones, v. 29: Oxford, Blackwells, p. 21-38.

Gluyas, J., and C. A. Cade, 1997, Prediction of porosity in compacted sands: In: Reservoir quality prediction in sandstones and carbonates (eds. Kupecz, J.A., Gluyas, J. and Bloch, S.) AAPG Memoir, v. 69, p. 19-28.

Gluyas, J. G., ed., 1997, Poroperm predictions for reserves growth exploration: Ula trend Norwegian North Sea: Reservoir quality pr, v. 69: edictions in sandstones and carbonates, American Association of Petroleum Geologist Memoir, 201-210 p.

Gluyas, J. G., A. G. Robinson, D. Emery, S. M. Grant, and N. H. Oxtoby, eds., 1993, The link between petroleum emplacement and sandstone cementation: Petroleum Geology of the North west Europe, Geological Society of London, v. 4, 1395-1402 p.

Hanor, J. S., 1980, Dissolved methane in sedimentary brines; potential effect on the PVT properties of fluid inclusions: Economic Geology, v. 75, p. 603-609.

Harris, N. B., 2006, Low-porosity haloes at stylolites in the feldspathic Upper Jurassic Ula sandstone, Norwegian North Sea: An integrated petrographic and chemical mass-balance approach: Journal of Sedimentary Research, v. 76, p. 444-459.

Haszeldine, R. S., A. J. Cavanagh, and G. L. England, 2003, Effects of oil charge on illite dates and stopping quartz cement: calibration of basin models: Journal of Geochemical Exploration, v. 78-9, p. 373-376.

Hawkins, P. J., 1978, Relationship between diagenesis, porosity reduction, and oil emplacement in late Carboniferous sandstone reservoirs, Bothamsall Oilfield, E Midlands: Journal of the Geological Society, v. 135, p. 7-24.

Hendry, J. P., and N. H. Trewin, 1995, Authigenic quartz microfabrics in Cretaceous turbidites - evidence for silica transfer processes in sandstones: Journal of

Sedimentary Research Section a-Sedimentary Petrology and Processes, v. 65, p. 380-392.
Higgs, K. E., H. Zwingmann, A. G. Reyes, and R. H. Funnell, 2007, Diagenesis, porosity evolution, and petroleum emplacement in tight gas reservoirs, Taranaki Basin, New Zealand: Journal of Sedimentary Research, v. 77, p. 1003-1025.
Home, P. C., ed., 1987, Ula: Geology of the Norwegian oil and gas fields: London, Graham and Trotman, 143-151 p.
Karlsen, D. A., T. Nedkvitne, S. R. Larter, and K. Bjørlykke, 1993, Hydrocarbon composition of authigenic inclusions: application to elucidation of petroleum reservoir filling history: Geochimica et Cosmochimica Acta, v. 57, p. 3641-3659.
Land, L. S., and K. L. Millken, 2000, Regional loss of SiO_2 and $CaCO_3$ and gain of K_2O during burial diagenesis of Gulf Coast mudrocks, USA, *in* R. H. Worden, and S. Morad, eds., Quartz cementation in sandstones, v. 29: Oxford, nternational Association of Sedimentologists Special Publications, p. 183-197.
Lander, R. H., and O. Walderhaug, 1999, Predicting porosity through simulating sandstone compaction and quartz cementation: American Association of Petroleum Geologists Bulletin, v. 83, p. 433-449.
Lowry, W. D., 1956, Factors in loss of porosity by quartzose sandstones of Virginia: American Association of Petroleum Geologists Bulletin, v. 40, p. 489-500.
Marchand, A. M. E., R. S. Haszeldine, C. I. Macaulay, R. Swennen, and A. E. Fallick, 2000, Quartz cementation inhibited by crestal oil charge: Miller deep water sandstone, UK North Sea: Clay Minerals, v. 35, p. 201-210.
Marchand, A. M. E., R. S. Haszeldine, P. C. Smalley, C. I. Macaulay, and A. E. Fallick, 2001, Evidence for reduced quartz-cementation rates in oil-filled sandstones: Geology, v. 29, p. 915-918.
Marchand, A. M. E., P. C. Smalley, R. S. Haszeldine, and A. E. Fallick, 2002, Note on the importance of hydrocarbon fill for reservoir quality prediction in sandstones: American Association of Petroleum Geologists Bulletin, v. 86, p. 1561-1571.
McBride, E. F., 1963, A classification of common sandstones: Journal of Sedimentary Petrology, v. 33, p. 664-669.
Midtbø, R. E. A., J. M. Rykkje, and M. Ramm, 2000, Deep burial diagenesis and reservoir quality along the eastern flank of the Viking Graben. Evidence for illitization and quartz cementation after hydrocarbon emplacement: Clay Minerals, v. 35, p. 227-237.
Molenaar, N., J. Cyziene, S. Sliaupa, and J. Craven, 2008, Lack of inhibiting effect of oil emplacement on quartz cementation: Evidence from Cambrian reservoir sandstones, Paleozoic Baltic Basin: Geological Society of America Bulletin, v. 120, p. 1280-1295.
Morad, S., K. Al-Ramadan, J. M. Ketzer, and L. F. De Ros, 2010, The impact of diagenesis on the heterogeneity of sandstone reservoirs: A review of the role of depositional facies and sequence stratigraphy: American Association of Petroleum Geologists Bulletin, v. 94, p. 1267-1309.
Nedkvitne, T., D. A. Karlsen, K. Bjorlykke, and S. R. Larter, 1993, Relationship between reservoir diagenetic evolution and petroleum emplacement in the Ula field, North Sea: Marine and Petroleum Geology, v. 10, p. 255-270.
O'Connor, S., H. Rasmussen, R. Swarbrick, and J. Wood, 2011, Integrating a hydrodynamically-titled OWC and a salt-withdrawal depositional model to explore the Ula Trend: Geofluids, v. 11, p. 388-400.
Oxtoby, N. H., ed., 1994, The Ula field: North Sea Formation waters: London, The Geological Society London. Memoir No. 15, 74 p.

Partington, M. A., B. C. Mitchener, N. J. Milton, and A. J. Fraser, 1993, Genetic sequence stratigraphy for the North Sea Late Jurassic and Early Cretaceous: distribution and prediction of Kimmeridgian–Late Ryazanian reservoirs in the North Sea and adjacent areas, v. 4, p. 347-370.

Ramm, M., and K. Bjorlykke, 1994, Porosity depth trends in reservoir sandstones - assessing the quantitative effects of varying pore-pressure, temperature history and mineralogy, Norwegian shelf data: Clay Minerals, v. 29, p. 475-490.

Ramm, M., A. W. Forsberg, and J. Jahren, 1997, Porosity-depth trends in deeply buried Upper Jurassic Reservoirs in the Norwegian Central Graben: an example of porosity preservation beneath the normal economic basement by grain coating microquartz: In: Reservoir quality prediction in sandstones and carbonates (eds. Kupecz, J.A., Gluyas, J. and Bloch, S.) AAPG Memoir, v. 69, p. 177-200.

Robinson, A., and J. Gluyas, 1992, Duration of quartz cementation in sandstones, North Sea and Haltenbanken Basins: Marine and Petroleum Geology, v. 9, p. 324-327.

Saigal, G. C., K. Bjorlykke, and S. Larter, 1992, The effects of oil emplacement on diagenetic processes; examples from the Fulmar reservoir sandstones, central North Sea: American Association of Petroleum Geologists Bulletin, v. 76, p. 1024-1033.

Sathar, S., R. H. Worden, D. R. Faulkner, and P. C. Smalley, 2012, The Effect of Oil Saturation On the Mechanism of Compaction In Granular Materials: Higher Oil Saturations Lead To More Grain Fracturing and Less Pressure Solution: Journal of Sedimentary Research, v. 82, p. 571-584.

Scholle, P. A., 1977, Chalk diagenesis and its relation to petroleum exploration: oil from chalks, a modern miracle: Americam Association of Petroleum Geologists Bulletin, v. 61, p. 982-1009.

Scholle, P. A., and B. Halley, eds., 1985, Burial diagenesis: out of sight, out of mind!: Out of sight, out of mind!, Society of Sedimentary Geology Special Publication, 309-334 p.

Sneider, R. M., ed., 1990, Introduction: Reservoir description of sandstones: Sandstone petroleum reservoirs: New York, Springer-Verlag, 1-3 p.

Taylor, M. S. G., A. LeROY, and M. Førland, 1999, Hydrocarbon systems modelling of the Norwegian Central Graben fairway trend, v. 5, p. 1325-1338.

Taylor, T. R., M. R. Giles, L. A. Hathon, T. N. Diggs, N. R. Braunsdorf, G. V. Birbiglia, M. G. Kittridge, C. I. Macaulay, and I. S. Espejo, 2010, Sandstone diagenesis and reservoir quality prediction: Models, myths, and reality: American Association of Petroleum Geologists Bulletin, v. 94, p. 1093-1132.

Trewin, N. H., and A. E. Fallick, 2000, Quartz cement origins and budget in the Tumblagooda Sandstone, Western Australia, *in* R. H. Worden, and S. Morad, eds., Quartz cement in sandstone. Special Publication of the International Association of Sedimentologists v. 29: Oxford, Blackwells, p. 219-229.

Underhill, J. R., ed., 1998, Jurassic: Petroleum Geology of the North Sea:Basic Concepts and Recent Advances, Blackwell Science, 656 p.

Vagle, G. B., A. Hurst, and H. Dypvik, 1994, Origin of quartz cement in some sandstone from the Jurassic of the Inner Moray Firth (UK): Sedimentology, v. 41, p. 363-377.

Walderhaug, O., 1990, A fluid inclusion study of quartz cemented sandstones from offshore mid-Norway - possible evidence for continued quartz cementation during oil emplacement: Journal of Sedimentary Petrology, v. 60, p. 203-210.

Walderhaug, O., 1994a, Precipitation rates for quartz cement in sandstones determined by fluid inclusion microthermometry and temperature history modelling: Journal of Sedimentary Research Section a-Sedimentary Petrology and Processes, v. 64, p. 324-333.

Walderhaug, O., 1994b, Temperatures of quartz cementation in Jurassic sandstones from the Norwegian continental shelf - evidence from fluid inclusions: Journal of

Sedimentary Research Section a-Sedimentary Petrology and Processes, v. 64, p. 311-323.
Walderhaug, O., 1996, Kinetic modeling of quartz cementation and porosity loss in deeply buried sandstone reservoirs: American Association of Petroleum Geologists Bulletin, v. 80, p. 731-745.
Walderhaug, O., R. H. Lander, P. A. Bjorkum, E. H. Oelkers, K. Bjorlykke, and P. H. Nadeau, 2000, Modelling quartz cementation and porosity in reservoir sandstones: examples from the Norwegain continental shelf: In: Quartz cementation in sandstones (eds. Worden, R.H. and Morad, S.) International Association of Sedimentologists Special Publications, v. 29, p. 39-50.
Weibel, R., H. Friis, A. M. Kazerouni, J. B. Svendsen, J. Stokkendal, and M. L. K. Poulsen, 2010, Development of early diagenetic silica and quartz morphologies - Examples from the Siri Canyon, Danish North Sea: Sedimentary Geology, v. 228, p. 151-170.
Wilkinson, M., and R. S. Haszeldine, 2011, Oil charge preserves exceptional porosity in deeply buried, overpressured, sandstones: Central North Sea, UK: Journal of the Geological Society, v. 168, p. 1285-1295.
Wilkinson, M., R. S. Haszeldine, R. M. Ellam, and A. Fallick, 2004, Hydrocarbon filling history from diagenetic evidence: Brent Group, UK North Sea: Marine and Petroleum Geology, v. 21, p. 443-455.
Wilkinson, M., R. S. Haszeldine, and A. E. Fallick, 2006, Hydrocarbon filling and leakage history of a deep geopressured sandstone, Fulmar Formation, United Kingdom: American Association of Petroleum Geologists Bulletin, v. 90, p. 1945-1961.
Worden, R. H., 2006, Dawsonite cement in the Triassic Lam Formation, Shabwa Basin, Yemen: A natural analogue for a potential mineral product of subsurface CO2 storage for greenhouse gas reduction: Marine and Petroleum Geology, v. 23, p. 61-77.
Worden, R. H., M. W. French, and E. Mariani, 2012, Amorphous silica nanofilms result in growth of misoriented microcrystalline quartz cement maintaining porosity in deeply buried sandstones: Geology, v. 40, p. 179-182.
Worden, R. H., and S. Morad, 2000, Quartz cementation in sandstones: a review of the key controversies In: Quartz cementation in sandstones (eds. Worden, R.H. and Morad, S.) International Association of Sedimentologists Special Publications, v. 29, p. 1-20.
Worden, R. H., N. H. Oxtoby, and P. C. Smalley, 1998, Can oil emplacement prevent quartz cementation in sandstones?: Petroleum Geoscience, v. 4, p. 129-137.
Worden, R. H., and J. C. Rushton, 1992, Diagenetic K-feldspar textures - A TEM study and model for diagenetic feldspar growth: Journal of Sedimentary Petrology, v. 62, p. 779-789.
Worden, R. H., E. A. Warren, P. C. Smalley, T. J. Primmer, and N. H. Oxtoby, 1995, Evidence for resetting of fluid inclusions from quartz cements in oil fields - discussion: Marine and Petroleum Geology, v. 12, p. 566-570.

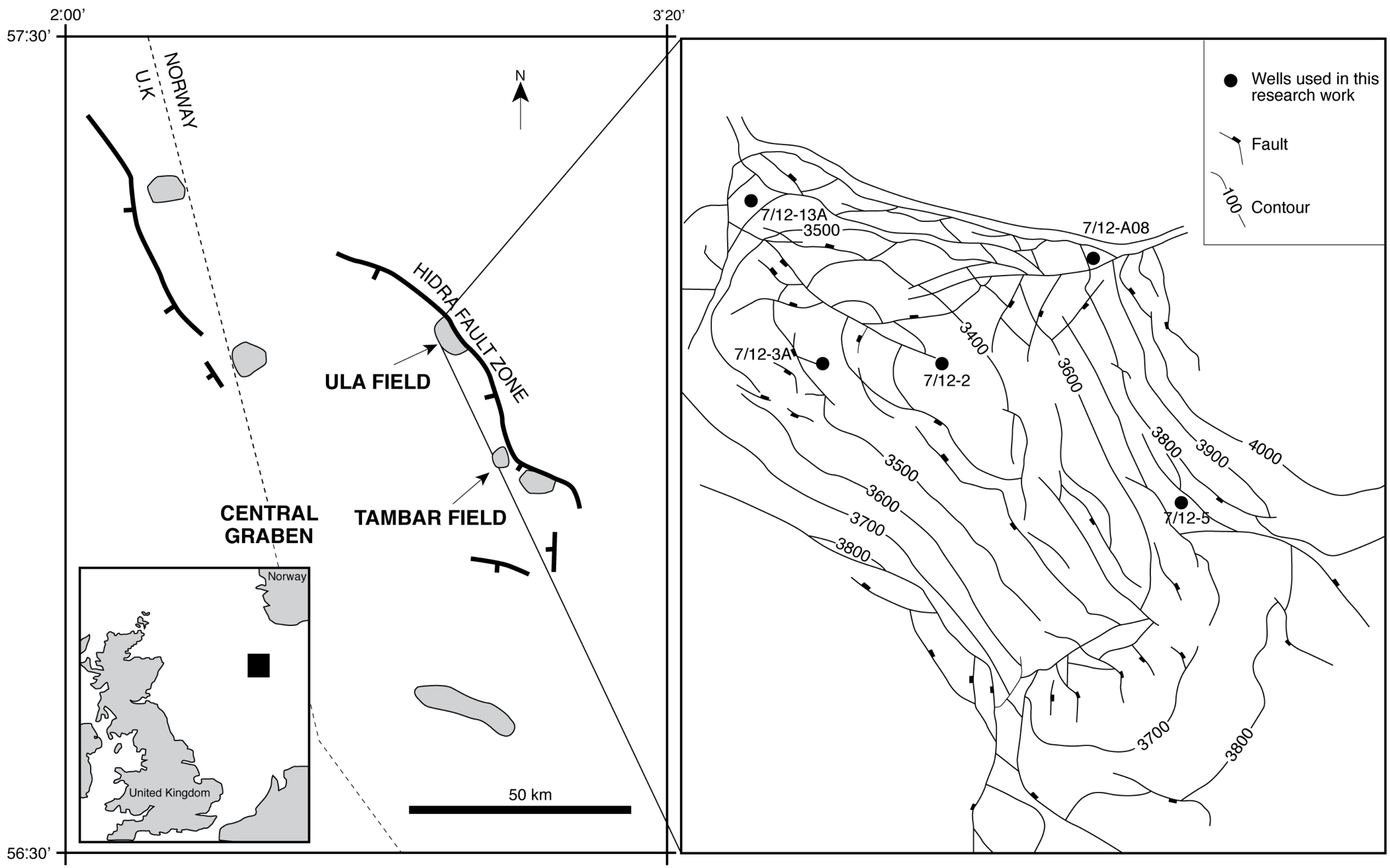
2°00'
3°20'
57°30'
56°30'
U.K
NORWAY
N
HIDRA FAULT ZONE
ULA FIELD
TAMBAR FIELD
CENTRAL GRABEN
Norway
United Kingdom
50 km
Wells used in this research work
Fault
Contour
100
7/12-13A
7/12-A08
7/12-3A
7/12-2
7/12-5
3400
3500
3600
3700
3800
3900
4000

Figure 1

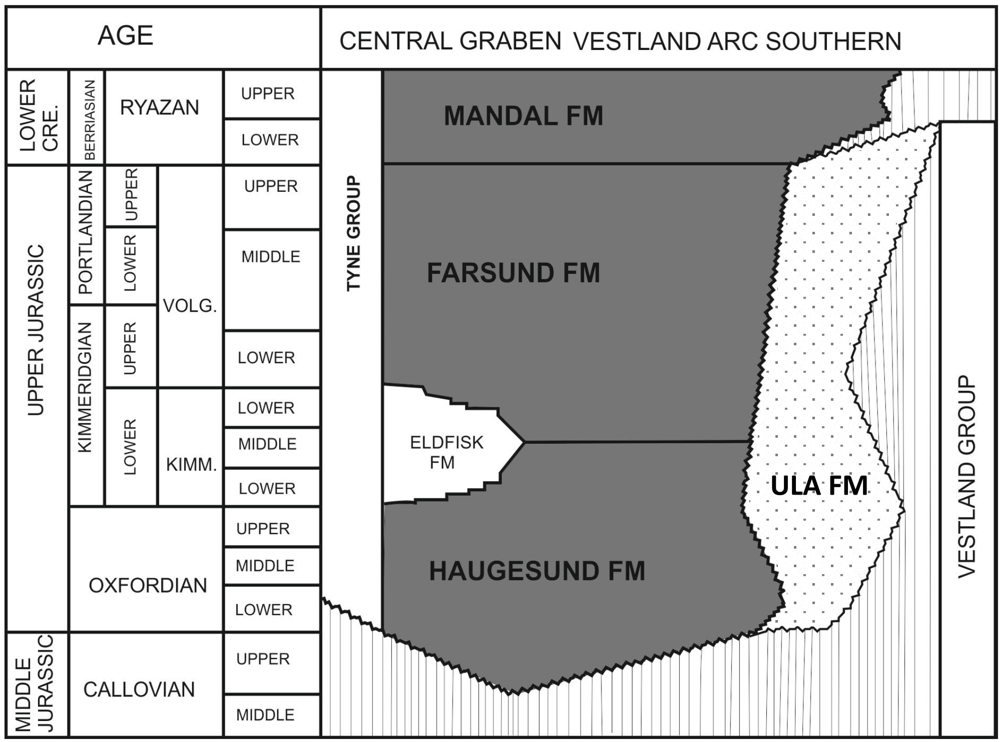
AGE
CENTRAL GRABEN VESTLAND ARC SOUTHERN
LOWER CRE.
BERRIASIAN
RYAZAN
UPPER
LOWER
UPPER JURASSIC
PORTLANDIAN
UPPER
LOWER
VOLG.
UPPER
MIDDLE
LOWER
KIMMERIDGIAN
UPPER
LOWER
KIMM.
LOWER
MIDDLE
LOWER
OXFORDIAN
UPPER
MIDDLE
LOWER
MIDDLE JURASSIC
CALLOVIAN
UPPER
MIDDLE
TYNE GROUP
MANDAL FM
FARSUND FM
ELDFISK FM
HAUGESUND FM
ULA FM
VESTLAND GROUP

Figure 2

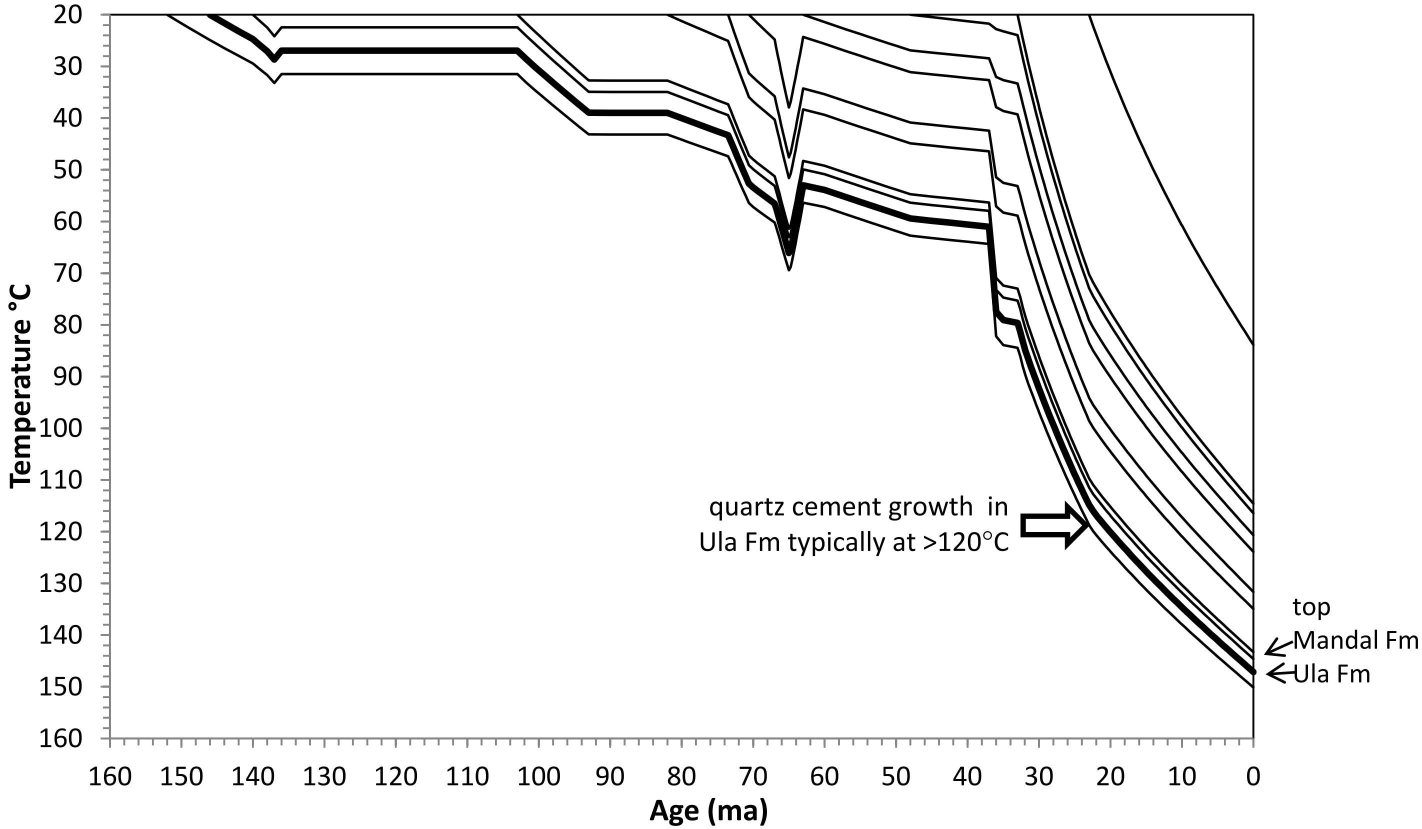

Temperature °C
20
30
40
50
60
70
80
90
100
110
120
130
140
150
160
160
150
140
130
120
110
100
90
80
70
60
50
40
30
20
10
0
Age (ma)
quartz cement growth in
Ula Fm typically at >120°C
top
Mandal Fm
Ula Fm

Figure 3

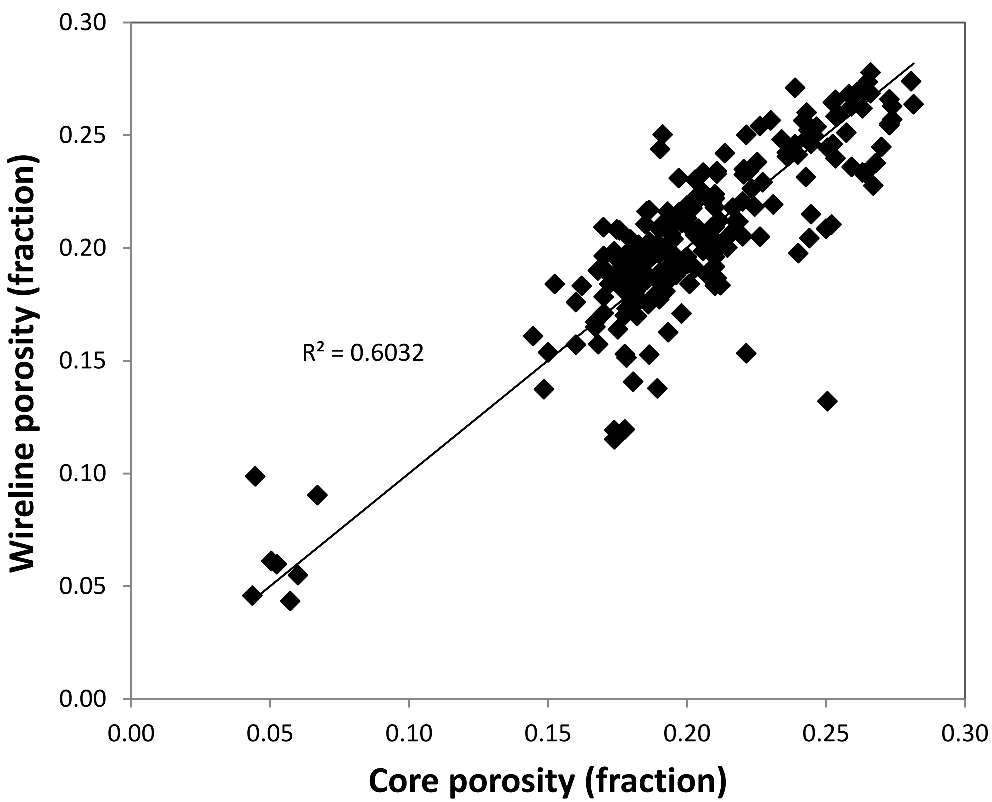

0.30
0.25
0.20
0.15
0.10
0.05
0.00
Wireline porosity (fraction)
R² = 0.6032
0.00 0.05 0.10 0.15 0.20 0.25 0.30
Core porosity (fraction)

Figure 4

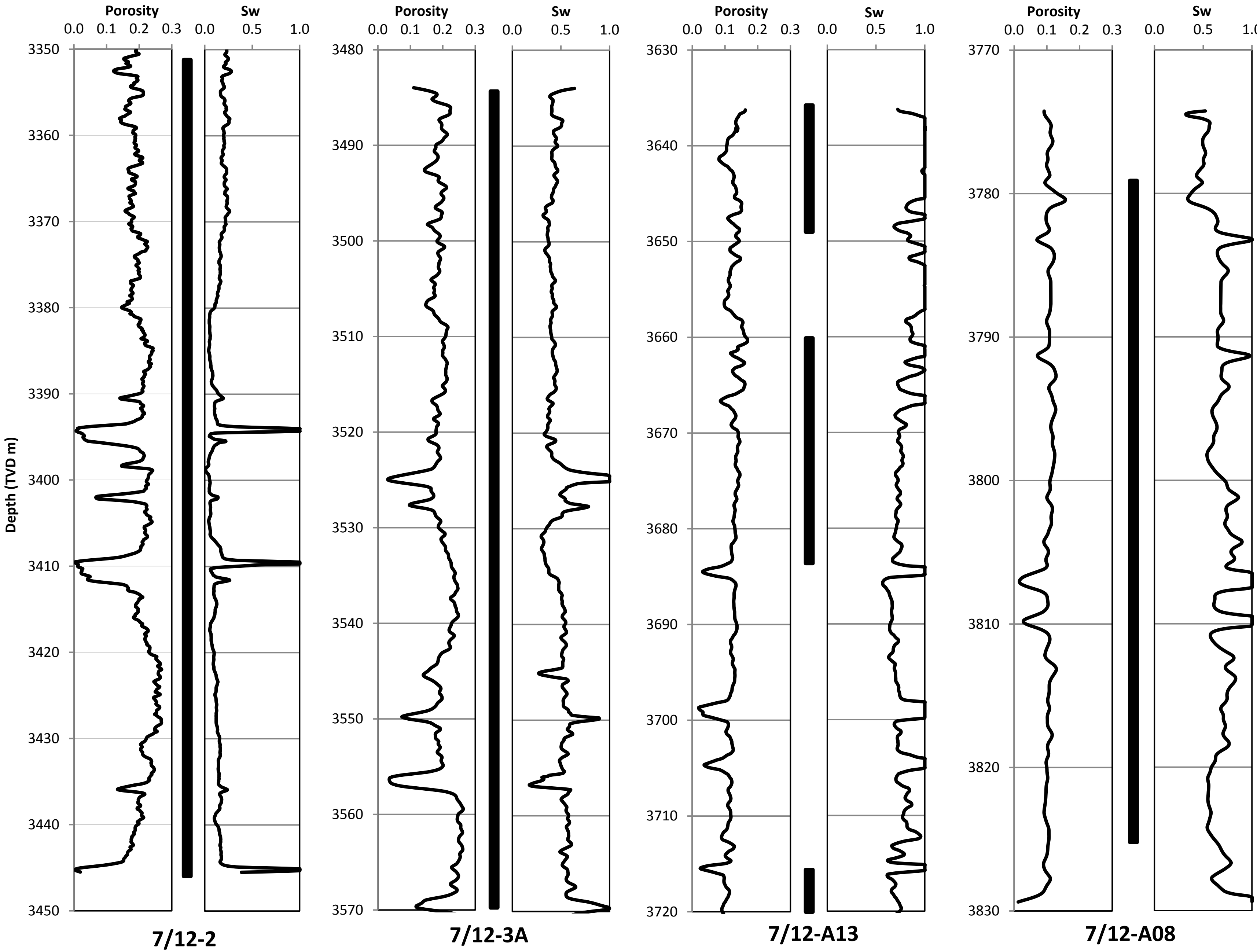

Porosity
Sw
0.0 0.1 0.2 0.3
0.0 0.5 1.0
Depth (TVD m)
3350
3360
3370
3380
3390
3400
3410
3420
3430
3440
3450
7/12-2
3480
3490
3500
3510
3520
3530
3540
3550
3560
3570
7/12-3A
3630
3640
3650
3660
3670
3680
3690
3700
3710
3720
7/12-A13
3770
3780
3790
3800
3810
3820
3830
7/12-A08

Figure 5

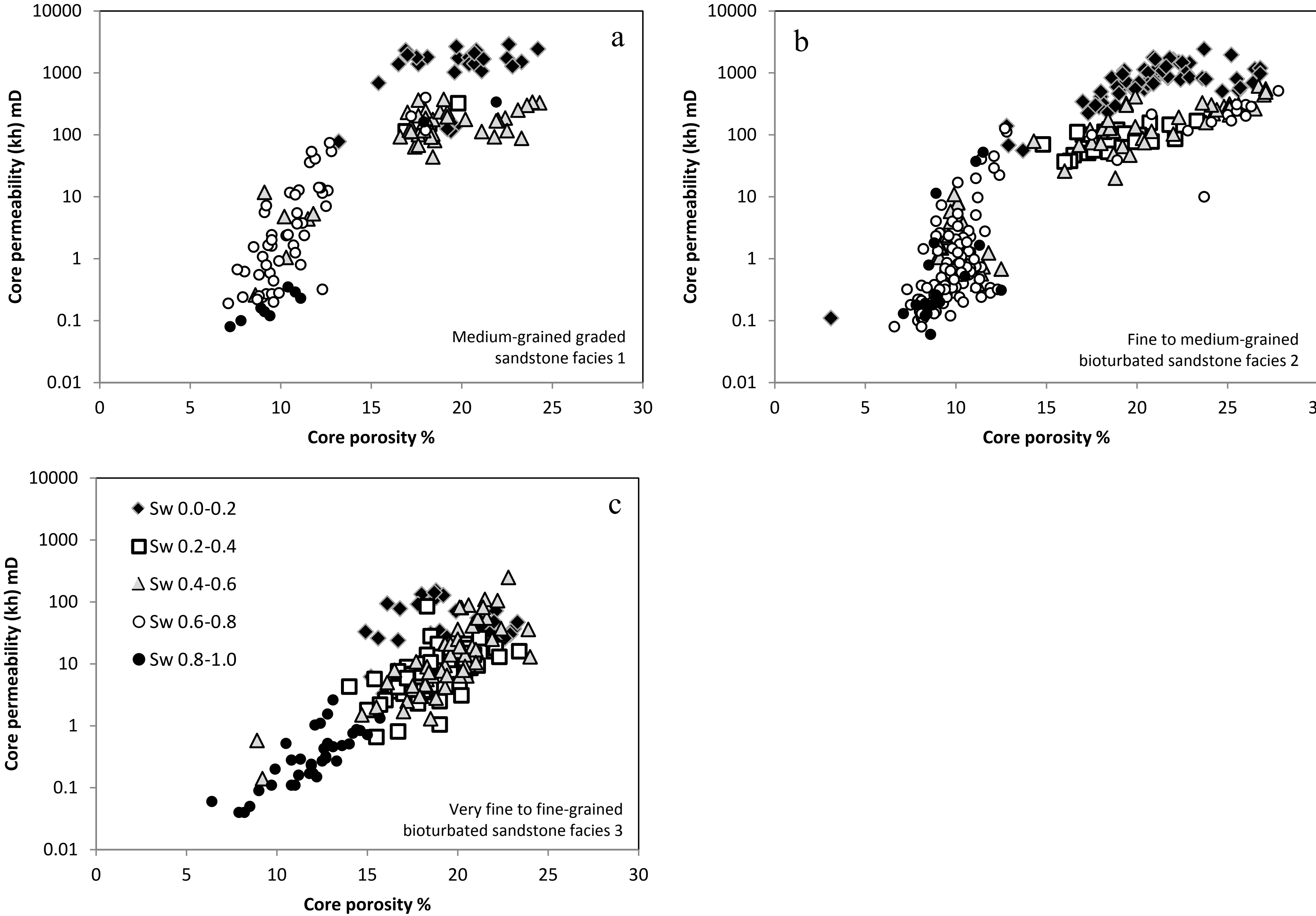

a
Medium-grained graded sandstone facies 1
b
Fine to medium-grained bioturbated sandstone facies 2
c
Very fine to fine-grained bioturbated sandstone facies 3
Core permeability (kh) mD
Core porosity %
10000
1000
100
10
1
0.1
0.01
0
5
10
15
20
25
30
Sw 0.0-0.2
Sw 0.2-0.4
Sw 0.4-0.6
Sw 0.6-0.8
Sw 0.8-1.0

Figure 6

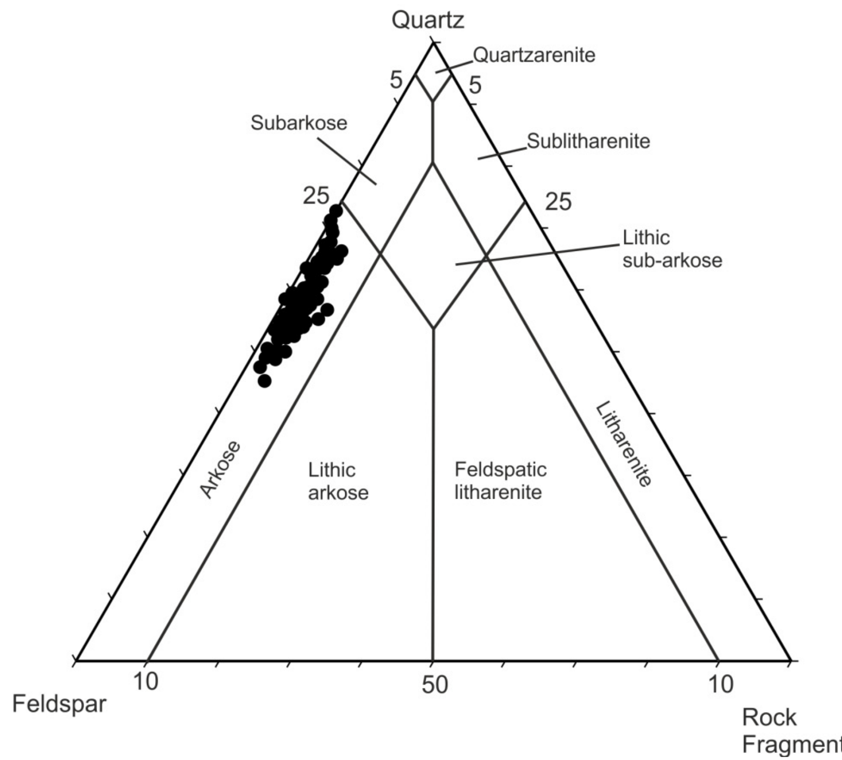

Quartz
Quartzarenite
5
5
Subarkose
Sublitharenite
25
25
Lithic
sub-arkose
Arkose
Lithic
arkose
Feldspatic
litharenite
Litharenite
10
50
10
Feldspar
Rock
Fragment

Figure 7

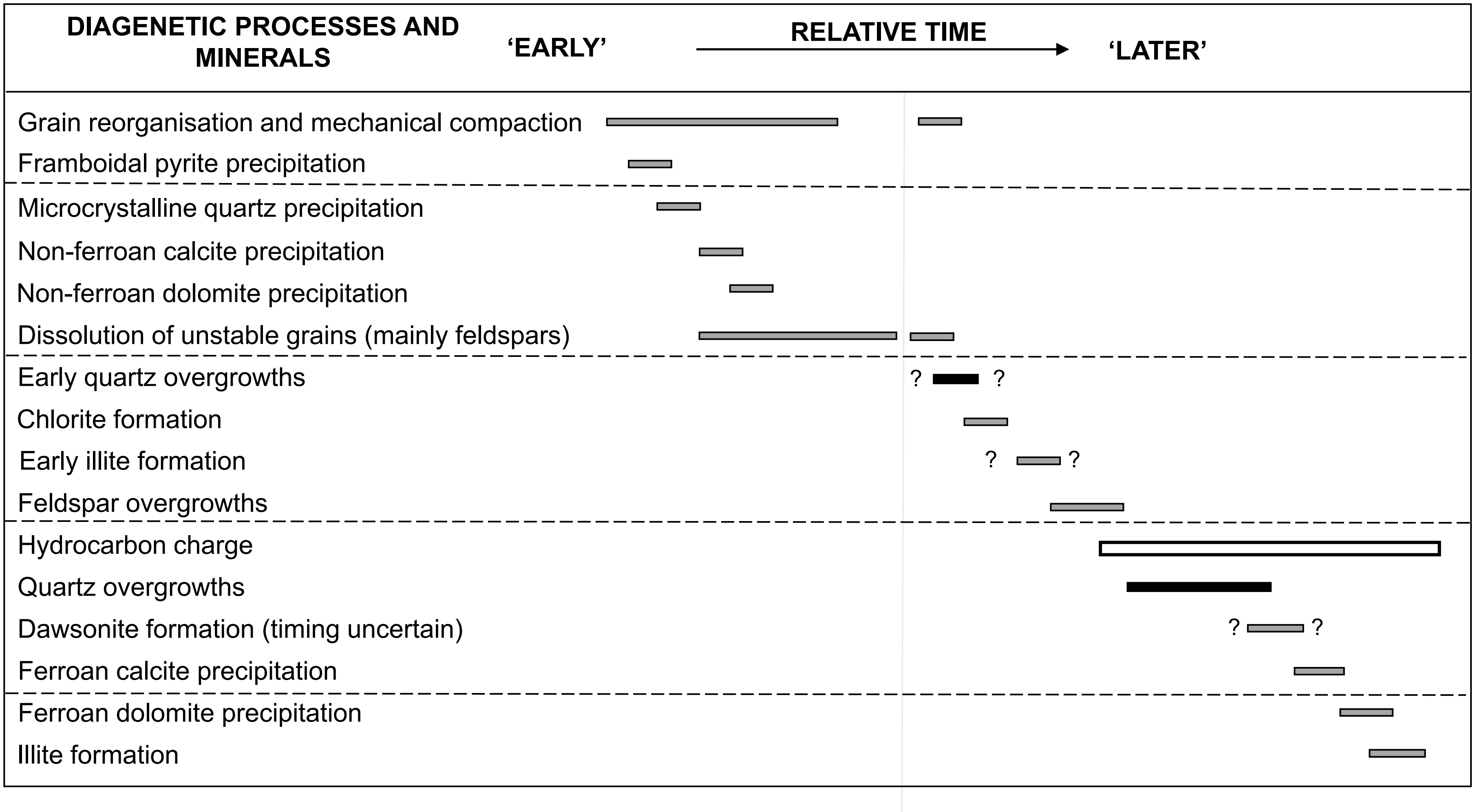
DIAGENETIC PROCESSES AND MINERALS
'EARLY'
RELATIVE TIME
'LATER'
Grain reorganisation and mechanical compaction
Framboidal pyrite precipitation
Microcrystalline quartz precipitation
Non-ferroan calcite precipitation
Non-ferroan dolomite precipitation
Dissolution of unstable grains (mainly feldspars)
Early quartz overgrowths
? ?
Chlorite formation
Early illite formation
? ?
Feldspar overgrowths
Hydrocarbon charge
Quartz overgrowths
Dawsonite formation (timing uncertain)
? ?
Ferroan calcite precipitation
Ferroan dolomite precipitation
Illite formation

Figure 8

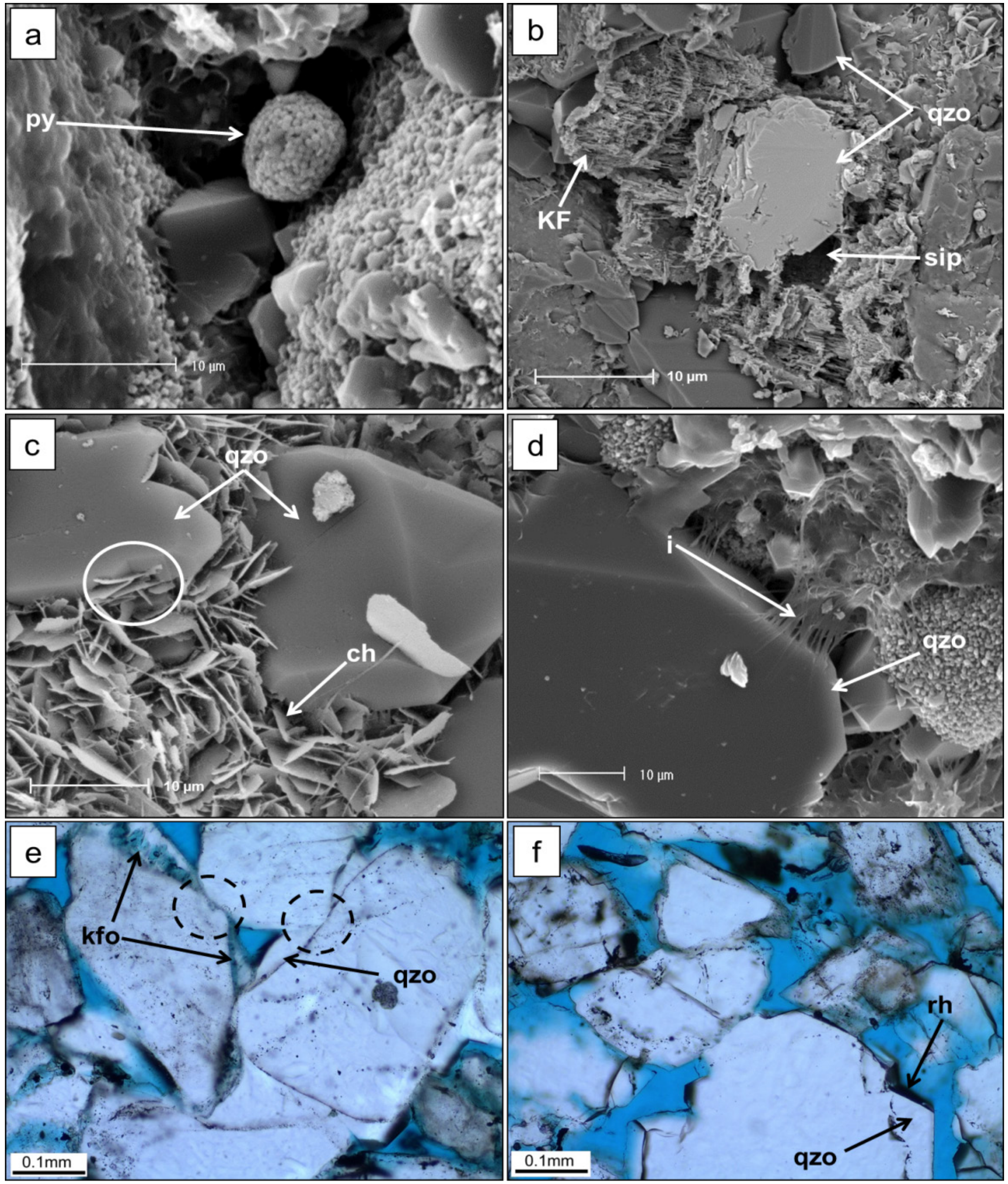
a
py
10 µm
b
qzo
KF
sip
10 µm
c
qzo
ch
10 µm
d
i
qzo
10 µm
e
kfo
qzo
0.1mm
f
rh
qzo
0.1mm

Figure 9

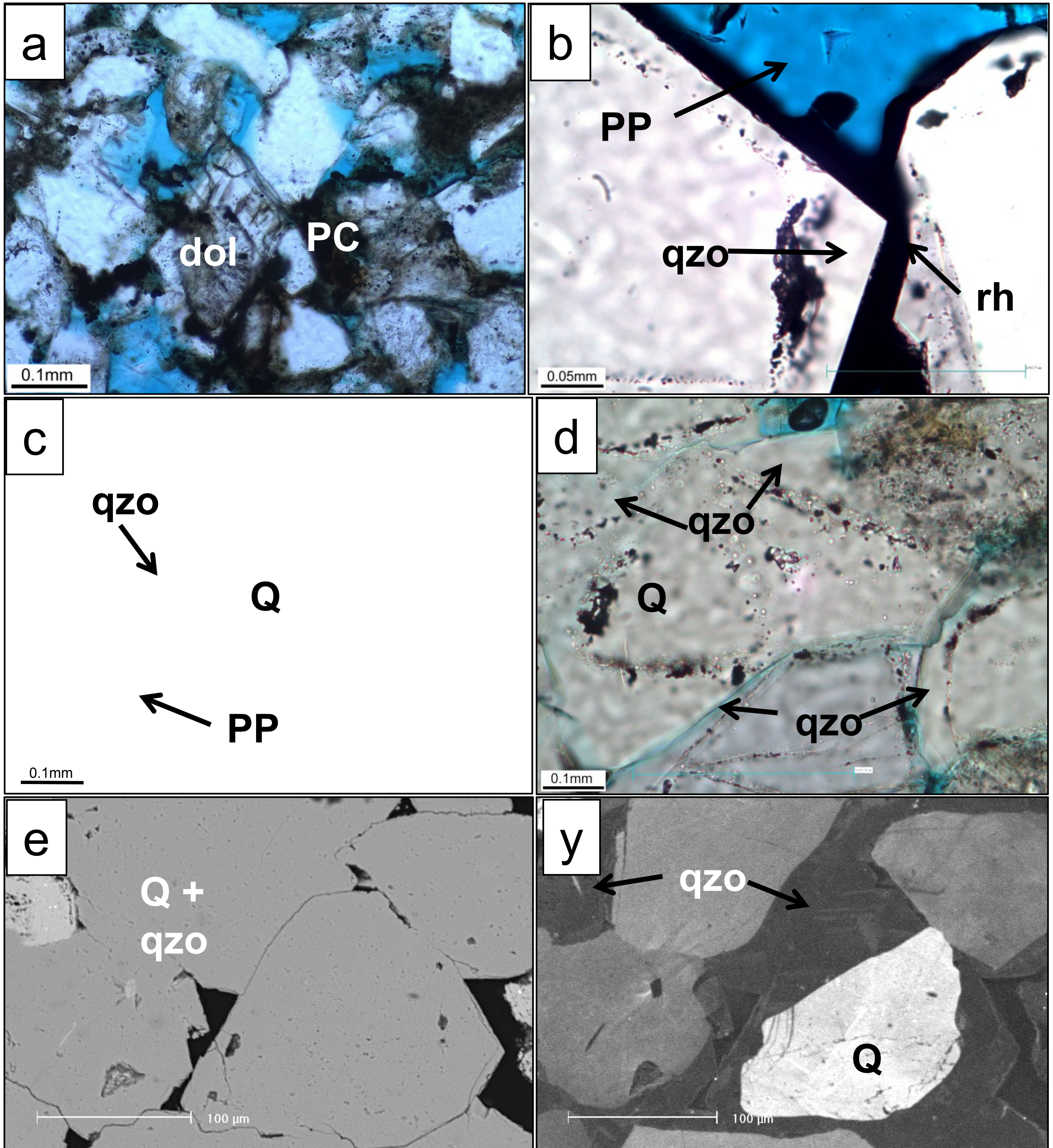
a
0.1mm
dol
PC
b
PP
qzo
rh
0.05mm
c
qzo
Q
PP
0.1mm
d
qzo
Q
qzo
0.1mm
e
Q +
qzo
100 µm
y
qzo
Q
100 µm

Figure 10

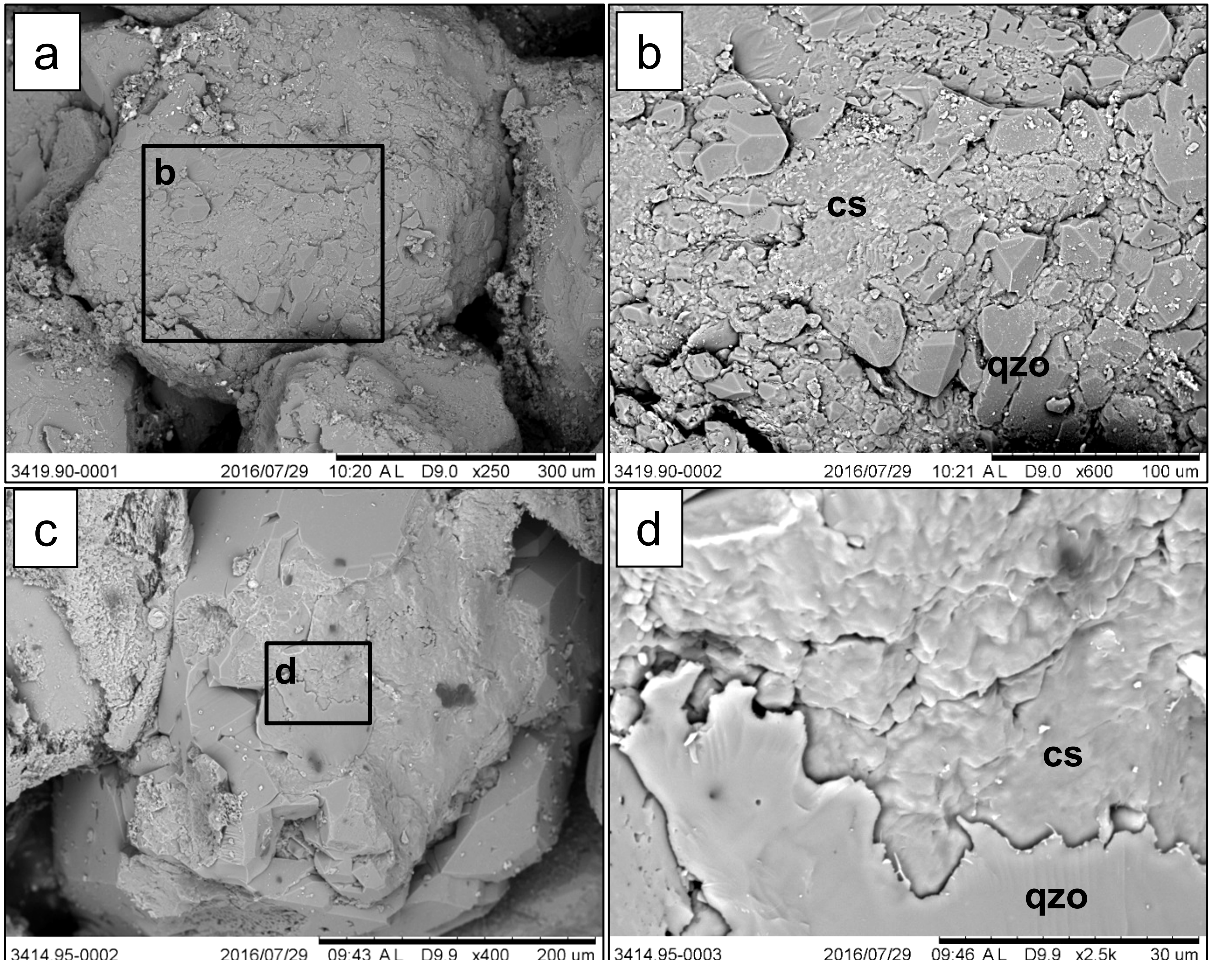

a
b
3419.90-0001 2016/07/29 10:20 A L D9.0 x250 300 um
b
cs
qzo
3419.90-0002 2016/07/29 10:21 A L D9.0 x600 100 um
c
d
3414.95-0002 2016/07/29 09:43 A L D9.9 x400 200 um
d
cs
qzo
3414.95-0003 2016/07/29 09:46 A L D9.9 x2.5k 30 um

Figure 11

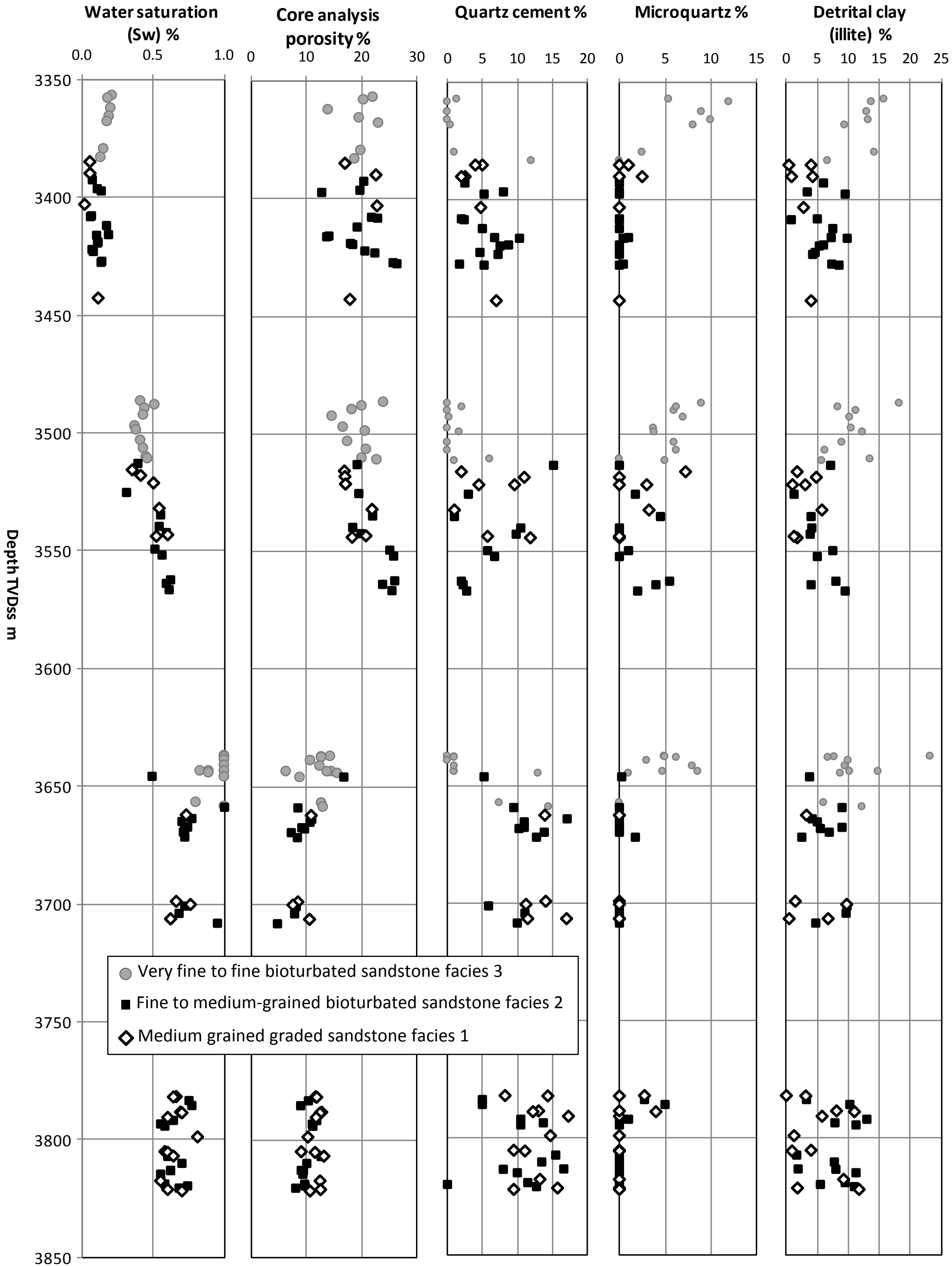
Water saturation (Sw) %
Core analysis porosity %
Quartz cement %
Microquartz %
Detrital clay (illite) %
Depth TVDss m
Very fine to fine bioturbated sandstone facies 3
Fine to medium-grained bioturbated sandstone facies 2
Medium grained graded sandstone facies 1

Figure 12

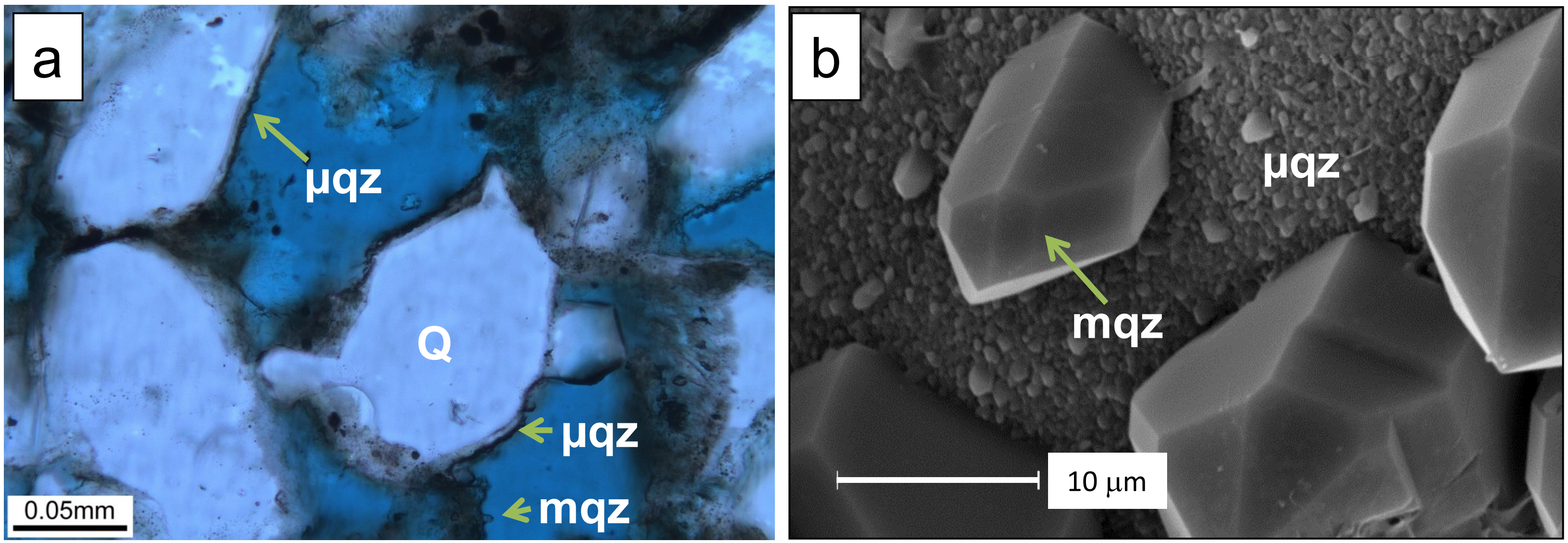

Figure 13

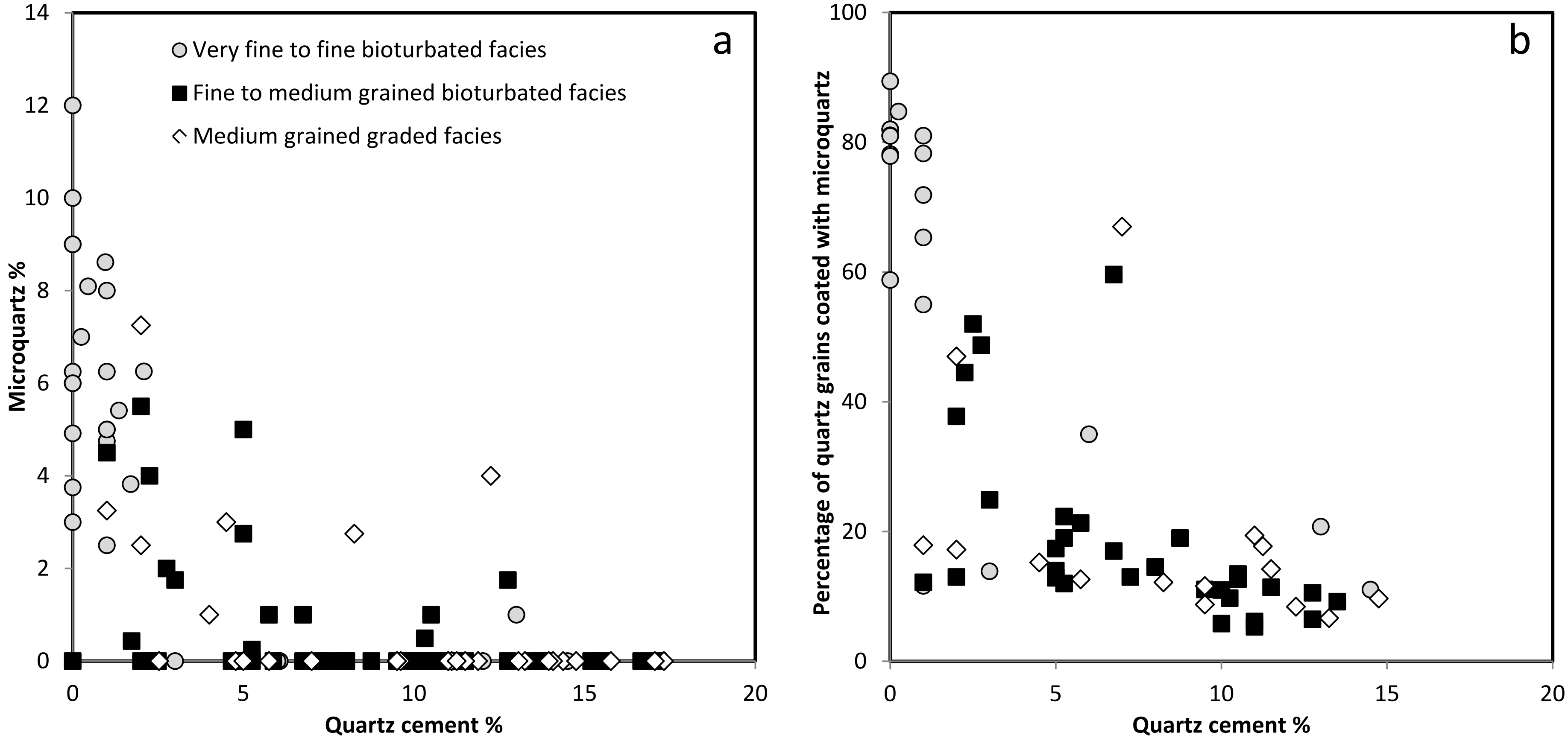

a
Very fine to fine bioturbated facies
Fine to medium grained bioturbated facies
Medium grained graded facies
Microquartz %
Quartz cement %
0
2
4
6
8
10
12
14
0
5
10
15
20
b
Percentage of quartz grains coated with microquartz
Quartz cement %
0
20
40
60
80
100

Figure 14

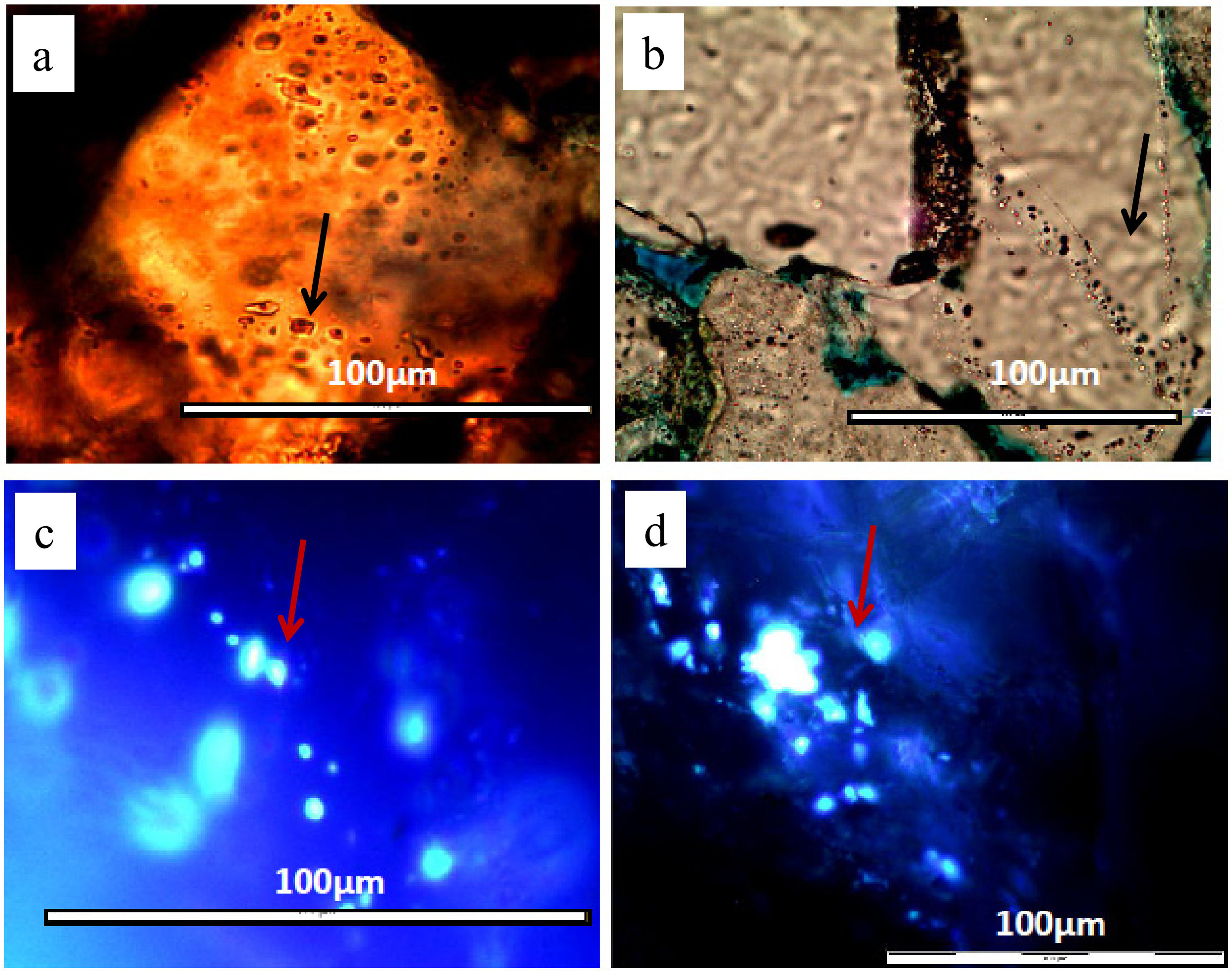

Figure 15

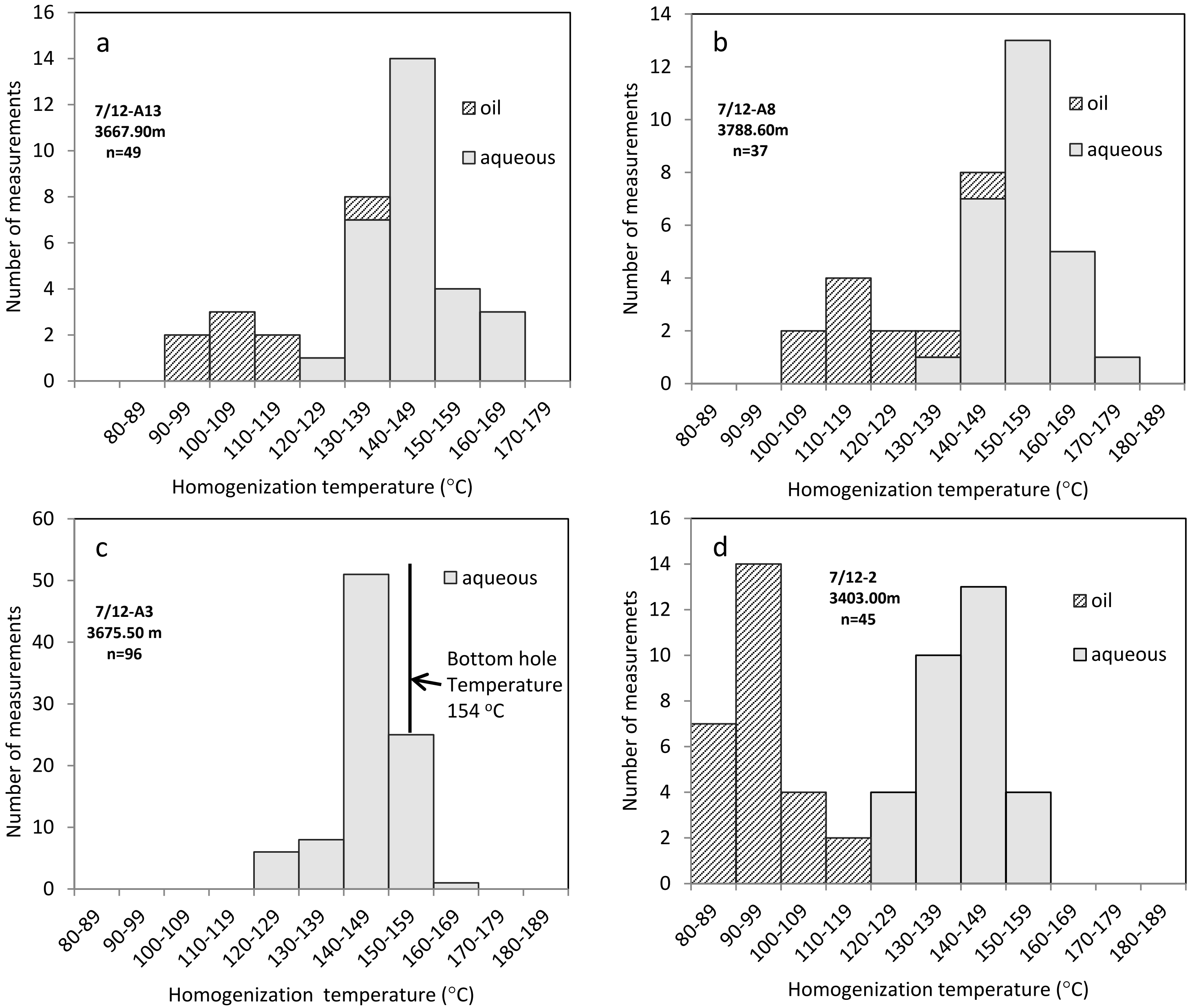
a
7/12-A13
3667.90m
n=49
oil
aqueous
Number of measurements
Homogenization temperature (°C)
80-89
90-99
100-109
110-119
120-129
130-139
140-149
150-159
160-169
170-179
b
7/12-A8
3788.60m
n=37
oil
aqueous
Number of measurements
Homogenization temperature (°C)
180-189
c
7/12-A3
3675.50 m
n=96
aqueous
Bottom hole
Temperature
154 °C
Number of measurements
Homogenization temperature (°C)
d
7/12-2
3403.00m
n=45
oil
aqueous
Number of measuremets
Homogenization temperature (°C)

Figure 16

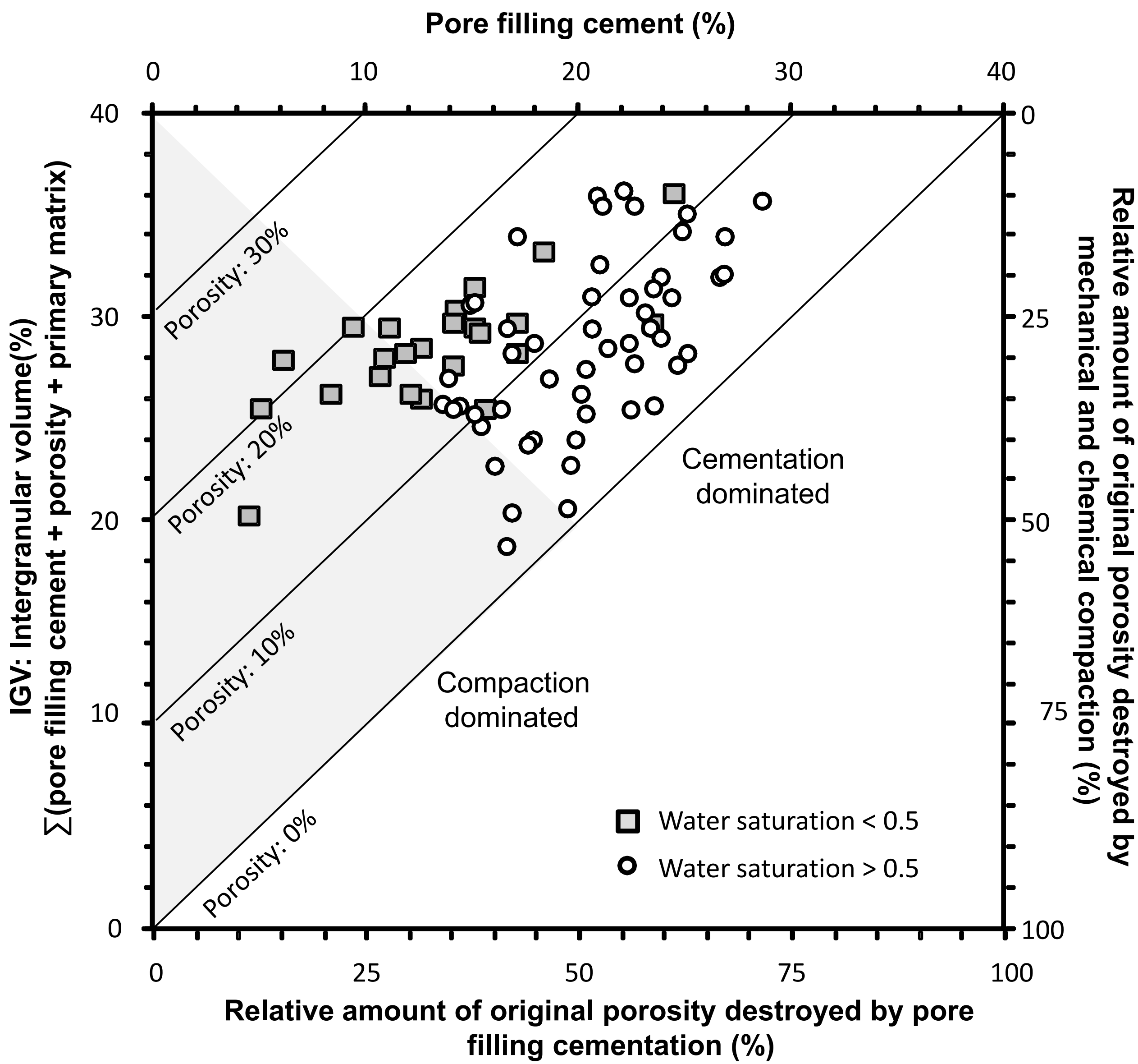
Pore filling cement (%)
0
10
20
30
40
IGV: Intergranular volume(%)
∑(pore filling cement + porosity + primary matrix)
Relative amount of original porosity destroyed by mechanical and chemical compaction (%)
Relative amount of original porosity destroyed by pore filling cementation (%)
0
25
50
75
100
Porosity: 30%
Porosity: 20%
Porosity: 10%
Porosity: 0%
Cementation dominated
Compaction dominated
Water saturation < 0.5
Water saturation > 0.5

Figure 17

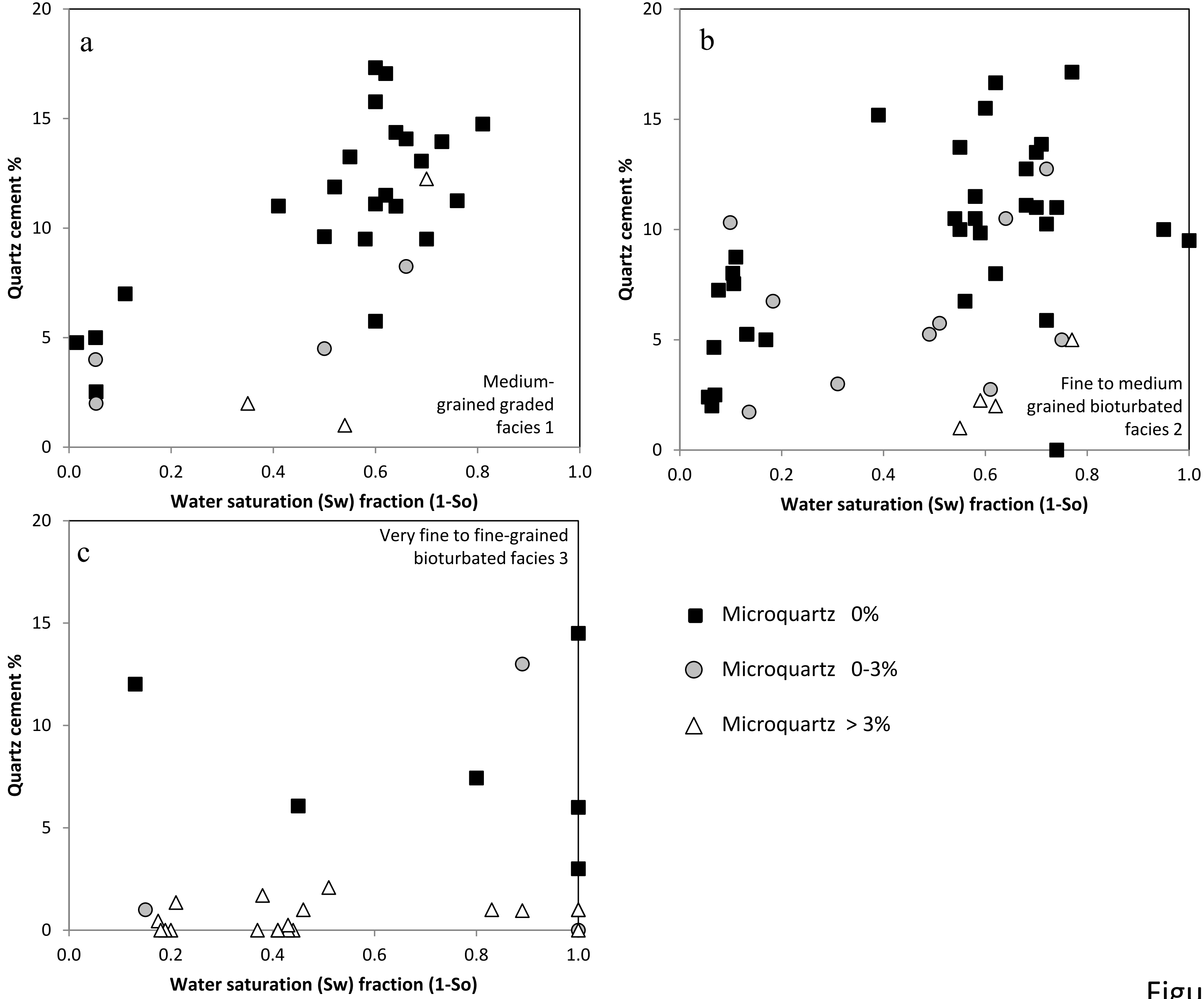
a
Medium-grained graded facies 1
b
Fine to medium grained bioturbated facies 2
c
Very fine to fine-grained bioturbated facies 3
Quartz cement %
Water saturation (Sw) fraction (1-So)
0
5
10
15
20
0.0
0.2
0.4
0.6
0.8
1.0
Microquartz 0%
Microquartz 0-3%
Microquartz > 3%

Figure 18

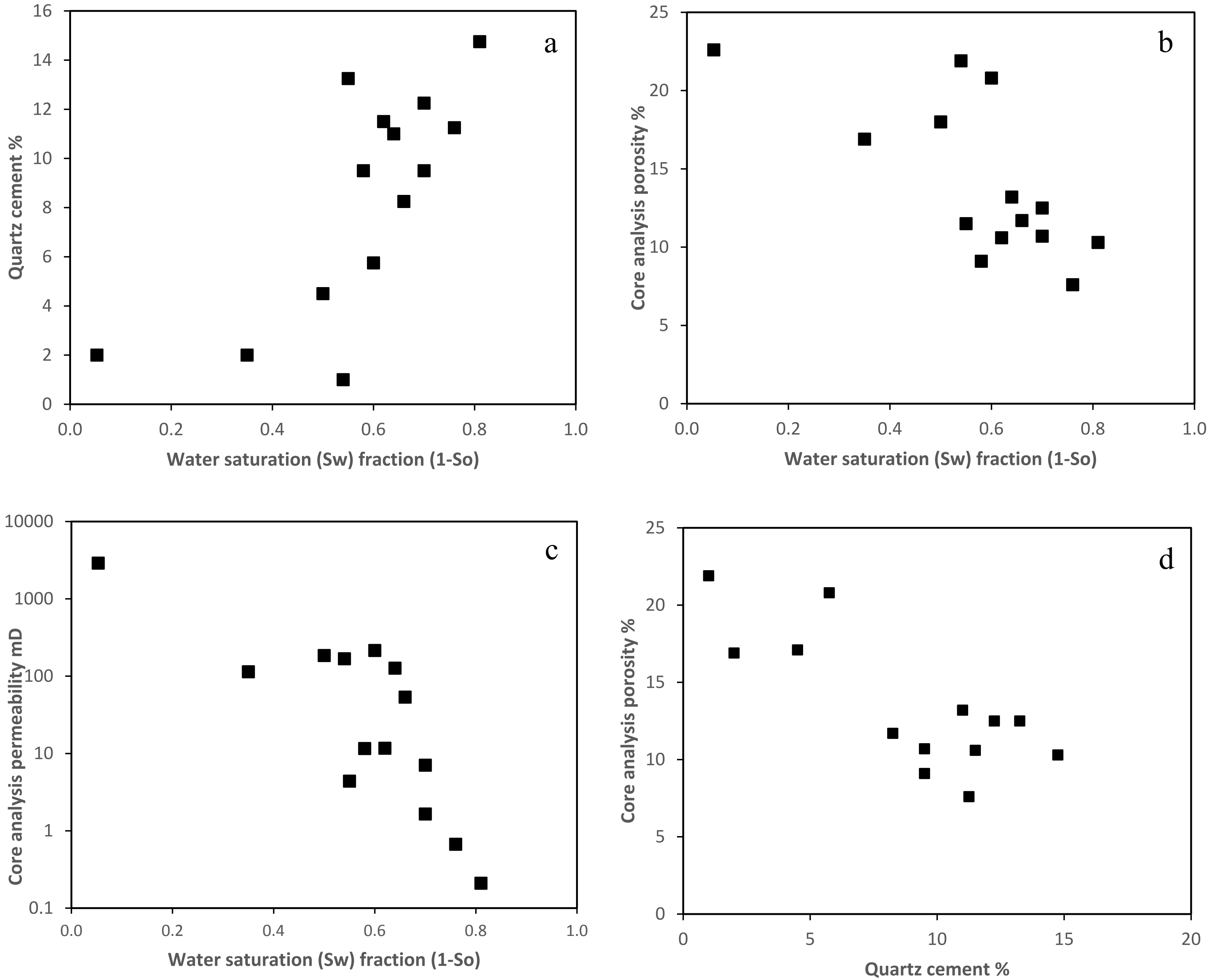

a
Quartz cement %
Water saturation (Sw) fraction (1-So)
b
Core analysis porosity %
Water saturation (Sw) fraction (1-So)
c
Core analysis permeability mD
Water saturation (Sw) fraction (1-So)
d
Core analysis porosity %
Quartz cement %

Figure 19

Parameters	Water saturation	Coarse grained sandstone facies - 1					Medium biotubated sandstone facies - 2					Very fine-fine biotubated sandstone facies - 3				
		MIN	AVERAGE	MAX	STDEV	NUM	MIN	AVERAGE	MAX	STDEV	NUM	MIN	AVERAGE	MAX	STDEV	NUM
Horizontal permeability (mD)	< 0.5	18.9	1117	2896	901	38	0.1	557	2424	520	99	0.6	25	249	36	152
	> 0.5	7.1	76	400	104.7	83	0.1	53	551	108	187	0.1	17	82	31	39
Core porosity %	< 0.5	13.2	19.3	24.2	2.5	38	3.1	20.2	27.0	3.6	99	8.9	19.1	24.0	2.2	152
	> 0.5	7.1	13.9	24.3	5.1	83	6.6	12.8	27.8	5.7	187	6.4	12.1	23.9	2.8	39
Quartz overgrowths %	< 0.5	2.0	4.8	11.0	3.0	8	1.7	5.9	15.2	3.5	17	0.0	1.5	12.0	3.2	16
	> 0.5	1.0	11.4	17.3	4.0	22	0.0	9.5	17.1	4.6	31	0.0	3.9	14.5	4.9	13
Detrital clay %	< 0.5	0.4	2.9	4.8	1.7	8	0.8	5.7	9.8	2.6	17	5.8	11.5	18.3	3.5	16
	> 0.5	0.0	4.6	11.8	3.9	22	1.7	5.9	13.0	3.1	31	6.0	11.5	23.2	4.9	13
Microcrystalline quartz %	< 0.5	0.0	1.3	7.3	2.5	8	0.0	0.2	1.8	0.5	17	0.0	5.9	12.0	3.4	16
	> 0.5	0.0	0.6	4.0	1.3	22	0.0	0.9	5.5	1.7	31	0.0	3.7	8.6	3.2	13
Total dolomite %	< 0.5	0.0	0.0	0.0	-	8	0.0	0.0	0.0	-	17	0.0	0.9	3.5	0.9	16
	> 0.5	0.0	0.0	0.0	-	22	0.0	0.0	0.0	-	31	0.0	0.2	1.4	0.2	13
Petrographic (visible) porosity %	< 0.5	12.7	15.5	20.0	2.6	8	6.1	14.4	20.3	3.40	17	6.0	11.8	16.3	3.4	16
	> 0.5	3.0	8.6	15.5	3.2	22	0.0	7.7	18.5	4.90	31	4.0	7.7	15.3	3.3	13
Intergranular volume %	< 0.5	20.3	26.6	29.5	3.6	8	25.5	29.1	36.1	2.70	17	24.8	33.3	44.5	4.5	16
	> 0.5	20.4	28.3	35.8	4.1	22	18.8	29.7	42.5	5.50	31	18.3	28.7	36.9	6.1	13

Well	7/12-A13	7/12-A8	7/12-A3	7/12-2
Depth TVD m	3667.90	3788.60	3675.50	3403.00
Part of figure 15 refered to	Fig. 15a	Fig. 15b	Fig. 15c	Fig. 15d
Lithofacies	Coarse grained graded facies	Medium-fine grained bioturbated facies	Coarse grained graded facies	Coarse grained graded facies
Water saturation %	88	70	62	5
Porosity %	11	13	20	20
Permability mD	3.65	7.06	332	1024
Quartz cement %	15	15	12	7

The effect of oil emplacement on quartz cementation in a deeply buried sandstone reservoir

Richard H Worden[1], Mohammed Bukar[1], Philip Shell[2]

1 Department of Earth, Ocean and Ecological Sciences, University of Liverpool, Liverpool, L69 3GP, UK

2. BP Exploration (Epsilon) Ltd, Oman Branch, PC 130 (Al Azaiba), Muscat, Sultanate of Oman

Key words: quartz cementation, quartz cement inhibition, diagenesis, oil charging, reservoir quality

Abstract

Quartz~~ cement~~ is an important, porosity-occluding cement in sandstone reservoirs that have been subjected to elevated temperature (>80 º-100 ºC) for a substantial period of time. The effect of oil emplacement on quartz cementation in reservoir sandstones is ~~controversial~~controversial; ~~with~~ some studies have concluded~~ing~~ that early oil emplacement can inhibit quartz cementation leading to the preservation of porosity, while other studies ~~claim~~ have concluded that quartz cementation appears largely unaffected by oil emplacement. Here we have studied shallow marine, Upper Jurassic sandstones from ~~the~~ Ula Field, Norwegian North Sea, with reservoir temperatures ~~in the region~~ of approximately 150 ºC, in order to determine whether oil emplace-

ment had a significant ~~effect~~ impact on diagenesis with particular attention to quartz cementation. Following sedimentological description of ~~the~~ cores, samples above and below the oil-water contact have been collected, adjacent to core analysis plug points. These samples then underwent a series of studies, including petrographic point counting with a transmitted light microscope, scanning electron microscopy (SEM), backscattered electron microscopy (BSEM), cathodoluminescence microscopy (SEM-CL), and fluid inclusion studies. These data were integrated with routine core analysis and petrophysical log data. Density and resistivity log data have been used to determine the precise oil saturation of each sample studied. The distributions of all potential controls on porosity and permeability, such as grain size, sorting, matrix clay content, degree of bioturbation, the presence of grain ~~-~~coatings, and dolomite cement, as well as the amount of quartz cement, have been assessed. The presence of primary oil inclusions within quartz cement shows that oil ingress into the Ula reservoir commenced prior to the onset of quartz cementation. Very fine-grained, matrix-~~-~~rich, bioturbated and microquartz-~~-~~cemented sandstones have uniformly low quartz cement contents irrespective of oil saturation. Medium-grained, graded, matrix-poor, microquartz-poor sandstones have quartz cement ranging from 1 % to greater than 17 %, associated with core porosities of about 22 % and 7 %, respectively. ~~However, sandstones of the same facies (i.e. coarse and fine to medium grain size, and uniform low matrix clay content, similar depositional mineralogy and negligible grain coating materials) that have high oil saturations have significantly less quartz cement than equivalent samples with low oil saturations.~~ Higher oil saturations equate to higher porosities and permeabilities in the medium-grained, graded, matrix-poor, microquartz-poor sandstones, ~~coarser, matrix- and microquartz-poor facies that~~which cannot be explained by any control other than the amount of quartz cement as a function of pore fluid type. Oil emplacement therefore appears to have inhibited quartz cementation at high oil saturations and can be viewed as a significant control on reservoir quality. The significance of this study is that the presence of oil in a sandstone reservoir, at the time that quartz cement was growing, can have a considerable impact on reservoir quality. Models that seek to predict quartz cement and reservoir quality in sandstones need to account for the timing of oil emplacement compared to other diagenetic processes~~presence of oil on the amount of quartz cement~~.

Introduction

The aim of this paper is to determine whether oil charge exerted a control on quartz cementation, and consequently preserved porosity, in sandstones from the Upper Jurassic ~~aged~~ Ula Formation in Ula Field, Norwegian North Sea.

Understanding whether oil charge has stopped or retarded quartz cementation in the Ula Formation could impact the prediction of porosity and permeability (reservoir quality) distribution, leading to (i) increased accuracy in volumetric reserve estimation (e.g. stock tank oil initially in place: STOIIP) and (ii) being able to forecast well performance pre-drill, allowing ~~the~~ wells with better delivery to be drilled first. The accurate understanding and prediction of reservoir quality is therefore key in order to obtain predictable well flow-rates throughout the lifetime of a field/reservoir (Sneider, 1990). However, the prediction of reservoir quality is, and will continue to be, a key challenge for petroleum exploration and reservoir development. Defining and reducing risk associated with reservoir quality is especially important in sandstone reservoirs that have been subjected to elevated temperatures (typically taken to be >100 °C) because of quartz, and other deep burial-related, cements (typically taken to be >100 °C), or high effective stress because of compaction (Taylor et al., 2010).

Quartz cement is volumetrically the most important cement in deeply buried sandstones (Worden and Morad, 2000). The Where quartz cement has been demonstrated to be the main control on reservoir quality, being abilitye to predict areas within reservoirs, or individual sandstone units, where quartz cement quantity appears to be anomalously low could lead to an improved prediction of the distribution of porosity and permeability in reservoirs where quartz cement has been demonstrated to be the main control on reservoir quality. –The concept that oil emplacement could inhibit quartz cementation and influence preservation of porosity in sandstone reservoirs became known to many geologists from Johnson's (1920) publication “The cementation process”, later developed in a series of papers (Hawkins, 1978; Lowry, 1956; Scholle, 1977; Scholle and Halley, 1985). -However, the question of the inhibiting effect of oil on mineral reactions in oil fields remains open and is highly contentious (Sathar et al., 2012; Taylor et al., 2010).

All diagenetic reactions take place through an aqueous phase, by dissolution, transport and re-precipitation (Worden and Morad, 2000). Hence, for diagenetic reaction to occur there must be aqueous fluid water present to dissolve the mineral grains, an aqueous fluid to transport dissolved material, and to facilitate water at the site of mineral precipitation. In an oil or gas field, displacement of the aqueous fluid by hydrocarbons within the pore -space disrupts the pathway between the reactants and sites of precipitation. As oil saturation increases (i) the residual (irreducible) water becomes isolated within a continuous hydrocarbon phase, (ii) the aqueous pathway becomes tortuous and diffusion rate decreases, or (iii) grain surfaces become coated by oil if the sandstone is mixed- or oil-wet (Barclay and Worden, 2000a). As a consequence, most of those working on diagenesis and sandstone reservoir quality assumed, up to the early-to-mid 1990s, that early oil emplacement halted cementation and preserved porosity.

Many empirical studies from different basins and from reservoirs of different ages have used, or discussed, the concept that early oil emplacement is a mechanism for porosity preservation in sandstones (Bjørnseth and Gluyas, 1995; Dixon et al., 1989; Emery et al., 1993; England et al., 2003; Gluyas and Cade, 1997; Gluyas et al., 1993; Haszeldine et al., 2003; Higgs et al., 2007; Marchand et al., 2000; Marchand et al., 2001; Marchand et al., 2002; Robinson and Gluyas, 1992; Saigal et al., 1992; Wilkinson and Haszeldine, 2011; Wilkinson et al., 2004; Wilkinson et al., 2006). These studies assumed that replacing formation water with oil simply stopped water-mediated geochemical reactions. However, ~~in recent years,~~ several other workers have suggested that quartz cementation can continue unhindered even after oil emplacement (Aase and Walderhaug, 2005; Bjørkum and Nadeau, 1998; Ehrenberg, 1990, 1993; Midtbø et al., 2000; Molenaar et al., 2008; Ramm and Bjorlykke, 1994). To explain this rather different interpretation of diagenetic processes, it was assumed that the combined diagenetic processes of dissolution-diffusion-precipitation utilise residual water that clings to grain surfaces, and that this film of water apparently permits mineral diagenesis to continue unhindered.

Comprehensive overviews of the empirical and theoretical arguments for and against oil emplacement inhibiting quartz cementation (Worden and Morad, 2000; Worden et al., 1998) concluded that the rate of quartz cementation that is synchronous with, or after, oil emplacement in sandstone is probably reduced relative to rates of quartz cementation in the underlying aquifer. These reviews concluded that quartz cementation should be strongly inhibited if (i) the system has mixed wettability or is oil-wet, (ii) the silica is externally supplied, (iii) the rate of diffusion is rate controlling, or (ivii) advection is an important part of the transport process. However, even in internally-sourced silica systems with diffusion as the transport control, the overall rate of quartz cementation should be inhibited due to added tortuosity reducing the net rate of diffusion.

One of the main difficulties in definitively addressing the controversial question of oil inhibition of quartz cement is the large number of potential controls on quartz cementation, such as: (i) primary depositional factors (e.g. facies, grain size, sorting, detrital mineralogy, matrix clay content), (ii) diagenetic factors (e.g. grain coating clay and other minerals, pre-quartz, pore-filling cements, the source of silica), and (iii) pore system characteristics (e.g. wettability and tortuosity). It is also important to consider the oil-filling history of each facies. It is, therefore, possible that previous studies have compared fundamentally different rocks, with different controls on quartz cementation, when attempting to prove or disprove the effect of oil emplacement on quartz cementation. In this study, we have taken samples with variable oil and water saturations, as defined by wireline log data. We have been careful to only compare sandstones from the same facies. We have also carefully quantified the presence, type and extent of grain coating materials and taken account of pore-filling cements and only made comparisons between rocks that appear to be as similar as possible (apart from oil saturation). Key questions to be addressed are;

~~1.~~ What was the timing of oil emplacement relative to quartz cementation in the Ula Formation?

~~2.~~1. ~~How much quartz would be expected if no oil were present in the Ula Formation?~~

~~3.~~2. What other potential influences/controls are there on quartz cementation in the Ula Formation?

~~4.~~3. Is there a difference in the quartz cement volume as a function of oil saturation for rocks that share similar pre-oil filling characteristics?

~~5.~~4. Can any differences in quartz cement volume be attributed to oil emplacement?

Geological background

Ula Field is an offshore oil accumulation~~field~~ located in blocks 7/12 in the southern Norwegian sector of the North Sea (Fig. 1). Ula is located 280 km (149 miles) southwest of Stavanger at the eastern margin of the Central Graben along the Hidra Fault zone (Fig. 1) (Nedkvitne et al., 1993). In addition to Ula Field, three other fields, Gyda, Tambar and Tambar East~~ fields~~, combine to make up the Ula-Gyda-Tambar (UGT) area (O'Connor et al., 2011). Ula Field was chosen to undertake this study due to the abundance of available core and supporting downhole data, which not only gives good geographical coverage of the whole field but also gives good stratigraphic coverage through the oil leg, transition zone and water leg.

Ula Field consists of Mesozoic sediments in an anticlinal structure formed by late Jurassic rifting and subsequent inversion in the Cretaceous and Tertiary (Brown et al., 1992). ~~Within the Ula field, t~~The main reservoir in the field is the Upper Jurassic Ula Formation (Fig. 2) (Bergan et al., 1989; Karlsen et al., 1993; Partington et al., 1993; Underhill, 1998). The Upper Jurassic Mandal Formation is considered to be the source of the petroleum, beginning expulsion from the deeper parts of the Central Graben during the late Cretaceous. Petroleum is still being generated in the UGT area from the Mandal Formation source rock (Taylor et al., 1999). Within the UGT area, the Mandal Formation also provides the seal for the underlying Jurassic sandstones (Bjørnseth and Gluyas, 1995).~~.~~

The Upper Jurassic Ula Formation is a marine sandstone, up to 200m thick, that prograded across Haugesund Formation outer-shelf mudstones following a sea level drop in the Kimmeridgian (Harris, 2006). ~~The~~ Ula sandstones~~Formation is~~ are typically very fine- to medium-grained~~ (coarse grained in places)~~, well-sorted, and locally can ~~locally~~ be glauconitic with some beds rich in shale fragments. ~~The~~ Ula Formation sandstones have been ~~was~~ described as arkosic (using the McBride, 1963, classification scheme) and ~~was~~ were probably sourced from nearby Triassic sandstone outcrops (Gluyas, 1997). Much of t~~T~~he Ula Formation has been interpreted to be intensively burrowed (Baniak et al., 2014; Baniak et al., 2015) and, even where no burrows are evident, physical sedimentary structures ~~are nonetheless~~can be absent, suggesting that the unit has been intensively bioturbated. Facies subdivisions are largely based on grain size and matrix content ; facies 1 is a normally-graded, medium~~ to coarse~~-grained sandstone, with low detrital clay content, facies 2 is a bioturbated fine- to medium-grained sandstone with variable detrital clay content, facies 3 is a very fine to fine-grained sandstone that is intensively bioturbated with a high detrital clay content. Trace fossils are ~~limited~~ dominated by~~to~~ *Ophiomorpha*, suggesting a high energy, shallow marine (*Skolithos* ichnofacies) origin for the sandstone (Baniak et al., 2015). The Ula Formation contains pervasively carbonate-cemented intervals that have negligible porosity and have been interpreted to result from bedded accumulation of shell debris followed by early diagenetic dissolution and reprecipitation as calcite cement (Gluyas, 1997). Core analysis porosity in the Ula Formation typically lies between ~~14~~ 7 and 28%. Permeability mostly falls between 650 to 850 mD for the better reservoir units (with extremes between 0.2 and 2800 mD) (Karlsen et al., 1993).

The Ula Formation in Ula Field underwent more than 2000m of subsidence after the early Oligocene and is slightly overpressured, possibly as a result of the rapid late Tertiary subsidence (Fig. 3) (Harris, 2006; O'Connor et al., 2011). The Ula reservoir has been reported to have a slightly tilted oil-water contact (O'Connor et al., 2011). Reservoir temperature at 3,450 m (11,319 ft) is 143 to 145°C (Home, 1987).

Methods and material

One hundred and twenty two samples of conventional core plugs from four wells were obtained for petrographic analysis from the BP core store at Reslab laboratories in Stavanger, Norway (Appendix 1). These petrographic samples were taken directly adjacent to plug points for conventional core analysis, thus ensuring that the petrographic data tied to the core analysis data. Of the four wells, well 7/12-2 is in the oil leg, and 7/12-A8 is in the water leg, 7/12-3A and 7/12-A13 traverse the oil and water legs. The core sample suite covers the range of present subsurface depths between about 3350 and 3850 m (10,991 and 12,631 ft) TVD, and spans the thickness of the whole reservoir.

Samples were impregnated with blue resin and then made into polished thin sections. Sandstone modal composition was obtained, in the laboratories at Liverpool University~~house~~, by point counting all thin sections at 400 counts per section. Point counting was performed using a x10 objective but higher power objectives were used where necessary, e.g. for finer grained materials and grain coatings. The grid-spacing was selected to ensure that the whole thin section was covered. Quartz cement was differentiated from quartz grains by virtue of the presence of a trail of inclusions on quartz grain surfaces. Grain sizes and grain coatings were determined for each sample using a Meiji 9000 microscope fitted with an Infinity 1.5 camera. Images were collected and long axes of 100 grains per sample and were measured using Infinity Analyser software, with the images and camera calibrated to standards of known size. Fifty quartz grains per sample were measured ~~,~~ in ~~house~~the laboratories at Liverpool University, for the percentage of grain-coating microcrystalline quartz coverage (noting that negligible clay mineral coats were observed) of the freely-exposed grain surfaces, using visual estimates compared to standard grain-coverage images. Only potential sites for quartz cementation (i.e. facing pores, not coated with dead-oil or with clay matrix) that were coated with microcrystalline quartz were measured and expressed as a percentage of all potential sites for quartz cementation.

Scanning electron microscope (SEM) examination of all samples was undertaken using a Philips XL 30 SEM with tungsten filament with an accelerating voltage of 20 kV, and 8 nA beam current for both secondary electron (SE) and backscattered electron microscopy (B)SEM. The SEM examination was carried out on polished sections and freshly fractured, stub-mounted samples coated with carbon and gold respectively. Energy dispersive X-ray analysis (EDAX) provided qualitative compositional analysis of clay minerals, carbonate cements and feldspars. Oil-~~-~~stained samples were soaked in acetone to remove the oil stains which caused problems for the vacuum system in the gold coater. The scanning elect~~g~~ron microscope-cathodoluminescence (SEM-CL) images of quartz cemented grains were ~~collected to calibrate the light optics-determined amounts of quartz cement. SEM-CL images were~~ collected at 10 kV by integrating the signals from 16 discrete frames using a slow scanning raster; this took about 8 minutes for each image. The p~~P~~etrographically-~~-~~defined quartz cement content was compared to the amount of quartz cement discernible from SEM-CL images for three samples, one with high, one with intermediate, and one with a low quartz cement content, to ensure that the point count determination of quartz cement~~ing~~ was consistent.

Doubly polished fluid inclusion wafers for fluid inclusion~~s~~ microthermometric studies were selected to cover all facies from both the water leg and the oil leg and prepared from core samples. An Olympus BX-60 petrographic microscope was used for thermometry equipped with a Linkam THMSG 600 heating and cooling stage. This enabled the measurement of the phase transition temperatures from -180 to 600 °C with an accuracy of between ± 0.1 to ± 1.0. Observations were made with different magnifications (objectives 10x, 20x, 50x and 100x). Inclusions were photographed with Digital Camera Olympus DP71 for the purpose of the fast mapping of inclusion locations. Homogenisation temperature measurements were made on each inclusion in each small piece of fluid inclusion wafer and then freezing point depression measurements were made on each identified inclusion to prevent modification of the homogenisation temperature (Worden et al., 1995). Fluid inclusion samples were also studied using a mercury UV source to differentiate oil inclusions from aqueous inclusions with a record being kept of the presence and absence (and relative abundance) of petroleum inclusions.

Petrophysical and conventional core analysis data were made available by BP Norway. ~~Core plugs were taken at 25 cm-spacings with p~~Porosity and permeability were measured for BP Norway using modern industry-standard methods and corrected for ~~taking account of subsurface conditions~~ confining stress. The permeability data reported here were all collected from plugs drilled parallel to bedding (horizontal permeability). The provided data excluded any anomalous data from fractured plugs. The plugs were collected using industry standard approaches at one every 25 cm (9.84 inches), irrespective of be boundaries to ensure a representative petrophysical dataset. The petrophysical log suites provided for this study were: caliper, bulk density, neutron porosity, sonic transit time, gamma ray, and shallow and deep resistivity. Porosity was calculated for each of the logs using the bulk density log (g/cm^3) and the following relationship:

$$\text{fractional porosity} = (\rho_{mbd} - \rho_{amd})/(\rho_{fd} - \rho_{amd}) \qquad \text{(eq 1)}$$

Where:

ρ_{mbd} = measured bulk density for each sample (from petrophysical logs)

ρ_{amd} = average mineral density

ρ_{fd} = fluid density

The average mineral density employed was 2.66 g/cm^3 (the density of quartz); this average is reasonable since there is a proportion of feldspar with lower density and a proportion of carbonate minerals with higher density. The average fluid density was assumed to be 1.00 g/cm^3.

Water saturation was calculated from the petrophysical log data for each 10 cm depth-interval using the Archie equation. Hole conditions were not an issue in the studied section because it did not include poorly-lithified or soluble sections such as mudstones or evaporites. Values of n, a, and m were fixed at 2.0, 0.81 and 2.0, respectively, as used by the field operators, following industry standard methods and calibration. Deep induction resistivity log data were used since these give true formation resistivity, unaffected by invasion of the formation by drilling fluids (Asquith and Gibson, 1982). The reported formation water resistivity for ~~the Ula Field~~Ula Field is 0.025 ohm.m (Oxtoby, 1994).

Results

Wireline and core analysis data

The calculated density log porosity values correlate well with the core analysis porosity values suggesting that the (wireline) density log porosity values are credible (Fig. 4). The density log-derived porosity and water saturation values for each well are illustrated in Figure 5. The log-derived porosity of the four wells seems to be highest at the shallowest positions with porosity routinely > 20% at the crest of the field but no higher than 10-15 % at the flanks of the field (Fig. 5). The wells included in this study show a wide variation in water saturations; well 7/12-2 has low water saturation, wells 7/12-A13 and 7/12-A08 have high water saturation. Well 7/12-3A has low to intermediate water saturation. The very low porosity and high water saturation spikes (e.g. for well 7/12-2) represent pervasively calcite cemented intervals.

The core analysis data have been split between the three main facies as determined by sedimentological facies description of the core and then further split by the wireline-calculated water saturations (~~see~~ Fig. 5). Porosity-permeability data for each facies, split by water saturation, are displayed in Figure 6 showing that samples with lowest water saturations, especially from facies 1 and facies 2, have the highest porosity and permeability values.

Facies and detrital minerals

The ~~new~~ point count data confirm that the Ula Formation reservoir is an arkosic sandstone (Fig. 7). The wells used in this study and different facies within the core are not differentiated on the ternary QFL diagram since the data lie in one cluster. The main variations in different facies are in terms of: grain size, clay content and degree of bioturbation. A full listing of petrographic data is given in Appendix 1.

Facies 1 is medium~~ to coarse~~-grained, moderately well-sorted (0.52 ϕ), with low detrital clay content (mean 4.2 %, Table 1) and no direct sign of bioturbation. Facies 1 tends to be in upward-fining (i.e. graded) beds that are devoid of small-scale sedimentary structures. Point counting results show that the most dominant detrital mineral~~ in facies 1~~ is monocrystalline quartz (mean 34 %), followed by K-feldspar (mean 11 %) and plagioclase (14 %). Polycrystalline quartz and traces of rock fragments are also present in this facies.

Facies 2 is a fine- to medium-~~-~~grained sandstone that is moderately- to well-sorted (0.62 ϕ), with a variable detrital clay content ranging from 0.8 to 13.0 % (mean 6.5 %) (Table 1). Facies 2 is bioturbated with no remaining primary sedimentary structures due to bioturbation with cm-scale horizontal burrows, identified as *Ophiomorpha* or *Palaeophycus*. The dominant detrital mineral grains in facies 2 are monocrystalline quartz (mean 28 %), K-feldspar (mean 9 %), plagioclase (mean 15%) and rock fragments (<3 %).

Facies 3 is a very fine- to fine-grained sandstone that is moderately-sorted (0.83 ϕ) with a high detrital clay content, based on point-~~-~~count data ranging from 5.7 to 23.2 % (mean 11.5 %) (Table 1). Facies 3 is intensively bioturbated with vertical and horizontal burrows identified as *Teichichnus* or *Rhizocorallian*. The dominant detrital mineral grains in facies 3 are monocrystalline quartz (mean 27 %), K-feldspar (mean 7 %), and plagioclase (mean 11 %). This facies has localised accumulations of stratigraphically-localized shell fragments and only a small amount of rock fragments.

Detrital clays are present as mm- to cm-sized patches and thin discontinuous layers. Detrital clay~~ and~~ is most~~re~~ abundant in the very fine to fine-grained bioturbated facie~~unit~~s. ~~The highest clay contents (of u~~Up to 26 % detrital clay is~~) are~~ found in the very fine- to fine-~~-~~grained, highly bioturbated facies and the lowest clay of <1 % are found in the mediumcoarse-grained, graded sandstones with nodevoid of evidence of bioturbation. From the SEM observations indicate that the clay mineralogy of thede-trital clay matrix is dominated by illite and chlorite, as shownconfirmed by XRD analyseis (trace not illustrated in this paper).

Overall paragenesis

A summary paragenetic sequence is presented in Figure 8, with supporting photomicrographs and SEM images in Figures 9, 10 to, 11 and 13, . The sequence is subdivided into 'early' and 'late' diagenesis. Early diagenetic events took place in depositional pore waters, and their evolving derivatives, at relatively shallow depths, with an influence of depositional and influxing meteoric water (Morad et al., 2010), whereas subsequent'late' diagenesis during burial occurred after the main phase of burial-related compaction and is characterised by growth at higher temperatures.

Early diagenesis

Early diagenesis commenced with admixing and infiltration of detrital clay into the newly deposited sediment, largely due to bioturbation. This resulted in patchy distribution of detrital clays and created locally cleaner pathways that potentially promoted later throughput of diagenetic fluids. This was accompanied by initial compactional porosity-loss, mainly through the reorganisation of grains and mechanical compaction into a stable framework. Framboidal pyrite (Fig. 9a) is associated with detrital clay and precipitated in a reducing environment at relatively shallow depth, during the decay of organic fragments by sulphate-reducing bacteria (Burley & Worden, 2003). Some beds are completely cemented with early diagenetic calcite and have negligible porosity. Dissolution of stratigraphically-restricted shelly carbonate fragments, and the growth of locally pervasive minor non-ferroan calcite within primary pores, occurred during early diagenesis. This led to total occlusion of porosity (see later section on wireline log analysis). Some beds are thus completely cemented with early diagenetic calcite and have negligible porosity. These nodular or bedded early calcite-cemented samples have been excluded from further data analysis (i.e. no point count data for samples with pervasive calcite cement included in Appendix 1) since they do not inform the discussion about the effect of oil emplacement on burial diagenesis (quartz cementation).

Bacterial sulphate reduction, responsible for framboidal pyrite growth (Fig. 9a), led to acidification, which resulted in minor dissolution of unstable grains and created minor amounts of secondary porosity (Fig. 9b). These minor, partially-dissolved grains were typically replaced by small quantities of patchy, early diagenetic chlorite (Fig. 9c). Chlorite predominantly occurs as minor pore-filling rosettes. Volumetrically, pore-filling chlorite is present in small quantities (typically < 1 %). Chlorite appears to be facies-related with the majority occurring in the very fine- to fine-grained, matrix rich, bioturbated facies 3. Grain-coating chlorite is not present in the studied Ula Formation reservoir sandstones.

Microcrystalline quartz locally coats grains (Fig. 9d). By reference to evidence from equivalent Upper Jurassic outcrops at Brora, on the NE coast of Scotland, UK, ~~; the~~ ~~m~~microcrystalline quartz ~~(dealt with in detail in a subsequent section)~~ was probably sourced from the dissolution of unstable siliceous bioclasts (e.g. sponge spicules), at shallow burial depths (< 60 °C) (Vagle et al., 1994).

~~Dissolution of stratigraphically restricted shelly carbonate fragments, and the growth of locally pervasive minor non-ferroan calcite within primary pores, occurred during early diagenesis. This led to total occlusion of porosity (see later section on wireline log analysis). Some beds are thus completely cemented with early diagenetic calcite and have negligible porosity. These nodular or bedded early calcite-cemented samples have been excluded from further data analysis (i.e. no point count data included in Appendix 1) since they do not inform the discussion about the effect of oil emplacement on burial diagenesis (quartz cementation).~~ Further dissolution of feldspar (Fig. 9e) seems to have resulted in the precipitation of a small quantity of early (i.e. pre-compactional) quartz overgrowths, present within quartz-quartz grain contact zones (Figs. 9e-f). Early diagenesis terminated with the end of the main phase of burial-related compaction, which is generally assessed as moderate to strong as evidenced by the prevalence of long and sutured grain contacts.

Late diagenesis

Minor feldspar dissolution continued beyond the main phase of compaction, as indicated by locally significant, but volumetrically-minor, secondary pores that have no evidence of compaction. This phase of grain dissolution liberated Al and Si and potentially contributed to~~resulted in~~ the precipitation of the diagenetically-dominant, post-compactional quartz overgrowths (Table 1~~; the focus of the next section~~) and minor quantities of clay minerals (Fig. 9e) (Barclay and Worden, 2000b). The switch from feldspar dissolution to feldspar growth (Worden and Rushton, 1992), required ~~Tthere must have been~~ a switch from cation-poor and/or ~~feldspar-dissolving (~~low pH ~~)~~ to cation rich and/or ~~(~~moderate pH~~)~~ pore-waters ~~that resulted in the precipitation of minor feldspar overgrowths~~ (Fig. 9e). This change also ~~and~~ led to local growth of minor quantities of dawsonite (sodium aluminum hydroxycarbonate) within primary pores (Worden, 2006)~~ within primary pores~~. Minor quantities of late illite precipitated, locally coating quartz overgrowths at this late stage (Fig. 9d).

Non ferroan and ferroan dolomite cement are present in the Ula Formation (Ula field), with the most volumetrically-important being rhombic ferroan dolomite (Fig. 10a). The mean point count volume for total dolomite is ~0.7 %, (Table 1). Ferroan and non-ferroan dolomite are only present in very fine to fine bioturbated sandstones with abundant matrix (facies 3; Table 1). The ferroan dolomite replaces and locally crosscuts quartz cement and ~~thus~~ so ~~seems to have~~ formed after quartz cement. ~~The~~ ~~h~~Hydrocarbon influx start~~seems to have occurr~~ed after the ~~start~~ onset of the main phase of quartz cement growth since residual hydrocarbon is present on quartz cement surfaces (Fig. 10b).

Quartz diagenesis

Both grain-coating microcrystalline quartz and quartz overgrowths are present in the Ula Formation~~ are~~.

The Ula ~~Formation~~ sandstones have~~s~~ variable amounts of quartz overgrowth cement ranging from high porosity sandstones with relatively small amounts of quartz cement (i.e. a few percent quartz cement) (Figs. 10a, b and c) to pervasively quartz-cemented samples in which the porosity is almost totally occluded (Figs. 10,d, e and f). Quartz overgrowths are not visibly zoned when studied using SEM-CL (Figs. 10e and f). ~~SEM-CL confirms the volumetric importance of quartz cement in the Ula~~

~~Formation.~~ The euhedral edges of quartz overgrowths are locally stained by dead oil or bitumen (Fig. 10b). However, some low porosity sandstones in the finest grained and most clay-rich facies 3 have little quartz cement due to other pore-filling materials such as abundant pore-filling clay and localised Fe-dolomite (Fig. 10a, Table 1). Quartz overgrowths are euhedral when facing open pores (Figs. 10b, c and e). The boundaries between detrital quartz grains and quartz overgrowths are typically characterized by a dust rim composed of fine-grained clay minerals or fluid inclusions (Figs. 10b, c and d). Quartz overgrowths can range in thickness from < 10 µm to > 50 µm. At sites where overgrowths from neighbouring grains interlock, porosity tends to be locally fully occluded. Quartz overgrowths are least abundant in facies type 3 but facies 1 and 2 have highly variable quantities of quartz overgrowths (Table 1).

The quartz cement-poor, medium-grained graded samples from low water saturation samples from 7/12-2 notably have relatively clean, largely unmodified (i.e. as-deposited) detrital quartz grain surfaces (Fig. 11). Such grains are marked by a lack of microquartz cement coatings and no more than nascent, patchy and very thin quartz overgrowths (Figs. 11b and d). These clean quartz grains from the oil leg have subtly uneven surfaces that resemble detrital grains from modern environments.

Quartz cement seems to increase in overall abundance with increasing depth for the medium-grained graded facies 1 (Fig. 12). The same pattern of increasing quartz cement with depth can be discerned for the fine- to medium-grained bioturbated facies 2 but there is no pattern for the relatively quartz cement-poor very fine to fine-grained bioturbated facies 3 (Fig. 12)

Light optics revealed a very fine-grained, colourless mineral coating with low to intermediate birefringence in some samples (Fig. 13a); SEM observation confirmed that this is microcrystalline quartz (Fig. 13b, Table 1). The quantity of microquartz is greatest in the very fine- to fine-grained bioturbated facies 3, with much less in the fine- to medium-grained and bioturbated facies 2 and medium-grained graded ~~and coarse~~ facies 1 ~~and 2~~ (Figs. 12 and 14a, Table 1). There is no systematic pattern of microquartz variation with depth of burial (Fig. 12). Some samples have unusually large amounts of microquartz, others have low to negligible amounts. The microquartz crystals tend to be < 5 µm in size and vary in shape from anhedral (typically rounded) to euhedral. Microquartz tends to sit on detrital grain surfaces but locally forms thick irregular coatings that extend into neighbouring pores and pore-filling patches. Microcrystalline quartz cement appears to be dominant only in facies 3 (very fine to fine bioturbated sandstone with abundant matrix) but it is typically present in small amounts in the coarser facies although one or two samples from ~~the~~ the medium-grained graded facies 1 and fine- to medium-grained bioturbated facies 2 ~~medium and coarse facies~~ contain several percent microquartz. ~~These~~ Facies 3 samples tend to have commensurately smaller amounts of quartz cement than the microquartz-poor medium-grained graded facies 1 and fine- to medium-grained bioturbated facies 2 ~~that have little microquartz~~ (Table 1; Fig. 14a). As well as point counting microquartz, the percentage of detrital quartz grains that are coated with microcrystalline quartz was determined by visually estimating 50 grains per section for a subset of the samples (Fig. 14b). Medium-grained graded facies 1 sandstones have~~s~~ grains that are, on average, about 10 to 20% coated with microquartz and have low overall point counted quantities of microquartz (Figs. 14a and b). Very fine- to fine-grained bioturbated facies 3 sandstones containss some grains that are approaching 100% grain coating with microquartz. Fine- to medium-grained bioturbated facies 2 sandstones tend to have intermediate degrees of grain coating by microquartz (Fig. 14b).

Fluid inclusion Analysis

Samples for fluid inclusion study were selected from both oil and water legs. Homogenization temperatures were measured for aqueous inclusions and petroleum inclusions in 12 samples in wells 7/12-2, 7/12-A3, 7/12-5, 7/12-A08, and 7/12-A13 of the Ula Formation. Primary fluid inclusions that fluoresced under UV illumination are present in quartz overgrowths (Fig. 15) showing that some oil was present during the growth of quartz. Non-fluorescent primary aqueous fluid inclusions are also present in quartz overgrowths. Petroleum inclusions are generally larger in size (Fig. 15a-d) and have a higher vapour-liquid ratio than aqueous inclusions and were therefore easier to work with. Aqueous inclusions range in diameter from 1 to 17 µm. Petroleum inclusions range in diameter from 7 to 38 µm. The liquid to vapor ratio for aqueous fluid inclusion was consistently about 8:1 and for petroleum inclusion was about 5:1. All the homogenisation temperatures recorded here are from inclusions within quartz overgrowths or sitting located between detrital quartz grains and their quartz overgrowths. Only homogenization temperatures that were reproducible within (<5 ºC) were recorded. All inclusions homogenised to liquid upon heating. Aqueous inclusion populations tend to be unimodal between 120 and 174 ºC with the lowest recorded aqueous inclusion homogenization temperature being 103 °C. Petroleum inclusions homogenized between about 80 and 142 ºC. Pressure corrections were not made to the aqueous inclusion homogenisation temperatures because the formation water was probably saturated with methane at the time of trapping (Hanor, 1980), implying that the measured homogenisation temperatures are representative of the actual trapping temperature for the aqueous inclusions. Homogenisation temperatures of inclusions trapped in quartz are not likely to have been re-equilibrated and so represent the true trapping temperature (Worden et al., 1995). The oil inclusions cannot easily be used to reveal the conditions of trapping since the precise PVT properties of the trapped petroleum are not known.

Histograms of homogenization temperatures four representative samples are given in Figure 16 and summarized in Table 2. The present-day formation temperature for well 7/12-A3 is 154°C (determined from drill stem testing) which compares favorably with the homogenisation temperatures (Fig. 16) although the modal fluid inclusion homogenization temperature is lower than the present day temperature.

Discussion

Quartz cementation in the presence of oil

The presence of primary oil inclusions in quartz cement indicates that some oil was present in the reservoir when this authigenic mineral was being precipitated. The very lowest homogenisation temperatures for the aqueous inclusions is 103°C, although a more typical minimum homogenisation temperatures for the aqueous inclusions is 120°C (Fig. 16) which is somewhat higher than the threshold of 80°C widely assumed to be the temperature above which quartz cement grows (Walderhaug, 1996). The oil saturation at the time of the growth of quartz cement, and thus inclusion trapping, is not known although it is noteworthy that the fluid inclusion sample with highest oil saturation at the present day (7/12-2, 3403.00m) has the lowest percentage of quartz cement (Table 2) and was visually estimated to have a relatively great abundance of petroleum inclusions (Fig. 15). Having some oil in the pore network clearly does not automatically preclude quartz cementation.

Quartz cement modeling in the presence of oil

~~In recent years s~~Simple modeling approaches have been developed to try to link quartz cement abundance with burial and thermal histories (Bjørkum et al., 1998; Lander and Walderhaug, 1999; Walderhaug, 1990, 1994a, b, 1996; Walderhaug et al., 2000). These ~~fundamental~~ models were calibrated by examining quartz cement quantities in different sandstones from one basin (Norwegian North Sea) and relating these quantities~~m~~ to the burial history of each sandstone reservoir in the calibration dataset. All of these models assumed that quartz cement is internally-derived and that the main control is the rate of quartz precipitation. The timing of quartz cementation in each well was derived by using aqueous fluid inclusion temperatures from the sandstones in the calibration dataset and the assumption that quartz cementation was continuous from the lowest recorded aqueous inclusion homogenization temperature onwards (despite there being punctuated fluid inclusion records reported) (Walderhaug, 1994a). Geometric characteristics were accounted for by examining grain size (and relating this to available surface area) and the fraction of grains that are quartz (as opposed to feldspars, lithics, etc.). The published models were thus calibrated using a number of basic assumptions. Interestingly, the models were also calibrated utilising the fundamental assumption~~ing~~ that emplacement of oil did not inhibit quartz cementation. Since the published ~~The~~ models (Walderhaug, 1990, 1994a, b, 1996; Walderhaug et al., 2000) involved the assumption that oil had no effect on quartz cement growth. ~~, they~~These models therefore seem to be fundamentally unsuitable for attempting to model~~ing~~ any effect of oil emplacement on quartz cementation. However, for medium-grained graded facies 1 and fine- to medium-grained bioturbated facies 2 in the oil leg of Ula oil field, the relative quantity of quartz cement and the elevated porosity look anomalous compared to the quantities found in the water leg (Table 1, Fig. 12). There are a finite number of controls on anomalously high porosity-low quartz cemented sandstones (Bloch et al., 2002); these possible controls will now be examined.

Main controls on porosity-loss above and below the oil-water contact

A comparison of the effects of cementation and compaction using a plot of pore-filling cement versus intergranular volume (also known as a Houseknecht-type plot) ~~based on petrographic data~~ (Fig. 17) shows that there is a difference in what process has controlled porosity-loss as a function of position in the oil field. On average, the oil leg samples occupy a central position in the diagram showing a combination of compaction and cementation leading to the final porosity. In contrast the ~~oil~~ water leg samples sit mainly within the cementation field. The main cement is quartz so that it could be concluded that quartz cement dominates in the high water saturation zone while there has been less cement in the high oil saturation zones (Fig. 17). In contrast, it could also be concluded that compaction has been relatively more important than cementation in the oil leg ~~than~~ compared to the water leg so that there is a need to compare cement volumes for initially similar samples (same facies) between the oil and water legs.

Grain size, detrital clay and grain-coating microcrystalline quartz and quartz cementation

Grain size is broadly uniform within each facies so that this cannot be invoked as the primary cause of variable amounts of quartz cement in the various facies -(Table 1, Appendix 1). Similarly, both fine- to medium-grained bioturbated and medium-grained graded sandstone samples each have approximately consistent quantities of detrital matrix clay, so this, too, can be excluded as a control on quartz cement within each facies (Fig. 12; Table 1). It is noteworthy that very fine to fine bioturbated facies 3 has a far higher quantity of matrix clay than medium and coarse facies 1 and 2. However, for the water leg samples from the three facies, there is a well-developed, inverse correlation between the amount of detrital clay and the amount of quartz cement (Table 1). This suggests that the more argillaceous-rich, finer-grained, heavily bioturbated samples have experienced inhibition of quartz cement compared to the cleaner medium- and coarse-grained sandstones. Ferroan dolomite is not a major mineral cement but it too correlates with primary facies and detrital clay content possibly (Table 1).

Microquartz is an abundant, and pervasively grain-coating, of cement found on detrital quartz grains by microquartz is prevalent, in the very fine- to fine-grained bioturbated facies 3 (Fig. 14). Quartz cementation appears to have been inhibited by microquartz coats irrespective of pore fluid type (Fig. 12; Table 1). This effect has

~~previously~~ been reported previously (Aase et al., 1996; French and Worden, 2013; French et al., 2010; French et al., 2012; Hendry and Trewin, 1995; Ramm et al., 1997; Weibel et al., 2010; Worden et al., 2012). It is ~~noteworthy~~ significant that a small subset of fine- to medium-grained bioturbated facies 2 samples contain measurable microquartz (Fig. 14a). These samples have commensurately reduced amounts of quartz cement and elevated porosity. For example, samples of fine- to medium-grained bioturbated facies 2 in well 7/12-3A at 3,559-3,566 m (11,677-11,699 ft) TVDss contain a few percent microquartz (Fig. 12) and have anomalously elevated porosity as a consequence of the inhibition of quartz cement (Figs. 5 and 12).

When grain-coating microquartz percentage, and ~~degree~~ percentage of surface area of grain-coating by microquartz, are plotted against quartz cement (Fig. 14a), it is apparent that samples from medium-grained graded facies 1 (and fine- to medium-grained bioturbated facies 2) show a large range of quartz cement volumes irrespective of the amount of microquartz. Although microquartz exerts a control on the development of quartz overgrowths, it is not particularly abundant in medium-grained graded facies 1 or fine- to medium-grained bioturbated facies 2 and it cannot explain the full range of abundance of quartz cement. This suggests that there is an additional control, other than microquartz, that has determined~~ing~~ the amount of quartz cement in facies 1 and 2.

Since grain-coating microquartz is only observed in large amounts in very fine- to fine-grained bioturbated facies 3, it seems likely that this is the only facies in which there was an abundant potential source for the microquartz. Microquartz in Upper

Jurassic sandstones from the North Sea is typically attributed to detrital sponge spicules (Aase et al., 1996; Vagle et al., 1994). Based on the literature-based interpretation that the microquartz was sourced from replaced sponge spicule fragments, it can thus be inferred that detrital fragments of sponge spicules were preferentially concentrated in the finest-~~-~~grained sand fraction. We here speculate that the grading of the silica bioclasts into the finest sand fraction may be a consequence of their fragility and consequent attritional diminution during transport from their original location on the marine shelf. While these silica bioclasts have successfully led to the inhibition~~ed~~ of quartz cement (good for reservoir quality), they are found in the finest sandstones (facies 3) that also contain abundant matrix clay so that the reservoir quality has been detrimentally controlled by other factors.

Quantity of quartz cement above and below the oil-water contact for rocks of the same pre-oil filling characteristics?

The characteristics of the three different primary facies above and below the oil-water contact (and in the transition zone) are summarized in Table 1. The three facies have been defined by grain size, matrix clay content and sedimentary structures (including grading and degree of bioturbation) and so have self-consistent grain size and sorting characteristics and detrital mineralogy (Fig. 7). They also have consistent quantities of detrital clay and grain-coating microcrystalline quartz (Table 1). Samples that have been fully cemented with early diagenetic calcite, i.e. with all pore space filled very soon after deposition, have been removed from the analysis since they cannot record the effects of oil emplacement of burial diagenetic processes. The amounts of ferroan dolomite observed in pores are approximately consistent for the different facies (Table 1). The quantity of petrographically-defined quartz cement has been plotted against specific water saturation for each sample, derived using log data with the data split by the petrographically-defined microquartz content (Fig. 18). This approach shows that low water saturations (and therefore high oil saturations) equate to less quartz cement in medium-grained graded facies 1 (Fig. 18a) and fine- to medium-grained bioturbated facies 2 (Fig. 18b), relative to samples of these same facies from the water ~~-~~leg. ~~Medium and coarse grained samples with relatively high water saturation also tend to have reduced amounts of quartz cement for increasing quantities of microquartz (Fig. 18).~~ There does not appear to be a simple relationship between water saturation and quartz cement content for very fine to fine bioturbated facies 3 (Fig. 18c) although large quantities of microquartz in this facies equate to negligible amounts of quartz cement in all cases. The lack of correlation of water saturation with quartz cement for the very fine to fine bioturbated facies may be a result of: (1) the large quantity of pre-existing detrital clay that left less room for quartz cement to grow (Fig. 12; Table 1), or~~.~~ (2) the great abundance of grain-coating microquartz that prevented quartz cement precipitating (Figs. 12,~~ and~~ 14, 18c; Table ~~2~~1).

Focusing on the medium-grained graded facies 1 sandstones that have less than 20% grain coating, it is possible to discern a good correlation between water saturation and quartz cement content (Fig. 19a). There are good inverse relationships between water saturation and core analysis porosity and permeability (Figs. 19b-c). There is also a good inverse relationship between quartz cement and core analysis porosity (Fig. 19d) confirming that quartz cement is the master control on reservoir quality.

The conclusion from the data detailed in Table 1 and Figures 18 and 19 is that for medium-grained graded facies 1 sandstones, that have virtually identical and small amounts of detrital clay, ferroan dolomite, and grain-coating microquartz, samples from the oil leg appear to have less quartz cement, higher porosity and higher permeability than samples from the water leg. The same is broadly true for fine- to medium-grained bioturbated facies 2 sandstones (Table 1) but very fine to fine bioturbated facies 3 samples tend to have a relatively small quantity of quartz cement irrespective of oil saturation. Facies 3 sandstones have smaller quantities of quartz cement than facies 1 and 2 due to the combined effects of grain coating microquartz (Fig. 14) and relatively minor extra amounts of ferroan dolomite and abundant matrix clay (Table 1).

The assessment of the effects of compaction versus cementation (Fig. 17) shows that water leg samples tend to be more cementation-dominated than oil leg samples. For samples of the same facies, with the same microquartz content, this difference is the result of there being more quartz cement in the water leg than the oil leg (Fig. 18a). We can thus surmise that the growth of quartz cement in the oil leg has been inhibited relative to growth in the water leg.~~It seems likely that this difference is the result of prolonged (or more intense) quartz cementation in the water leg resulting in more quartz cement relative to the oil leg.~~

Synthesis: has oil slowed quartz cementation and therefore caused preservation of porosity?

The key question addressed by this study is whether emplacement of oil during diagenesis led to inhibition of quartz cementation in the Ula Formation in Ula Field. ~~When compared, s~~Samples ~~for similar facies~~ from the oil leg have higher porosities and less quartz cement than comparable samples from the water leg for facies 1 and facies 2 (Table 1, Fig. 18). This difference cannot be explained by demonstrable variances in abundance of microcrystalline quartz coatings (Figs. 12 and 14), grain size, grain-coating chlorite or the presence of other subordinate pore-filling cements (Table 1). We therefore propose that the differences in porosity and quartz cement abundance as a function of oil saturation may be directly attributed to differences in the dominant fluid type within the pore ~~-~~space of these samples.

In essence, the rate of quartz cement growth will be limited to the slowest step in the sequence of steps: supply, transport and precipitation. Having oil present in the pore space during quartz cementation (as shown by oil inclusions in quartz cement; Figs. 15, 16) may have caused the rate of quartz *precipitation* to slow significantly relative to similar samples with high water saturation and therefore led to less quartz cement being precipitated. However, the recorded reduced abundance of quartz cement in the oil leg samples (in medium-grained graded facies 1 and fine- to medium-grained bioturbated 2) could also be the result of reduced rates of silica *supply* in the oil leg (presumably from internal, stylolite-related~~,~~ sources). Alternatively, there may have been reduced rates of silica *transport* in the presence of oil due either to slowed advection (resulting from relative permeability effects) or slowed diffusion (resulting from tortuosity effects) (Worden et al., 1998). The lack of correlation between IGV and quartz cement content (Table 1, Appendix 1) could be used to infer that pressure solution (chemical compaction) has not been affected by the emplacement of oil if we assume that quartz cement was only supplied by local, intra-facies pressure solution. However we cannot be sure that quartz cement in facies 1 and 2 sandstones has not been supplied by feldspar-clay reactions (Barclay and Worden, 2000b), pressure solution in surrounding mudstones (Land and Millken, 2000) or clay-rich sandstones (Trewin and Fallick, 2000), export of biogenic silica from finer sandstone facies (e.g. facies 3) (Worden and Morad, 2000) or even mass flux from deeper in the basin (Giles et al., 2000). Although we cannot be sure which of supply, transport and precipitation rate has been slowed by the presence of oil we can state that the overall process of quartz cementation has been significantly slowed in cleaner, less fine-grained, minimally microquartz-coated sandstones, by the presence of oil in the pore network.

Conclusion

1. Oil was present during quartz cementation in the Ula Formation in Ula Field as revealed by the presence of oil inclusions suggesting oil ingress into the reservoir began when the reservoir was at a temperature of about ~100-120°C.
2. Aqueous fluid inclusion homogenisation temperature data from primary inclusions in quartz cement shows that Qquartz cementation seems to have started at an absolute minimum of 103°C with most quartz cement growing at >120°C, if assume that the lower homogenisation temperatures for

aqueous inclusions in quartz are regarded as being representative of minimum growth temperature.

3. For sandstones of the same depositional facies, with ~~the same~~similar grain size, similar ~~same~~ detrital clay content, similar ~~same~~ low quantity of grain coating microquartz and similar ~~same~~ low quantity of ferroan dolomite, there is less quartz cement in the oil leg than in the water leg, particularly for facies 1 (~~coarse~~medium-grained graded sandstone) and facies 2 (fine- to medium-grained bioturbated sandstone).
4. For facies 3 (fine- to very fine-grained bioturbated sandstone) there appears to be little quartz cement, regardless of whether oil was present during diagenesis or not. This can be attributed to the (relatively) large quantity of grain-coating microquartz and detrital clay associated with this facies.
5. A small number of the coarse-grained sandstone samples in the water leg also have a few percent grain-coating microquartz. These have unusually reduced quantities of quartz cement showing that microquartz, as well as oil emplacement, can inhibit quartz cementation.
6. Emplacement of oil before, or during, quartz cementation has inhibited the growth of quartz cement in the Ula Formation in the cleaner, fine- to medium-grained and medium-grained graded, minimally microquartz cemented sandstones.

FIGURE CAPTIONS

Figure 1. Location map of the Central Graben showing Ula Field with insert map of the North Sea region (lower left). The map shows the study area in the black square and inserted field structural map right showing major bounding faults structures and well locations (modified from Nedkvitne et al., 1993).

Figure 2. Generalized stratigraphy of Ula Field~~ modified from Fraser et al. (2002)~~. The Mandal Formation is the main regional source rock; the Ula Formation is the reservoir under consideration.

Figure 3. Thermal ~~and burial history~~ curves ~~of~~ for Ula Field from well 7/12-6 (Fig. 1), ~~grey~~ the heavier black line represents the top of the Ula reservoir interval. The combined ~~B~~burial and thermal history ~~curve~~ was modelled using ~~Thermodel for Windows~~BasinMod software.

Figure 4. Comparison of core analysis porosity and wireline-derived porosity for well 7/12-A13.

Figure 5. Plots of density-derived porosity and Archie-derived water saturation (S_w) from four of the five Ula field wells used in this study.

Figure 6. Plots of core analysis porosity and permeability subdivided by wireline derived water saturations for the three facies; (a) ~~Coarse~~Medium-grained graded sandstone facies, (b) Fine- to medium-grained bioturbated sandstone facies, (c) Very fine- to fine-grained bioturbated sandstone facies.

Figure 7. Ternary diagram showing the Ula Formation sandstone classification (McBride, 1963).

Figure 8. Generalised paragenetic sequence for the Ula Sandstone in Ula Field (7/12-2, 7/12-A3, 7/12-5, 7/12-A08 and 7/12-A13). Age ranges of diagenetic phases are estimated based on thin section~~s~~ and SEM observations.

Figure 9 a) SEM image showing framboidal pyrite (py) and microcrystalline quartz (μqz) formed early within intergranular area (7/12-A3, ~~3690.90~~3520.36 m ~~DD~~TVD, Sw 0.61) b) SEM image showing partial dissolution of detrital K-feldspar grain (KF) and later authigenic quartz within the secondary intragranular pore (sip) (Well 7/12-5, 3894.00 mDD, Sw 0.78). (c) quartz overgrowth (qzo) encloses pore-filling chlorite (ch) shown by circle (Well 7/12-5, 3894.00 mDD, Sw 0.78) suggesting quartz precipitation after chlorite. (d) late hairy illite (i) draped quartz overgrowths (7/12-A3 , ~~3690.90~~3520.36 m TVD~~DD~~, Sw 0.61). (e) Optical thin section photomicrograph (plane polarised) showing feldspar overgrowths (kfo) and quartz overgrowths both of which thin at grain contacts (circled) suggesting precipitation after main phase of compaction (7/12-A3, ~~3675.50~~3515.76 m ~~DD~~TVD, Sw 0.~~63~~35). (f) residual hydrocarbons (rh) which stain earlier quartz overgrowths (7/12-2, ~~3440.00~~3407.93 m~~DD~~ TVD, Sw 0.06~~43~~).

Figure 10 (a) Thin section photomicrograph (plane polarised light) showing patchy clay minerals (PC) and dolomite cement (dol) (7/12-2, ~~3419.9~~3389.92 m~~DD~~ TVD, Sw 0.~~13~~05). (b) Thin section image (plane polarised) showing quartz overgrowths which partially fills primary intergranular pore (PP) and stained by residual hydrocarbons (rh) (7/12-2, ~~3460.00~~3427.67 ~~mDD~~m TVD, Sw 0.~~24~~13). (c) Thin section photomicrograph (plane polarised light) showing clean primary porosity (PP) ~~low~~ medium to high volume of quartz overgrowths (qzo) and uncoated quartz grain (Q) (7/12-A~~2~~13, ~~3437.30~~3706.32 m~~DD~~ TVD, Sw 0.62~~.12~~). (d) Thin section photomicrograph (plane polarised light) showing quartz overgrowths (qzo) occluding primary pores around quartz grain 7/12-A3, ~~3686.60~~3525.35 m TVD~~DD~~, SW 0.~~60~~31). (e and f) Backscattered electron image and cathodoluminescence image of the same sample differentiating between detrital quartz (Q) and quartz overgrowths (qzo) in the later. Note that at it much easier to observe quartz cement-grain boundaries using light optical images than ~~e problem of quantifying the volume of quartz overgrowths from the~~ backscattered electron images. (7/12-A3, 3525.35 m TVD, SW 0.31~~3686.60 mDD, Sw 0.60~~).

Figure: 11. SEM micrographs of minimally quartz cemented samples of medium-grained graded facies 1 from the oil leg revealing the lack of microquartz or any other sort of grain coating material. The exposed quartz grain surfaces contain nascent quartz cement but are largely in their original, depositional, state. qzo: quartz overgrowth, cs: clean grain surface free of microquartz but also with no quartz cement growing. (a and inset b) 7/12-2, ~~3419.9~~3389.92 m ~~core depth~~TVD; Sw 0.05. (c and inset d) 7/12-2 ~~3414.95~~3384.98 m TVD~~core~~ depth; Sw 0.05.

Figure: 12. Variation of log-derived water saturation, core analysis porosity, quartz cement, microquart~~zz.~~ and detrital clay with true vertical depth for all the wells studied. Samples have been split into the three main facies. The diagram represents the aggregation of data from four wells; ~~with~~ the data are in depth order and do not represent the stratigraphic successio~~n~~y ~~necessarily repeated four times~~.

Figure 13. (a) Thin section image of microquartz~~-~~-coated sandstone (7/12-2; ~~3395~~3365.40~~70~~; m TVD~~DD~~; Sw 0.19). (b) SEM image showing grain-coating microcrystalline quartz (µqz) and mesoquartz (mqz) crystals (7/12-A3; ~~3690.90~~3534.87 m TVD~~DD~~; Sw 0.~~75~~55).

Figure14. Point-~~—~~counted quartz cement plotted against: (a) point-~~—~~counted microquartz cement for all samples, and (b) for a subset of the samples, the percentage of grains coated with microquartz. Samples with abundant microquartz (and grain coating) have little quartz cement suggesting that microquartz has effectively inhibited quartz overgrowths. However, there are many samples with little microquartz (and grain coating) that also have little low quantities of quartz overgrowths suggesting that there is another factor that has significantly affected the growth of quartz cement.

Figure 15. Thin section photomicrograph showing fluid inclusions; see Table 2 for details of samples in the images. (a) Plane polar showing fluid inclusion assemblage in quartz cement. (b) Plane polar photomicrograph showing fluid inclusion rim at the boundary between detrital quartz grain and quartz cement samples from water zone well 7/12-A3. (c and d) petroleum inclusion under fluorescence light samples from oil leg of 7/12-2.

Figure 16. Homogenization temperature measurements for aqueous and petroleum inclusions in selected samples of the Ula Formation. Note present-~~–~~day reservoir temperature is only available for well 7/12-A3

Figure 17. Diagram, based on petrographic data, illustrating styles of porosity ~~-~~loss in the Ula Formation (after Houseknecht, 1984). The oil leg samples (Sw < 0.5) have relatively more porosity lost to compaction than cementation. In contrast, the water leg samples (Sw > 0.5) have more porosity lost to cementation than compaction ~~and 64 % lost to~~. This diagram suggests that, on average, the water leg is more cemented than the oil leg.

Figure 18. Point-~~–~~counted quartz cement volume versus wireline-derived water saturation; (a) ~~coarse~~medium-grained graded sandstone facies 1 (b) fine- to medium-grained bioturbated sandstone facies 2 (c) very fine- to fine-~~–~~bioturbated facies 3. This diagram shows that the fine- to medium-grained bioturbated and medium-grained graded facies have less quartz cement in samples with low water saturation than those with higher water saturation. This suggests that oil emplacement has inhibited the growth of quartz cement. Note that microquartz coatings also play a role in diminishing the amount of amount of quartz cement.

Figure 19. Wireline-derived water saturation values for medium-grained graded sandstone facies 1 samples, that have less than 20% grain coating, compared to quartz cement and core analysis data. (a) Water saturation compared to quartz cement showing that these sandstones have decreasing quartz cement in samples with decreasing water saturations. Sandstones with water saturations less than 0.5 have less than 5% quartz cement; those with water saturations greater than 0.5 have up to 15% quartz cement. There is a good correlation between water saturation and quartz cement; this relationship could be used to predict quartz cement as a function of water saturation. (b) Water saturation compared to core analysis porosity showing that these sandstones have increasing porosity with decreasing water saturation. (c) Water saturation compared to core analysis permeability showing that these sandstones have increasing permeability with decreasing water saturation. (d) Quartz cement compared to core analysis porosity showing that less quartz cement equates to higher porosity.

TABLE CAPTIONS

Table 1. Average values of core analysis horizontal permeability porosity, and point count quartz cement, detrital clay, microquartz and ferroan dolomite volumes for the different facies, subdivided by high and low water saturation. A full listing of all petrographic and related data is available in Appendix 1.

Table 2. The properties of fluid inclusion samples in different wells of Ula Field.

References

Aase, N. E., P. A. Bjorkum, and P. H. Nadeau, 1996, The effect of grain-coating microquartz on preservation of reservoir porosity: American Association of Petroleum Geologists Bulletin, v. 80, p. 1654-1673.

Aase, N. E., and A. Walderhaug, 2005, The effect of hydrocarbons on quartz cementation: diagenesis in the Upper Jurassic sandstones of the Miller Field, North Sea, revisited: Petroleum Geoscience, v. 11, p. 215-223.

Asquith, G. B., and C. R. Gibson, 1982, Basic well log analysis for geologists: American Association of Petroleum Geologists, Methods in Exploration, p. 216.

Baniak, G. M., M. K. Gingras, B. A. Burns, and S. G. Pemberton, 2014, An example of a highly bioturbated, storm- influenced shoreface deposit: Upper Jurassic Ula Formation, Norwegian North Sea: Sedimentology, v. 61, p. 1261-1285.

Baniak, G. M., M. K. Gingras, B. A. Burns, and S. G. Pemberton, 2015, Petrophysical characterization of bioturbated sandstone reservoir facies in the Upper Jurassic Ula Formation, Norwegian North Sea, Europe: Journal of Sedimentary Research, v. 85, p. 62-81.

Barclay, S. A., and R. H. Worden, 2000a, Effects of reservoir wettability on quartz cementation in oil fields, *in* R. H. Worden, and S. Morad, eds., Quartz cementation in sandstones, v. 29, Special Publication of the International Association of Sedimentologists, p. 103-117.

Barclay, S. A., and R. H. Worden, 2000b, Geochemical modelling of diagenetic reactions in a sub-arkosic sandstone: Clay Minerals, v. 35, p. 57-67.

Bergan, M., B. Tørudbakken, and B. Wandås, 1989, Lithostratigraphic correlation of Upper Jurassic sandstones within the Norwegian Central Graben: sedimentological and tectonic implications, *in* J. D. Collinson, ed., Correlation in hydrocarbon exploration, Norwegian Petroleum Society, Graham and Trotman, London, p. 243-251.

Bjørkum, P. A., and P. H. Nadeau, 1998, Temperature controlled porosity/permeability reduction, fluid migration, and petroleum exploration in sedimentary basins: Australian Petroleum Production and Exploration Association Journal, v. 38, p. 453-464.

Bjørkum, P. A., E. H. Oelkers, P. H. Nadeau, O. Walderhaug, and W. M. Murphy, 1998, Porosity prediction in quartzose sandstones as a function of time, temperature, depth, stylolite frequency, and hydrocarbon saturation: American Association of Petroleum Geologists Bulletin, v. 82, p. 637-648.

Bjørnseth, H. M., and J. Gluyas, 1995, Petroleum exploration in the Ula Trend: Norwegian Petroleum Society Special Publications, v. 4, p. 85-96.

Bloch, S., R. H. Lander, and L. Bonnell, 2002, Anomalously high porosity and permeability in deeply buried sandstone reservoirs: Origin and predictability: American Association of Petroleum Geologists Bulletin, v. 86, p. 301-328.

Brown, A., A. W. Mitchell, I. R. Nilssen, I. J. Stewart, and P. T. Svela, 1992, Ula field: relationship between structure and hydrocarbon distribution: Structural and tectonic modelling and its application to petroleum geology: Norwegian Petroleum Society Special Publication, v. 1, p. 409-420.

Dixon, S. A., D. M. Summers, and R. C. Surdam, 1989, Diagenesis and preservation of porosity in Norphlet Formation (Upper Jurassic), southern Alabama: Americam Association of Petroleum Geologists Bulletin, v. 73, p. 707-728.

Ehrenberg, S. N., 1990, Relationship between diagenesis and reservoir quality in sandstones of the Garn Formation, Haltenbanken, mid-Norwegian continental shelf: American Association of Petroleum Geologists Bulletin, v. 74, p. 1538-1558.

Ehrenberg, S. N., 1993, Preservation of anomalously high porosity in deeply buried sandstones by grain-coating chlorite: examples from the Norwegian continental shelf: American Association of Petroleum Geologists Bulletin, v. 77, p. 1260-1260.

Emery, D., P. C. Smalley, N. H. Oxtoby, K. V. Ragnarsdottir, P. Aagaard, A. Halliday, M. L. Coleman, and R. Petrovich, 1993, Synchronous oil migration and cementation in sandstone reservoirs demonstrated by quantitative description of diagenesis [and discussion]: Philosophical Transactions of the Royal Society of London. Series A: Physical and Engineering Sciences, v. 344, p. 115-125.

England, G. L., R. S. Haszeldine, J. Cleverley, S. A. Barclay, B. W. D. Yardley, Q. J. Fisher, C. Graham, and A. Fallick, 2003, Applying Ion-Microprobe Technology in Reconstructing Quartz Cement History in an Upper Jurassic Sandstone Reservoir of the Outer Moray Firth Basin, North Sea, United Kingdom: American Association of Petroleum Geologists Annual meeting, South Lake Tulsa, Oklahoma.

French, M. W., and R. H. Worden, 2013, Orientation of microcrystalline quartz in the Fontainebleau Formation, Paris Basin and why it preserves porosity: Sedimentary Geology, v. 284, p. 149-158.

French, M. W., R. H. Worden, E. Mariani, W. C. Horn, C. E. Kliewer, W. A. Lamberti, R. R. Mueller, and C. Fischer, 2010, Low temperature porosity preserving microquartz from Upper Cretaceous sandstones of the Subhercynian Basin (Germany): Geochimica et Cosmochimica Acta, v. 74, p. A305-A305.

French, M. W., R. H. Worden, E. Mariani, R. E. Larese, R. R. Mueller, and C. E. Kliewer, 2012, Microcrystalline quartz generation and the preservation of porosity in sandstones: evidence from the Upper Cretaceous of the Sub-Hercynian Basin, Germany: Journal of Sedimentary Research, v. 82, p. 422-434.

Giles, M. R., S. L. Indrelid, G. V. Beynon, and J. Amthor, 2000, The origin of large-scale quartz cementation: evidence from large data sets and coupled heat-fluid mass transport modelling, *in* R. H. Worden, and S. Morad, eds., Quartz cement in sandstones, v. 29: Oxford, Blackwells, p. 21-38.

Gluyas, J., and C. A. Cade, 1997, Prediction of porosity in compacted sands: In: Reservoir quality prediction in sandstones and carbonates (eds. Kupecz, J.A., Gluyas, J. and Bloch, S.) AAPG Memoir, v. 69, p. 19-28.

Gluyas, J. G., ed., 1997, Poroperm predictions for reserves growth exploration: Ula trend Norwegian North Sea: Reservoir quality pr, v. 69: edictions in sandstones and carbonates, American Association of Petroleum Geologist Memoir, 201-210 p.

Gluyas, J. G., A. G. Robinson, D. Emery, S. M. Grant, and N. H. Oxtoby, eds., 1993, The link between petroleum emplacement and sandstone cementation: Petroleum Geology of the North west Europe, Geological Society of London, v. 4, 1395-1402 p.

Hanor, J. S., 1980, Dissolved methane in sedimentary brines; potential effect on the PVT properties of fluid inclusions: Economic Geology, v. 75, p. 603-609.

Harris, N. B., 2006, Low-porosity haloes at stylolites in the feldspathic Upper Jurassic Ula sandstone, Norwegian North Sea: An integrated petrographic and chemical mass-balance approach: Journal of Sedimentary Research, v. 76, p. 444-459.

Haszeldine, R. S., A. J. Cavanagh, and G. L. England, 2003, Effects of oil charge on illite dates and stopping quartz cement: calibration of basin models: Journal of Geochemical Exploration, v. 78-9, p. 373-376.

Hawkins, P. J., 1978, Relationship between diagenesis, porosity reduction, and oil emplacement in late Carboniferous sandstone reservoirs, Bothamsall Oilfield, E Midlands: Journal of the Geological Society, v. 135, p. 7-24.

Hendry, J. P., and N. H. Trewin, 1995, Authigenic quartz microfabrics in Cretaceous turbidites - evidence for silica transfer processes in sandstones: Journal of

Sedimentary Research Section a-Sedimentary Petrology and Processes, v. 65, p. 380-392.

Higgs, K. E., H. Zwingmann, A. G. Reyes, and R. H. Funnell, 2007, Diagenesis, porosity evolution, and petroleum emplacement in tight gas reservoirs, Taranaki Basin, New Zealand: Journal of Sedimentary Research, v. 77, p. 1003-1025.

Home, P. C., ed., 1987, Ula: Geology of the Norwegian oil and gas fields: London, Graham and Trotman, 143-151 p.

Karlsen, D. A., T. Nedkvitne, S. R. Larter, and K. Bjørlykke, 1993, Hydrocarbon composition of authigenic inclusions: application to elucidation of petroleum reservoir filling history: Geochimica et Cosmochimica Acta, v. 57, p. 3641-3659.

Land, L. S., and K. L. Millken, 2000, Regional loss of SiO_2 and $CaCO_3$ and gain of K_2O during burial diagenesis of Gulf Coast mudrocks, USA, *in* R. H. Worden, and S. Morad, eds., Quartz cementation in sandstones, v. 29: Oxford, nternational Association of Sedimentologists Special Publications, p. 183-197.

Lander, R. H., and O. Walderhaug, 1999, Predicting porosity through simulating sandstone compaction and quartz cementation: American Association of Petroleum Geologists Bulletin, v. 83, p. 433-449.

Lowry, W. D., 1956, Factors in loss of porosity by quartzose sandstones of Virginia: American Association of Petroleum Geologists Bulletin, v. 40, p. 489-500.

Marchand, A. M. E., R. S. Haszeldine, C. I. Macaulay, R. Swennen, and A. E. Fallick, 2000, Quartz cementation inhibited by crestal oil charge: Miller deep water sandstone, UK North Sea: Clay Minerals, v. 35, p. 201-210.

Marchand, A. M. E., R. S. Haszeldine, P. C. Smalley, C. I. Macaulay, and A. E. Fallick, 2001, Evidence for reduced quartz-cementation rates in oil-filled sandstones: Geology, v. 29, p. 915-918.

Marchand, A. M. E., P. C. Smalley, R. S. Haszeldine, and A. E. Fallick, 2002, Note on the importance of hydrocarbon fill for reservoir quality prediction in sandstones: American Association of Petroleum Geologists Bulletin, v. 86, p. 1561-1571.

McBride, E. F., 1963, A classification of common sandstones: Journal of Sedimentary Petrology, v. 33, p. 664-669.

Midtbø, R. E. A., J. M. Rykkje, and M. Ramm, 2000, Deep burial diagenesis and reservoir quality along the eastern flank of the Viking Graben. Evidence for illitization and quartz cementation after hydrocarbon emplacement: Clay Minerals, v. 35, p. 227-237.

Molenaar, N., J. Cyziene, S. Sliaupa, and J. Craven, 2008, Lack of inhibiting effect of oil emplacement on quartz cementation: Evidence from Cambrian reservoir sandstones, Paleozoic Baltic Basin: Geological Society of America Bulletin, v. 120, p. 1280-1295.

Morad, S., K. Al-Ramadan, J. M. Ketzer, and L. F. De Ros, 2010, The impact of diagenesis on the heterogeneity of sandstone reservoirs: A review of the role of depositional facies and sequence stratigraphy: American Association of Petroleum Geologists Bulletin, v. 94, p. 1267-1309.

Nedkvitne, T., D. A. Karlsen, K. Bjorlykke, and S. R. Larter, 1993, Relationship between reservoir diagenetic evolution and petroleum emplacement in the Ula field, North Sea: Marine and Petroleum Geology, v. 10, p. 255-270.

O'Connor, S., H. Rasmussen, R. Swarbrick, and J. Wood, 2011, Integrating a hydrodynamically-titled OWC and a salt-withdrawal depositional model to explore the Ula Trend: Geofluids, v. 11, p. 388-400.

Oxtoby, N. H., ed., 1994, The Ula field: North Sea Formation waters: London, The Geological Society London. Memoir No. 15, 74 p.

Partington, M. A., B. C. Mitchener, N. J. Milton, and A. J. Fraser, 1993, Genetic sequence stratigraphy for the North Sea Late Jurassic and Early Cretaceous: distribution and prediction of Kimmeridgian–Late Ryazanian reservoirs in the North Sea and adjacent areas, v. 4, p. 347-370.

Ramm, M., and K. Bjorlykke, 1994, Porosity depth trends in reservoir sandstones - assessing the quantitative effects of varying pore-pressure, temperature history and mineralogy, Norwegian shelf data: Clay Minerals, v. 29, p. 475-490.

Ramm, M., A. W. Forsberg, and J. Jahren, 1997, Porosity-depth trends in deeply buried Upper Jurassic Reservoirs in the Norwegian Central Graben: an example of porosity preservation beneath the normal economic basement by grain coating microquartz: In: Reservoir quality prediction in sandstones and carbonates (eds. Kupecz, J.A., Gluyas, J. and Bloch, S.) AAPG Memoir, v. 69, p. 177-200.

Robinson, A., and J. Gluyas, 1992, Duration of quartz cementation in sandstones, North Sea and Haltenbanken Basins: Marine and Petroleum Geology, v. 9, p. 324-327.

Saigal, G. C., K. Bjorlykke, and S. Larter, 1992, The effects of oil emplacement on diagenetic processes; examples from the Fulmar reservoir sandstones, central North Sea: American Association of Petroleum Geologists Bulletin, v. 76, p. 1024-1033.

Sathar, S., R. H. Worden, D. R. Faulkner, and P. C. Smalley, 2012, The Effect of Oil Saturation On the Mechanism of Compaction In Granular Materials: Higher Oil Saturations Lead To More Grain Fracturing and Less Pressure Solution: Journal of Sedimentary Research, v. 82, p. 571-584.

Scholle, P. A., 1977, Chalk diagenesis and its relation to petroleum exploration: oil from chalks, a modern miracle: Americam Association of Petroleum Geologists Bulletin, v. 61, p. 982-1009.

Scholle, P. A., and B. Halley, eds., 1985, Burial diagenesis: out of sight, out of mind!: Out of sight, out of mind!, Society of Sedimentary Geology Special Publication, 309-334 p.

Sneider, R. M., ed., 1990, Introduction: Reservoir description of sandstones: Sandstone petroleum reservoirs: New York, Springer-Verlag, 1-3 p.

Taylor, M. S. G., A. LeROY, and M. Førland, 1999, Hydrocarbon systems modelling of the Norwegian Central Graben fairway trend, v. 5, p. 1325-1338.

Taylor, T. R., M. R. Giles, L. A. Hathon, T. N. Diggs, N. R. Braunsdorf, G. V. Birbiglia, M. G. Kittridge, C. I. Macaulay, and I. S. Espejo, 2010, Sandstone diagenesis and reservoir quality prediction: Models, myths, and reality: American Association of Petroleum Geologists Bulletin, v. 94, p. 1093-1132.

Trewin, N. H., and A. E. Fallick, 2000, Quartz cement origins and budget in the Tumblagooda Sandstone, Western Australia, *in* R. H. Worden, and S. Morad, eds., Quartz cement in sandstone. Special Publication of the International Association of Sedimentologists v. 29: Oxford, Blackwells, p. 219-229.

Underhill, J. R., ed., 1998, Jurassic: Petroleum Geology of the North Sea:Basic Concepts and Recent Advances, Blackwell Science, 656 p.

Vagle, G. B., A. Hurst, and H. Dypvik, 1994, Origin of quartz cement in some sandstone from the Jurassic of the Inner Moray Firth (UK): Sedimentology, v. 41, p. 363-377.

Walderhaug, O., 1990, A fluid inclusion study of quartz cemented sandstones from offshore mid-Norway - possible evidence for continued quartz cementation during oil emplacement: Journal of Sedimentary Petrology, v. 60, p. 203-210.

Walderhaug, O., 1994a, Precipitation rates for quartz cement in sandstones determined by fluid inclusion microthermometry and temperature history modelling: Journal of Sedimentary Research Section a-Sedimentary Petrology and Processes, v. 64, p. 324-333.

Walderhaug, O., 1994b, Temperatures of quartz cementation in Jurassic sandstones from the Norwegian continental shelf - evidence from fluid inclusions: Journal of

Sedimentary Research Section a-Sedimentary Petrology and Processes, v. 64, p. 311-323.

Walderhaug, O., 1996, Kinetic modeling of quartz cementation and porosity loss in deeply buried sandstone reservoirs: American Association of Petroleum Geologists Bulletin, v. 80, p. 731-745.

Walderhaug, O., R. H. Lander, P. A. Bjorkum, E. H. Oelkers, K. Bjorlykke, and P. H. Nadeau, 2000, Modelling quartz cementation and porosity in reservoir sandstones: examples from the Norwegain continental shelf: In: Quartz cementation in sandstones (eds. Worden, R.H. and Morad, S.) International Association of Sedimentologists Special Publications, v. 29, p. 39-50.

Weibel, R., H. Friis, A. M. Kazerouni, J. B. Svendsen, J. Stokkendal, and M. L. K. Poulsen, 2010, Development of early diagenetic silica and quartz morphologies - Examples from the Siri Canyon, Danish North Sea: Sedimentary Geology, v. 228, p. 151-170.

Wilkinson, M., and R. S. Haszeldine, 2011, Oil charge preserves exceptional porosity in deeply buried, overpressured, sandstones: Central North Sea, UK: Journal of the Geological Society, v. 168, p. 1285-1295.

Wilkinson, M., R. S. Haszeldine, R. M. Ellam, and A. Fallick, 2004, Hydrocarbon filling history from diagenetic evidence: Brent Group, UK North Sea: Marine and Petroleum Geology, v. 21, p. 443-455.

Wilkinson, M., R. S. Haszeldine, and A. E. Fallick, 2006, Hydrocarbon filling and leakage history of a deep geopressured sandstone, Fulmar Formation, United Kingdom: American Association of Petroleum Geologists Bulletin, v. 90, p. 1945-1961.

Worden, R. H., 2006, Dawsonite cement in the Triassic Lam Formation, Shabwa Basin, Yemen: A natural analogue for a potential mineral product of subsurface CO2 storage for greenhouse gas reduction: Marine and Petroleum Geology, v. 23, p. 61-77.

Worden, R. H., M. W. French, and E. Mariani, 2012, Amorphous silica nanofilms result in growth of misoriented microcrystalline quartz cement maintaining porosity in deeply buried sandstones: Geology, v. 40, p. 179-182.

Worden, R. H., and S. Morad, 2000, Quartz cementation in sandstones: a review of the key controversies In: Quartz cementation in sandstones (eds. Worden, R.H. and Morad, S.) International Association of Sedimentologists Special Publications, v. 29, p. 1-20.

Worden, R. H., N. H. Oxtoby, and P. C. Smalley, 1998, Can oil emplacement prevent quartz cementation in sandstones?: Petroleum Geoscience, v. 4, p. 129-137.

Worden, R. H., and J. C. Rushton, 1992, Diagenetic K-feldspar textures - A TEM study and model for diagenetic feldspar growth: Journal of Sedimentary Petrology, v. 62, p. 779-789.

Worden, R. H., E. A. Warren, P. C. Smalley, T. J. Primmer, and N. H. Oxtoby, 1995, Evidence for resetting of fluid inclusions from quartz cements in oil fields - discussion: Marine and Petroleum Geology, v. 12, p. 566-570.